MARMARA UNIVERSITY
INSTITUTE FOR GRADUATE STUDIES IN PURE AND APPLIED SCIENCES

SYNTHESIS, CHARACTERIZATION AND PHOTOCATALYTIC ACTIVITIES OF MODIFIED CHALCOGENIDES

İBRAHİM KABA

MASTER THESIS
Department of Chemical Engineering

Thesis Supervisor
Assoc. Prof. Dr. Özge KERKEZ KUYUMCU

Thesis CO- Supervisor
Prof. Dr. Atıf KOCA

ISTANBUL, 2024

MARMARA UNIVERSITY
INSTITUTE FOR GRADUATE STUDIES
IN PURE AND APPLIED SCIENCES

SYNTHESIS, CHARACTERIZATION AND PHOTOCATALYTIC ACTIVITIES OF MODIFIED CHALCOGENIDES

İBRAHİM KABA

(524522001)

MASTER THESIS

Department of Chemical Engineering

Thesis Supervisor

Assoc. Prof. Dr. Özge KERKEZ KUYUMCU

Thesis CO- Supervisor

Prof. Dr. Atıf KOCA

ISTANBUL, 2024

ACKNOWLEDGEMENT

I would like to present my sincere gratitude to Assoc. Prof. Dr. Özge KERKEZ KUYUMCU, who supported me throughout my master's degree process for writing and managing projects and was the main person in the development of my thesis.

I would like to express my gratitude to my co-advisor Prof. Dr. Atıf KOCA for his laboratory support and guidance.

I would like to thank Res. Asst. Rabia Nur BOZKURT not only for her support but also for her friendship.

I would also like to thank my friends Sumru KALAÇ, İlayda İŞLEK, Sergen BAHMAL, Nida ELMALI, Elif Tuğba YILMAZ, Elif ÇUBUĞUUZUN, who always gave me positive support throughout my master's degree process.

I would like to thank The Scientific Research Commisions (BAPKO) of Marmara University for the project titled "Modifiye Kalkojenitlerin Sentezi, Tanımlanması ve Fotokatalitik Aktiviteleri" (Project Number: FYL-2024-11093).

I would like to thank Scientific and Technological Research Council of Turkey (TUBITAK) for supporting my thesis and serving as a scholar in the project titled "$Cd_xZn_{1-x}S$/Farklı İkili Yardımcı Katalizörlerin Sentezi ve Fotokatalitik H_2 Üretiminde Aktivitelerinin İncelenmesi" (Project Number: 123M629), which is a 1002 - A Rapid Support Module.

I would also like to thank TUBITAK again for being supported by the 2210-A Domestic General Master's Scholarship Program during my master's degree.

Finally, I would like to thank my dear mother Emine KABA, my dear father Zeki KABA, my brothers Havvanur and İlkay KABA, My uncle Bayram ÜRESİN, his wife Nurhayat ÜRESIN and my cousin Gamzenur ÜRESİN for their endless love and support.

July, 2024 **İbrahim KABA**

TABLE OF CONTENT

ABSTRACT

SYNTHESIS, CHARACTERIZATION AND PHOTOCATALYTIC ACTIVITIES OF MODIFIED CHALCOGENIDES

Hydrogen is a promising energy source for addressing environmental issues and photocatalytic hydrogen production from water is a promising renewable energy process. Cadmium sulfide (CdS) is a widely used photocatalyst; however, the photocorrosion problem causing the low stability and fast charge recombination problem causing the low photocatalytic activity are also well-known. To prevent the stability problem, $Cd_xZn_{1-x}S$ which has tunable optical properties has become forward. MoS_2 is used as an additive to semiconductor photocatalysts due to its wide contact interface, inhibition of charge recombination, low cost, high reactivity for H_2 evoluation reaction, and enhancement of visible light response. Transition metal carbides such as Mo_2C are excellent electrocatalysts for the production of H_2; additionally, they serve as good co-catalysts for most photocatalysts.

Modified $Cd_XZn_{1-X}S$ photocatalysts were examined in hydrogen production under solar illumination. In the first part of the study, $Cd_XZn_{1-X}S$ was prepared using 1,3-diaminopropane (DAP) and then MoS_2 added; in the second part of the study $Cd_{0.7}Zn_{0.3}S$ nanorod was prepared using ethylenediamine (EDA)/water and then MoS_2 and MoC-Mo_2C were added. Catalysts were characterized by XRD, TEM, SEM, UV-Vis DRS, and electrochemical applications. For the first part, a full factor design was carried out via Minitab 19 to investigate the factors affecting the produced hydrogen amount. Cd/Zn ratio, MoS_2 content, and photocatalyst loading were studied. Photocatalytic hydrogen production results were analyzed by ANOVA (Analysis of Variance) and it was concluded that for maximum hydrogen production, Cd/Zn ratio should be in the range of 0.5/0.5 and 0.7/0.3; MoS_2 content should be in the range of 2-4% and photocatalyst loading should be 10 mg. For the second part, $Cd_{0.7}Zn_{0.3}S$ nanorods were modified with various amounts of MoS_2 and MoC-MoC_2. N-$Cd_{0.7}Zn_{0.3}S$/1% MoS_2/1.0% MoC-Mo_2C catalyst showed the best result with 133.5 mmol H_2 g^{-1} h^{-1}, while the hydrogen production rate of N-$Cd_{0.7}Zn_{0.3}S$ was 37.2 mmol g^{-1} h^{-1}.

ÖZET

MODİFİYE KALKOJENİTLERİN SENTEZİ, KARAKTERİZASYONU VE FOTOKALİTİK AKTİVİTELERİ

Hidrojen, çevresel sorunları çözecek, umut vadeden bir enerji kaynağıdır ve sudan fotokatalitik hidrojen üretimi umut vadeden bir yenilenebilir enerji sürecidir. Kadmiyum sülfür (CdS) yaygın olarak kullanılan bir fotokatalizördür; ancak, düşük kararlılığa neden olan fotokorozyon sorunu ve düşük fotokatalitik aktiviteye neden olan hızlı yük rekombinasyonu sorunu da iyi bilinmektedir. Kararlılık sorununu önlemek için, ayarlanabilir optik özelliklere sahip $Cd_xZn_{1-x}S$ öne çıkmıştır. MoS_2, geniş temas yüzeyi, yük rekombinasyonunu engellemesi, düşük maliyeti, H_2 oluşumu reaksiyonu için yüksek reaktivitesi ve görünür ışık tepkisinin iyileştirilmesi nedeniyle yarı iletken fotokatalizörlere katkı maddesi olarak kullanılır. Mo_2C gibi geçiş metali karbürleri, H_2 üretimi için mükemmel elektrokatalizörlerdir; ayrıca, çoğu fotokatalizör için iyi yardımcı katalizörler olarak hizmet ederler.

Modifiye edilmiş $Cd_XZn_{1-X}S$ fotokatalizörleri solar ışık altında hidrojen üretiminde incelenmiştir. Çalışmanın ilk bölümünde, $Cd_XZn_{1-X}S$, 1,3-diaminopropan (DAP) kullanılarak hazırlanmış ve ardından MoS_2 eklenmiştir; çalışmanın ikinci bölümünde, $Cd_{0.7}Zn_{0.3}S$ nanoçubuklar, etilendiamin (EDA)/su kullanılarak hazırlanmış ve ardından MoS_2 ve MoC-Mo_2C eklenmiştir. Katalizörler XRD, TEM, SEM, UV-Vis DRS ve elektrokimyasal uygulamalarla karakterize edilmiştir. İlk bölümde, üretilen hidrojen miktarını etkileyen faktörleri araştırmak için Minitab 19 aracılığıyla tam faktör tasarımı gerçekleştirilmiştir. Cd/Zn oranı, MoS_2 içeriği ve fotokatalizör yüklemesi incelenmiştir. Fotokatalitik hidrojen üretim sonuçları ANOVA (Varyans Analizi) ile analiz edilmiştir ve maksimum hidrojen üretimi için Cd/Zn oranının 0.5/0.5 ile 0.7/0.3 aralığında; MoS_2 içeriğinin %2-4 aralığında ve fotokatalizör miktarının 10 mg olması sonucuna varılmıştır. İkinci kısım için, $Cd_{0.7}Zn_{0.3}S$ nanoçubuklar çeşitli miktarlarda MoS_2 ve MoC-Mo_2C ile modifiye edilmiştir. N-$Cd_{0.7}Zn_{0.3}S$/1% MoS_2/1.0% MoC-Mo_2C katalizörü 133.5 mmol H_2 g^{-1} h^{-1} ile en iyi sonucu gösterirken, N-$Cd_{0.7}Zn_{0.3}S$'nin hidrojen üretim hızı 37.2 mmol g^{-1} h^{-1}'dir.

SYMBOLS

H_2 : Hydrogen

O_2 : Oxygen

$E^o_{oxidation}$: Oxidation potential

$E^o_{reduction}$: Reduction potential

eV : Electronvolts

e^- : Electrons

h^+ : Holes

ΔH : Enthalpy change

W : Watt

mg : Milligram

mmol : Millimole

λ : The Greek letter lambda

t : Time

Eg : Band gap energy (eV)

ABBREVIATIONS

CB : Conduction band

VB : Valence band

EDTA : Ethylenediaminetetraacetic acid

LA : Lactic acid

TEOA : Triethanolamine

Na_2S/Na_2SO_3 : Sodium sulfur/sodium sulfite

$S^{-}{}_2$: Sulfide

$SO^{2-}{}_4$: Sulfate

MSs : Metal sulfides

CdS : Cadmium sulfide

ZnO : Zinc Oxide

ZnS : Zinc Sulfide

MoS_2 : Molybdenum disulfide

$Cd_xZn_{1-x}S$: Cadmium zinc sulfide

Cd/Zn : Cadmium zinc ratio

EDA : Ethylenediamine

DAP : 1,3-diaminopropane

HER : Hydrogen evolution reaction

MoC-Mo_2C : Molybdenum carbides

XRD : X-Ray Diffraction analysis

TEM : Transmission Electron Microscopy

HRTEM : High Resolution Transmission Electron Microscopy

STEM : Scanning Transmission Electron Microscopy

UV-Vis DRS : Ultraviolet–Visible Diffuse Reflectance Spectroscopy

SEM : Scanning Electron Microscope

LSV : Linear Sweep Voltammetry

ITO : Indium tin oxide

CVD : Chemical vapour deposition

LIST OF FIGURES

LIST OF TABLES

1. INTRODUCTION

Hydrogen is a viable energy source that can help solve environmental and energy issues [1]. Hydrogen has the highest specific energy among fuels. It is regarded as a worldwide energy solutions leader since the combustion process of hydrogen produces only water [2]. It has been extensively researched as an energy source due to its high energy density and minimal environmental effect [3]. It is accepted as a potential fuel due to the advantages of its use as a carbon-free solution, it can be used in transportation infrastructures and existing fuel storage, and its advantages can be mentioned as being suitable for long-term storage [4].

Green hydrogen, which is not dependent on fossil fuels, emits little or no carbon dioxide during manufacturing, making it renewable and clean. Today, renewable energy sources like solar and energy are employed in a variety of ways, as are ethanol, biogas, and wood. Green hydrogen generation is being investigated utilizing biomass-derived raw materials [5]. Hydrogen, whose only result when burnt is H_2O, has gained popularity as a clean energy carrier [6]. In terms of both challenges (fossil fuel depletion and toxic gaseous byproducts of fossil fuels), hydrogen generation using solar energy is seen as a very promising technology, and research is now underway. Among solar hydrogen generation techniques, semiconductor-based photocatalytic hydrogen production is regarded as a successful approach since it allows for the easy use of artificial indoor illumination or solar energy, resulting in widespread availability. As a result, significant efforts are being made to produce efficient, stable, low-cost, and environmentally friendly photocatalysts that use solar energy to provide additional hydrogen sustainably [7].

2. LITERATURE REVIEW

2.1. Photocatalytic Hydrogen Production and Mechanism

Photocatalytic hydrogen generation is one of several renewable hydrogen production processes.

The utilization of sunlight as a light source, as well as semiconductor catalysts that support it, is an important area of research in turning solar energy into chemical energy. Water splitting employing semiconductor photocatalysts is regarded as a promising and

environmentally friendly method for photocatalytic hydrogen generation [8]. In this process, solar energy is used to produce valuable chemical fuels such as hydrogen from the decomposition of water via a photocatalytic reaction involving a semiconductor, and research is being conducted to identify suitable semiconductors for this purpose, including metal oxides, metal hydroxides, oxynitrides, and sulfides [9][10]. High hydrogen production efficiency, accessible cost, optimization of bandgap, stability and other factors are considered the key characteristic parameters for water splitting. Inhibiting electron recombination and increasing photostability through the development of new catalysts and co-catalysts are other important research topics [11]. Generally, the photocatalytic H_2 generation process consists of three main steps: the semiconductor absorbs light to form electron-hole pairs, the photogenerated electron-hole pairs are separated and transferred to the surface of the semiconductor, and H_2 evolution on the semiconductor surface. The efficiency of photocatalytic H_2 production depends on the balance of kinetics and thermodynamics between these three processes. Studies are taking important steps to develop innovative photocatalysts with wide absorption spectrum and effective charge separation and transfer [12]. The Gibbs free energy shift for water splitting is + 237.13 kJ/mol, and two simultaneous redox processes occur, as seen in Equations (1.1) and Equation (1.2) below. Equation (1.3) represents the complete reaction [13].

$$H_2O \rightarrow \frac{1}{2} O_2 + 2H^+ + 2e^- \ (E°_{oxidation} = 1.23 \text{ eV}) \quad (1.1)$$

$$2H^+ + 2e^- \rightarrow H_2 \ (E°_{reduction} = 0 \text{ eV}) \quad (1.2)$$

$$H_2O \rightarrow H_2 + \frac{1}{2} O_2, \ \Delta G° = 237.13 \text{ kj/mol} \quad (1.3)$$

The water decomposition process is a thermodynamically involuntary event, which requires energy input to overcome the 1.23 eV energy barrier. To carry out the photocatalytic breakdown process of water, a semiconductor in the reaction medium must be activated by a photon with energy equal to or higher than its band gap energy. In this situation, electrons transfer from the valence band to the conduction band, leaving holes in the valence band. Photons create electrons (e^-) and holes (h^+). If the conduction band

(CB) of the photocatalyst is more negative than the H^+/H_2 reduction potential and the valence band (VB) is more positive than the O_2/H_2O oxidation potential, the electrons and holes produced by this photon have the capacity to reduce the H^+ cation and oxidize H_2O, respectively happens [13]. The semiconductor with a shorter band gap absorbs and utilizes sunlight more quickly, whereas the semiconductor with a wider band gap has a greater capacity for oxidation or reduction. Furthermore, the violent recombination of photogenerated carriers within a discrete semiconductor poses a significant hurdle for photocatalyst applications due to the existence of Coulomb forces [14]. Figure 2.1. illustrates the mechanism. The image depicts four steps: 1) light harvesting, 2) charge separation, 3) electron and hole transport to the photocatalyst's surface, and 4) redox reaction [15]. In other words, the conduction band (CB) of an ideal photocatalyst must be more negative than the H^+/H_2 reduction potential, and the valence band (VB) [16].

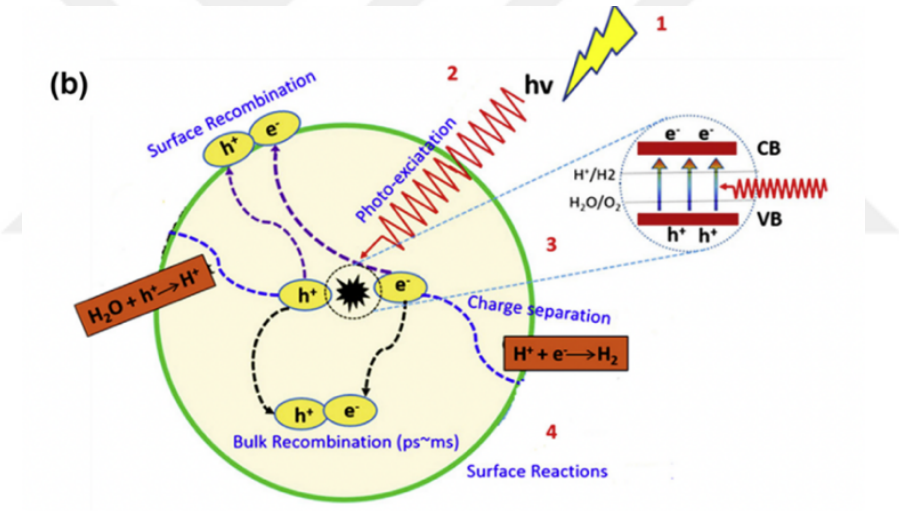

Figure 2.1 A schematic representation of the photocatalysis process and charge recombination [15].

2.2.Sacrificial Agents

Water splitting is an energetically rising process (ΔH = 286 kJ mol^{-1}), hence electron or sacrificial agents donor/hole scavengers play an essential role for photocatalytic hydrogen synthesis. The most often used sacrificial reagents for catalysis are methanol, ethylenediaminetetraacetic acid (EDTA), lactic acid (LA), triethanolamine (TEOA), and sodium sulfur/sodium sulfite (Na_2S/Na_2SO_3). Among these sacrificial components, S^{2-}

/SO_3^{2-}, or sulfur ion, has a comparatively strong reducing capacity and is the most utilized [17]. The sacrificial agent is irreversibly oxidized by the photon-generated vacancies instead of the water molecule. It becomes easier for electrons in the conduction band to reduce water and the oxygen (O_2) formation reaction becomes easier. At the same time, thanks to these agents, the back reaction of H_2 and O_2 is prevented. The sacrificial reagent helps control the hole recombination and the rate of electron, and the photocatalytic efficiency can be increased by the addition of the sacrificial agent [18]. For example, when examining the CdS photocatalyst, the pH becomes alkaline and produces hydrogen sulfide (HS^-) and sulfide (S_2^-) when dissolved in water. During the process, HS^- and S_2^- are rapidly oxidized into polysulfide (S_4^{2-}, S_5^{2-}) ions and sulfate (SO_4^{2-}). Na_2SO_3 is used to improve efficiency and activity. When the H_2 generation efficiency of the CdS photocatalyst was investigated using different sacrificial agents (Figure 2.2.), it was discovered that Na_2S/CdS or CdS/ Na_2SO_3 was greater than that of CdS/Na_2S/Na_2SO_3. It has been demonstrated that TEOA produces the most H_2, which can be attributed to strong interface connectivity and photo-generated holes on the CdS surface, which improves efficiency [17].

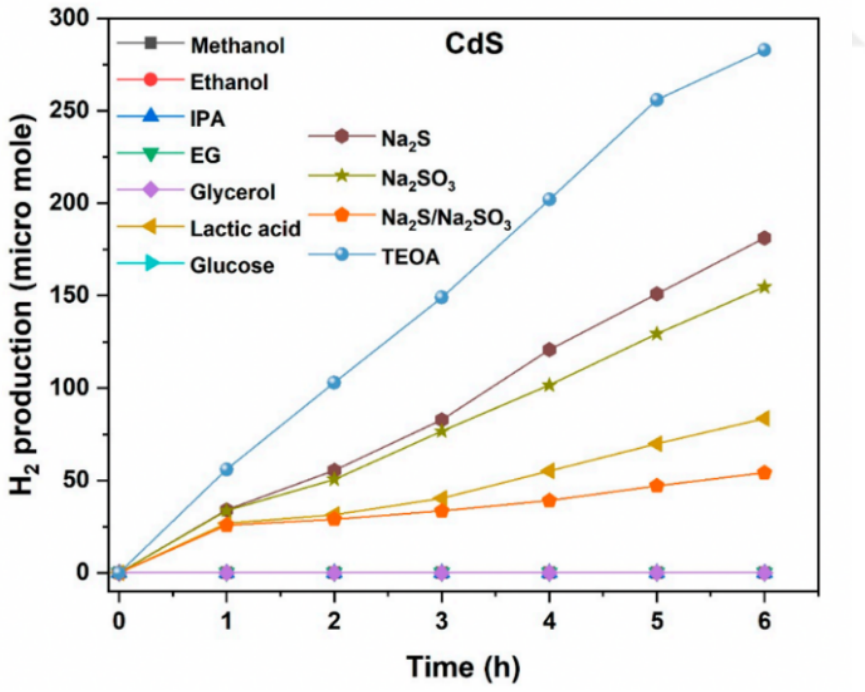

Figure 2.2 Photocatalytic H_2 generation efficiency of CdS with varied sacrificial agents [17].

2.3. Metal sulfides (MSs)

Among the numerous semiconductor materials studied, metal sulfides (MSs) are promising for H_2 production under obvious light [19].

2.3.1. Cadmium Sulfide (CdS)

CdS photocatalysts come in two crystal structures: cubic and hexagonal. Cubic crystals, also known as zinc blende phases, have a tetrahedral structure in terms of crystal morphology and are classified as equiaxed systems with faces [20]. Having a moderately shrinking band gap (2.4 eV), CdS seems warranted as a perfect photo driven catalyst. Generally, co-catalysts are used to prevent the recombination of photon-induced charges with CdS and improve H_2 production efficiency [21]. It exhibits great mobility, a low band gap, and a good energy band location, making it a prospective high-performance photocatalyst [22]. However, the photocatalytic H_2 production action on an uncovered CdS is extremely low, primarily due to the rapid recombination of photogenerated electrons and holes, the rapid reverse reaction between hydrogen and oxygen, and the large H_2 production overpotential [23]. It is susceptible to photo corrosion, and CdS nanoparticles easily agglomerate, resulting in inactivation. These issues lead CdS to have a poor photocatalytic hydrogen generation rate [24]. As a result, CdS can be paired with a cocatalyst to address some of its issues. Noble metals have a high electron density and strong electrical conductivity, making them useful cocatalysts for photocatalysts. However, its high cost and rarity limit its widespread utilization, hence non-noble metal cocatalysts are being developed [25]. Ma et al. used an atomic layer deposition (ALD) approach to develop a new type of CdS@ZnO core-shell the heterostructure. The rationally built thin ZnO shell not only permits light to be received through the CdS core, but it also forms an intimate heterojunction between the two. The number of deposition cycles controls the amount of ZnO shell coated on the CdS core, and the resultant CdS@ZnO with (100) ALD deposition cycles have a greatest photocatalytic evolution of H_2 rate of 11.36 mmol/g/hour. When Pt and PdS are used as co-catalysts, the H_2 evolution rates are further increased to 71.39 and 98.82 mmol g^{-1} h^{-1}, accordingly, which are 4.1 and 5.7 times greater than the maximum reported value (17.40 mmol g^{-1} h^{-1}). The H_2 production and % quantum efficiency of some co-catalysts added to the CdS photocatalyst are given in Table 2.1.

Table 2.1 Effect of different co-catalysts added on CdS.

Catalyst Type	Catalyst Amount (mg)	Light Intensity (W/m^2)	Hydrogen Production Amount (mmol g^{-1} h^{-1})	% Quantum Efficiencies	References
CdS/MoS_2	10	300 W xenon lamp	63.7	33.62	26
CdS/ZnS/ZnO	10	225 W Xenon arc lamp	51.4	26.88	27
CdS@ZnO core-shell /Pt	10	225 W Xe lamp	71.4	50.27	28
CdS@ZnO core-shell /PdS	10	225 W Xe lamp	98.8	69.59	28
CdS/CNTs/NiS	100	350 W Xe lamp	12.1	-	29
ZnO/CdS/ MoS_2	15	500 W Xenon lamp	10.3	-	30

2.3.2. Zinc Oxide (ZnO) and Zinc Sulfide (ZnS)

Many semiconductors, including zinc oxide (ZnO), zinc sulfide (ZnS), molybdenum disulfide (MoS_2), and bismuth vanadate ($BiVO_4$), have been shown to improve CdS's capacity to evolve H_2 via heterostructures [31]. Wide band gap ZnO, an inorganic semiconductor photocatalytic material, is widely used in different fields, such as biomedicine, sensors, solar cells and photocatalysis, especially in the photocatalytic degradation of organic pollutants; It has features such as being non-toxic, having stable chemical and physical properties, and high catalytic activity. In addition, this material is environmentally friendly and low-cost. They are synthesized in different morphologies (nanorods, nanospheres, nanotubes, nanowires, nanocrystals, etc.). In the studies, zinc

oxide nanoparticles (ZnO-NPs) are used as another important semiconductor photocatalytic material after TiO_2 [32]. ZnS has a greater band gap energy than CdS. ZnS's large band gap energy makes it an ideal surface passivating shell material for CdS [33]. ZnS is a semiconductor of the n-type photocatalyst with a broad bandgap of 3.68 eV. It has a negative redox potential in the conduction band (-1.36 eV) and valence band (+2.35 eV) and is chemically stable against oxidation and hydrolysis [34]. Although it has lower photocatalytic activity than TiO_2, for example, ZnS is still considered an outstanding semiconductor due to its stability, non-toxicity, fast electron mobility, and rapid formation of photogenerated electron-hole pairs. ZnS's wide band gap of 3.68 eV limits its applicability to UV light ($\lambda < 400$ nm), like TiO_2 [35]. Lin et al. developed an incompletely coated CdS/ZnS core/shell photocatalyst using a simple hydrothermal technique. Because of the defect energy levels created by zinc vacancies, the normal type-I heterojunction of CdS/ZnS develops to a type-II heterojunction and Z-scheme hybrid structure, allowing the ZnS shell to promptly transfer and collect photogenerated holes from the CdS core. Under optimum conditions, CdS/ZnS produced the most hydrogen (24.1 mmol g^{-1} h^{-1}) when exposed to visible light. After 9 hours of illumination at $\lambda = 420 \pm 5$ nm, the average apparent quantum yield is 9.3%. It shows excellent photocatalytic H2 evolution while being stable [36]. H_2 production and % quantum efficiency of some ZnS photocatalyst samples are given in Table 2.2.

Table 2.2 Hydrogen production and efficiency values of different ZnS samples.

Catalyst Type	Catalyst Amount (mg)	Light Intensity (W/m^2)	Hydrogen Production Amount (mmol g^{-1} h^{-1})	% Quantum Efficiencies	References
CdS/ZnS	10	300 W xenon lamp	24.1	9.3	36
CdS/ZnS	10	300-W Xe lamp	14.0	2.76	37
ZnO/ZnS/MoS2	-	100 W Xe lamp	10.4	25.4	38

2.3.3. Cadmium Zinc Sulfide ($Cd_XZn_{1-x}S$)

Based on the studies conducted on the CdZnS structure, it can be said that it is not a physical mixture like CdS/ZnS, but rather a type of solid solution. Due to this feature, it has better properties than CdS, ZnS and CdS/ZnS structures and shows a better photocatalytic activity due to the adjustable band gap [39]. However, the photocatalytic H_2 production effect on uncoated CdS is negligible, owing to the rapid recombination of photogenerated electrons and holes, the rapid reverse reaction between hydrogen and oxygen, and the significant H_2 production overpotential. It may be argued that ternary metal sulfides produce substantially superior outcomes in terms of band gap suited for hydrogen production. In comparison to $Cd_xZn_{1-x}S$ photocatalysts, ternary metal sulfide catalysts produce more hydrogen from water, are more stable, efficient, and have a better form structure. Its characteristics have made it famous in studies nowadays. Changing the x value can improve photocatalytic activity and yield the best band structure for photocatalytic H_2 generation [40][41]. $Cd_xZn_{1-x}S$ has a favorable band gap that varies with composition, allowing to produce H_2 when exposed to visible light. $Cd_xZn_{1-x}S$ are promising materials for short-wavelength laser diodes and high-density optical recording [42]. Different methods are utilized to synthesize $Cd_xZn_{1-x}S$ catalysts. The sol-gel procedure is the most extensively utilized method for producing semiconductor photocatalysts. The main advantage of the sol-gel process is the uniform mixing of metal ions at the molecular level, which promotes the production of polycrystalline particles with unique characteristics. The hydrothermal synthesis procedure is often carried out in steel pressure containers (autoclaves) at controlled temperatures and/or pressures using aqueous solutions. Temperatures can climb above the boiling point of water, resulting in vapor saturation pressure. The solvent amount and reaction temperature of solution introduced to the autoclave have a significant impact on the internal pressure generated. The solvothermal method is a variation on the hydrothermal technique in which the solvent is anhydrous. Because of the wide range of organic solvents with high boiling points available, the reaction temperature can be raised far higher than in the hydrothermal approach. In general, the solvothermal technique has been shown to be more effective in controlling semiconductor particle size, shape, distribution, and crystallinity than the hydrothermal method. Compared to the hydrothermal technique, the solvothermal method allows for better control over photocatalyst parameters such as

particle shape and size, crystallization, dispersion, and particle agglomeration behavior. Another crucial consideration in the solvothermal process is the solvent used. The role of the solvent is particularly crucial in this process, as varied physicochemical parameters of the solvent influence [43].

2.3.3.1. Parameters Affecting the $Cd_XZn_{1-x}S$ Catalyst

The parameters affecting the synthesized catalyst can generally be listed as follows: Change in cadmium and zinc ratio, autoclave synthesis temperature and parameters, changes in the morphological structure in different sizes and shapes due to the solvent used [44]. These affecting parameters are explained with examples from studies conducted over the years.

The band gap position in the $Cd_xZn_{1-x}S$ photocatalyst varies as the Cd/Zn ratio changes. The band gap narrows as the cadmium content increases and increases as the cadmium content declines. As the Zn content in the $Cd_xZn_{1-x}S$ photocatalyst grows, the edge potential of the conduction band decreases, increasing the band gap, which is undesirable for photocatalysis. The efficiency of H_2 generation under visible light can be enhanced by selecting a suitable band gap width and conduction band. Studies conducted with $Cd_xZn_{1-x}S$ photocatalyst in the literature have revealed that photocatalysts with high Cd content show the highest efficiency because of their low band gap [45][46][47].

Wang et al. (2011) used the solvothermal method to synthesize the $Cd_xZn_{1-x}S$ photocatalyst with various x ratios as nanorods and investigated its effectiveness in producing hydrogen from water. The study found that as the Cd/Zn ratio changes, the morphological structure changes, which affects the performance of the catalyst. Figure 2.3. shows the morphological structure change as Cd/Zn levels change. As the amount of Zn^{2+} increased, the length of the nanorods decreased, and their shape changed from rod-like to plate-like. The Zn^{2+} content in the precursor solutions was increased to 0.7 and 0.8 (x value) to produce nanoplates and microspheres composed entirely of small particles. As a result, hydrogen production efficiency remained poor even at high cadmium rates. The $Cd_{0.5}Zn_{0.5}S$ photocatalyst performed the best, with a quantum efficiency of 30.4% and hydrogen production of 10.97 mmol g^{-1} h^{-1}. The material's exceptional efficiency can be attributed to its fabrication into nanorods. As a result, it has been demonstrated that the morphological structure and nanoforms of the catalyst have a direct impact on its

activity. In this study, the change in the morphological structure of the $Cd_{0.5}Zn_{0.5}S$ photocatalyst by changing the autoclave solvothermal synthesis temperature is shown. Figure 2.4. shows the change in morphological structure according to the changing solvothermal synthesis temperature. In Figure 2.4c, only all of them were found to be nanorods in the 12 h synthesis. It was shown that 2 or 6 hours was not sufficient, and in the 24 h synthesis period, the nanorod form shifted towards nanoparticles [48].

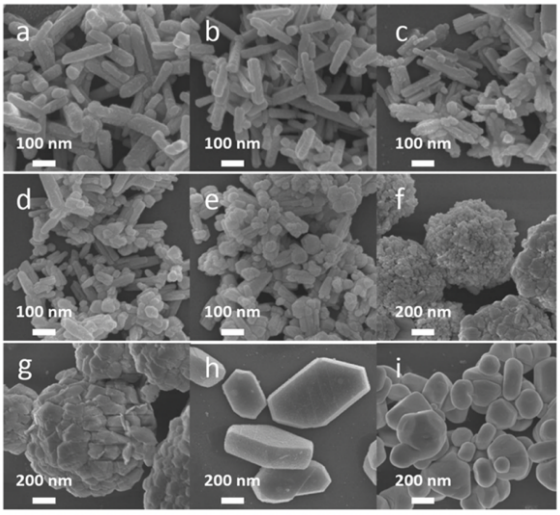

Figure 2.3 FESEM images of $Cd_xZn_{1-x}S$ generated using the solvothermal method at 180 °C for 24 hours [48].

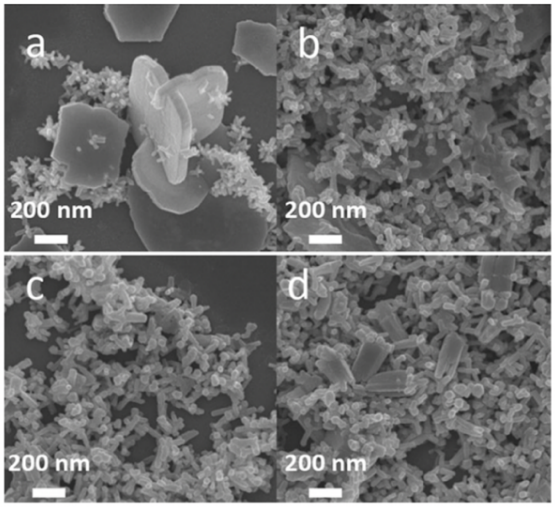

Figure 2.4 FESEM images of $Cd_{0.5}Zn_{0.5}S$ sample synthesized with different reaction times, hours increasing in order from a to b (2 hours, 6 hours, 12 hours, and 48 hours) [48].

Li et al. (2013) observed the Cd/Zn ratio of the band gap. Figure 2.5. shows the variation of the band gap according to the Cd/Zn ratio. The causes of visible light absorption and photoactive enhancement for the $Cd_xZn_{1-x}S$ solid solution were investigated and discussed by observing the changes in the energy distributions, charge distributions, and energies of the band particles. It has been demonstrated that the band gap decreases as the cadmium level increases [49].

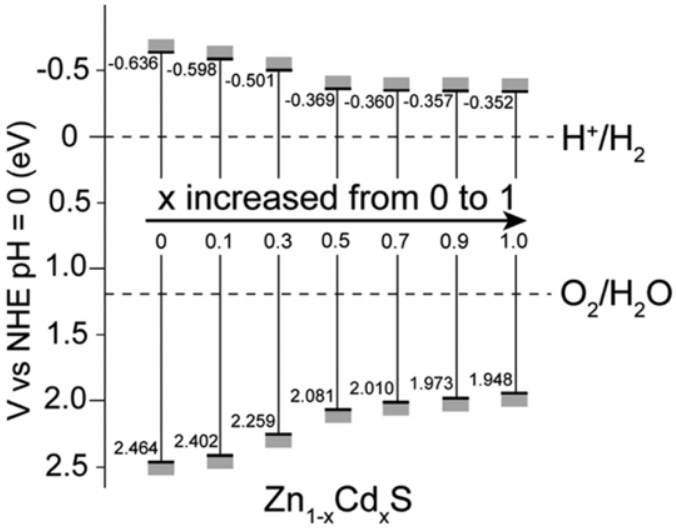

Figure 2.5 Change in conduction and valence band potentials of $Cd_xZn_{1-x}S$ (x = 0, 0.1, 0.3, 0.5, 0.7, and 1.0) photocatalyst with Cd/Zn ratio [49].

Wang et al. (2013) investigated the fabrication of $Cd_xZn_{1-x}S$ complex structures, such as micro flowers and microspheres, utilizing diethylenetriamine (DETA) and water solvents. The morphology of the $Cd_xZn_{1-x}S$ solid solution changed from micro flowers to microspheres as the Zn concentration increased. The photocatalytic reaction of H2 over solid solutions is further studied, with the highest H2 evolution rates achieved without co-catalysts at 1.8 mmol g^{-1} h^{-1}. The morphological shift caused varied BET and surface flaws, which resulted in varying photocatalytic activity. The $Cd_{0.2}Zn_{0.8}S$ microspheres demonstrated the highest photocatalytic capacity, producing about 1.8 mmol g^{-1} h^{-1}. After adding 1 wt% Pt to the surface of $Cd_{0.2}Zn_{0.8}S$, the speed of H_2 generation increased to 5 mmol g^{-1} h^{-1}.

Figure 2.6A displays SEM pictures of produced $Cd_xZn_{1-x}S$ samples. ZnS nanocrystals in form of pure are composed like microspheres coated with short nanorods. The

photocatalytic activity of $Cd_xZn_{1-x}S$ solid solution in H_2 generation was studied in a system containing 0.1 M Na_2S and aqueous Na_2SO_3. All $Cd_xZn_{1-x}S$ photocatalysts display greater activity than ZnS and CdS, implying that the formation and structure of the solid solution are important for hydrogen production (Figure 2.6Ba). Noble metals including Pt, Pd, and Rh were investigated as co-catalysts for increasing photocatalytic activity. Pt had the strongest positive effect on CdS photocatalytic activity. Adding Pt to $Cd_xZn_{1-x}S$ photocatalysts increases photocatalytic activity by up to 5 mmol g-1 h-1, which is nearly 1.8 times greater than the bare $Cd_xZn_{1-x}S$ solid solution catalyst (Figure 2.6Bb) [50].

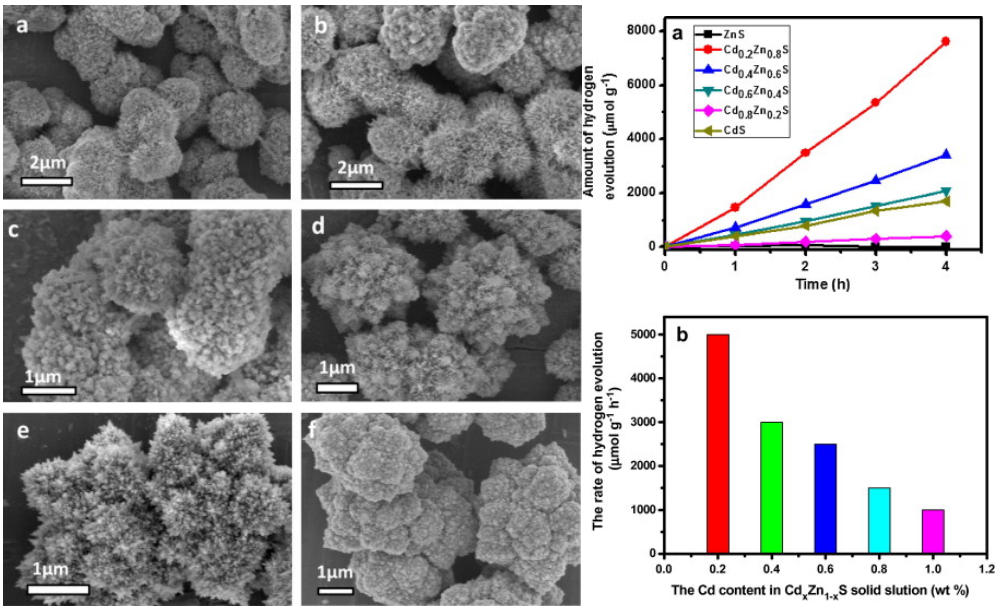

(A) (B)

Figure 2.6 (A) SEM images of $Cd_xZn_{1-x}S$ nanocrystals with changing of x values (x: 0, 0.2, 0.4, 0.6, 0.8, and 1); (B) (a) Hydrogen production of varying solid solution of $Cd_xZn_{1-x}S$ photocatalysts in using Na_2SO_3/Na_2S aqueous solutions. (b) H_2 evolution of $Cd_xZn_{1-x}S$ loading with using co-catalyst of Pt adding like 1 wt.% in Na_2SO_3/Na_2S aqueous solution [50].

Another parameter that affects photocatalytic activity is the morphological structure of the catalyst. Nanorod structures provide an increase in H_2 production capacity through water dissociation, where the long axis can offer a unidirectional light-excited electron-hole pair flow and a short transfer distance at the surface. The light absorption and

scattering properties of nanorod structures are generally open to improvement due to their high surface to volume ratios. It increases the activity in the fast and long-term load carrying ability of nanorod structures. With the richness of sulfur vacancies in the CdZnS nanorod photocatalyst, it greatly limits charge recombination thanks to electron capture sites [51]. In their study, Yu et al. (2020) synthesized the $Cd_xZn_{1-x}S$ catalyst in the form of a nanorod, examined the effectiveness of the catalyst, and found that the catalyst that produced the best hydrogen production was $Cd_{0.6}Zn_{0.4}S$ and produced 59.3 mmol h^{-1} g^{-1} H_2. The $Cd_xZn_{1-x}S$ catalyst synthesized in the form of nanorods was compared with CdS and ZnS and it was observed that it produced approximately 30 times more H_2 than pure CdS. Moreover, in the same study, the H_2 production results of the CdZnS photocatalyst synthesized as a nanorod could only be achieved by adding 1% Pt co-catalyst onto the CdS photocatalyst. This result shows that the CdZnS photocatalyst synthesized in a nanorod morphological structure provides high activity without using expensive co-catalysts such as Pt. It can be said that nanorod structures increase hydrogen production efficiency.

Wang et al. (2011) described a simple solvothermal approach (Using ethylenediamine (EDA) to CdS and ZnS in the form of a solid solution). The as-prepared affordable photocatalysts exhibit significantly greater hydrogen production activities than previously reported in the absence of additives and cocatalysts. $Cd_xZn_{1-x}S$ solid solution photocatalysts were successfully synthesized utilizing a simple solvothermal technique with EDA for the solvent and thioacetamide (TAA) for the sulfur source. According to the findings, due to EDA's different coordinating abilities with Cd^{2+} and Zn^{2+} ions, as well as its promoting effects on the development of ZnS and CdS, there is an evident morphological progression of the shape of metal complex microplates, leading to nanorods and nanoparticles. The $Cd_{1-x}Zn_xS$ catalysts were discovered to be homogeneous solid solutions containing $0.3 \leq x \leq 0.5$ in the precursor solution. Excellent photocatalytic activity was achieved without the use of pricey metal components or co-catalysts. It was discovered to be $Zn_{0.5}Cd_{0.5}S$, with a hydrogen generation rate of 1097 mmol h^{-1} ($\lambda \geq 420$ nm). AQE is almost 30.4% at 420 nm [48]. Table 2.3. shows the results of CDS catalysts used in bare form after research in the literature.

Table 2.3 Hydrogen production and efficiency values of different bare $Cd_xZn_{1-x}S$ samples.

Catalyst Type	Catalyst Amount (mg)	Light Intensity (W/m^2)	Hydrogen Production Amount (mmol g^{-1} h^{-1})	% Quantum Efficiencies	References
$Cd_{0.19}Zn_{0.81}S$	5	300 W Xe lamp	7.7	-	52
$Cd_{0.36}Zn_{0.64}S$	50	300 W Xe lamp	0.8	-	53
$Cd_{0.5}Zn_{0.5}S$	100	300 W Xe lamp	11.0	30.4	48
$Cd_{0.6}Zn_{0.4}S$	5	300 W Xe-arc lamp	42.7	17.6	7
$Cd_{0.6}Zn_{0.4}S$	-	300 W Xe lamp	59.3	-	51
$Cd_{0.5}Zn_{0.5}S$	50	1800 W/m^2	7.4	9.6	54
$Cd_{0.8}Zn_{0.2}S$	200	350 W Xe lamp	0.9	10.3	55

2.4. The Effect of Adding Co-catalysts.

Co-catalysts are added to the catalyst to improve hydrogen production efficiency and productivity. Co-catalysts are frequently used to address these issues, and their functional variety can effectively enhance the improvement of catalytic activity [56]. Metals like Ag, Pt, Ru, Pd, and Au are employed as both photocatalysts and cocatalysts because they have many active sites appropriate for photocatalytic reactions. Pt, as the most widely used co-catalyst, has the highest work function, which means it has the greatest ability to capture electrons from the semiconductor's conduction band and efficiently separate electron-hole pairs, resulting in many active sites for hydrogen evolution [57]. Platinum

is widely used as a photocatalyst for hydrogen evolution reaction (HER) from water, but its rarity and high cost limit its widespread use, necessitating the development of non-noble metal alternatives [58]. Gold, like Pt, is an expensive co-catalyst. Due to the high cost and limited features of these co-catalysts, research is being conducted on co-catalysts capable of replacing precious metals [59]. Studies are exploring the use of noble metal-free materials as co-catalysts for higher hydrogen production at an economic level. Metal chalcogenides are seen as a promising choice due to their unique electrical and optical properties, low cost, and abundant presence in the earth's crust [60]. Molybdenum disulfide (MoS_2), with a layered crystal structure, is considered an alternative for Pt [59].

2.4.1. Molybdenum disulfide (MoS_2)

MoS_2, one of the co-catalysts, is used as an additive to semiconductor photocatalysts due to its wide contact interface, inhibition of charge recombination, low cost, high reactivity for H_2 evaluation reaction, and enhancement of visible light response [47][61][62]. There are few studies in the literature on adding co-catalysts to the $Cd_xZn_{1-x}S$ catalyst. Zhao et al., (2016) synthesized $Cd_{0.5}Zn_{0.5}S/MoS_2$ photocatalyst by hydrothermal coprecipitation method and proposed photocatalyst catalyst showed higher activity and stability with 12.30 mmol g^{-1} h^{-1} hydrogen under visible light irradiation. Figure 2.7. illustrates the VB and CB edge potentials for MoS_2 and $Cd_{0.5}Zn_{0.5}S$ solution. A putative mechanism for increased H_2 production in $Cd_{0.5}Zn_{0.5}S/MoS_2$ photocatalysts is postulated. Once the $Cd_{0.5}Zn_{0.5}S/MoS_2$ photocatalyst is exposed to visible light, photogenerated electrons move from the $Cd_{0.5}Zn_{0.5}S$ solid solution to MoS_2, where they are converted into H_2, while holes oxidize the sacrificial material. As a result, the co-catalyst MoS_2 expedited the separation of pairs of electrons and holes, which is crucial for the photocatalytic reaction, while limiting their combination, resulting in considerable H_2 production for the $Cd_{0.5}Zn_{0.5}S/MoS_2$. However, when excess MoS_2 is added, the bulk of the $Cd_{0.5}Zn_{0.5}S$ surface may be coated by MoS_2 nanosheets, decreasing electron-hole pair formation, or the excess MoS_2 nanosheets may act as a photogenerated recombination center, leading in low photoactivity. As a result, it has been claimed that adding large amounts of co-catalyst has no positive effect on activity levels [45].

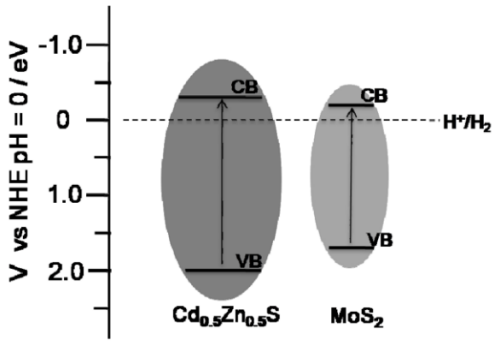

Figure 2.7 A schematic illustration of the potential and band locations of $Cd_{0.5}Zn_{0.5}S/MoS_2$ [45].

Wang et al., (2023) synthesized plate-on-plate structured 0.8% MoS_2-$Cd_{0.6}Zn_{0.4}S$ photocatalyst, which showed excellent photocatalytic hydrogen production (13.5 mmol g^{-1} h^{-1}), through an easy electrostatic self-assembly strategy, and the amount of hydrogen production increased by 1.3 times with the addition of MoS_2 compared to pure $Cd_xZn_{1-x}S$. Thus, $Cd_xZn_{1-x}S/MoS_2$ is a promising noble-metal free binary photocatalyst for hydrogen production and its structural effects on reaction yield is worth investigating [46]. $Cd_xZn_{1-x}S$ decorated with Au nanoparticles made by Chen et al., (2020) was assembled and synthesized. With pure $Cd_{0.5}Zn_{0.5}S$ containing 57.0 mmol g^{-1} h^{-1} H_2 with Au added, this production increased to 96.0 mmol g^{-1} h^{-1}. However, gold is also an expensive auxiliary. Thanks to the high cost and scope of these auxiliaries, auxiliary units that can replace precious metals will bring innovation [63].

Hinnemann et al. (2005) discovered that MoS_2 improved the activity of the hydrogen generation process, indicating that it was a suitable low-cost alternative co-catalyst to platinum [64]. Many investigations have demonstrated that MoS_2 may be used as a co-catalyst instead of Pt for various semiconductor photocatalysts (TiO_2, ZnS, CdS, $ZnIn_2S_4$, and CdZnS) [65] [1] [45]. Wei et al. (2014) produced the $MoS_2/ZnIn_2S_4$ nanocomposite and discovered that MoS_2 considerably improved hydrogen generation. As a key outcome, Pt and MoS_2 were evaluated as co-catalysts, and it was discovered that MoS_2 performed better under the identical circumstances [1]. MoS_2 has excellent electrical, optical, and catalytic capabilities, and its application with semiconductor catalysts improves H_2 generation efficiency [66]. Its structure has strong intralayer covalent connections separated by a small van der Waals gap, which is critical for catalysis [67].

Zhao et al., (2016) showed that the efficiency was increased by adding MoS_2 and found 12.3 mmol·$g^{-1}h^{-1}$ H_2 production with the $MoS_2/Cd_{0.5}Zn_{0.5}S$ photocatalyst. The reason for this is the photocatalyst with the structure $MoS_2/Cd_{0.5}Zn_{0.5}S$; Photon-generated electrons are transferred from the conduction band of the $Cd_{0.5}Zn_{0.5}S$ photocatalyst to the conduction band of MoS_2 to produce H_2, and the photon-generated holes oxidize the sacrificial agents [45]. Wang et al., (2023) used 0.8% $MoS_2/Cd_{0.6}Zn_{0.4}S$ catalyst and the best result was found to be 13.5 mmol $g^{-1}h^{-1}$. The amount of MoS_2 co-catalyst in the photocatalyst has been determined as a factor affecting H_2 production [46]. Furthermore, MoS_2 is regarded a Pt alternative since it is synthesized in sheet form (2D), like the structure of graphene [68]. These 2D ultra-intense MoS_2 nanotubes have higher catalytic activity and higher electron mobility than bulk MoS_2. According to Saadati et al. (2021), ultra-intense MoS_2 nanolayers have significant catalytic activity, which leads to the creation of active edge zones [69]. MoS_2-based photocatalysts have demonstrated better shape, crystal structure, electrical characteristics, and durability [70]. When bulk MoS_2 is synthesized in 2D and the number of nanolayers is adjusted, it transitions from an indirect band gap semiconductor to a direct band gap semiconductor. The band gap value theoretically changes from 1.3 eV to 1.8 eV when bulk MoS_2 is converted to monolayer MoS_2 [2]. Based on these collected literature investigations, it was established that generating MoS_2 nanosheet is more favorable.

In their research, Li et al. (2021) developed a 2D/2D $MoS_2/Cd_{0.5}Zn_{0.5}S$ catalyst, with the greatest hydrogen generation of 15.9 mmol $g^{-1}h^{-1}$ for 4.3% MoS_2 [71]. Yin et al. (2016) manufactured the MoS_2 co-catalyst as a nanosheet on the CdS nanorod photocatalyst and measured hydrogen generation at 49.8 mmol. $g^{-1}h^{-1}$. In this work, the hydrothermal technique was also employed; the autoclave was held at 220°C for 24 hours [61] [71] [72]. The catalyst's structure may be differentiated by modifying synthesis parameters such as reaction duration, temperature, and the kind and concentration of starting materials. All these characteristics influence the morphology, porosity, and particle size properties of the photocatalyst. Temperature during hydrothermal/solvothermal synthesis is another crucial element in catalyst production. To synthesize MoS_2 nanolayers, a temperature of 220 ºC was used for 24 hours [46]. Studies conducted with $Cd_xZn_{1-x}S/MoS_2$ are summarized in Table 2.4.

Table 2.4 Hydrogen production and efficiency values of different bare $Cd_xZn_{1-x}S/MoS_2$ samples.

Catalyst Type	Catalyst Amount (mg)	Light Intensity (W/m^2)	Hydrogen Production Amount ($mmol\ g^{-1}\ h^{-1}$)	% Quantum Efficiencies	References
$Cd_{0.5}Zn_{0.5}S$ / MoS_2	4	300 W Xe lamp	15.9	-	61
$Cd_{0.6}Zn_{0.4}S$ / MoS_2	30	300 W Xe lamp	13.5	21.81	46
$Cd_{0.5}Zn_{0.5}S$ / MoS_2	60	320 W/ m^2	12.3	31.69	45
$Cd_{0.5}Zn_{0.5}S$ / MoS_2	10	300 W Xe lamp	37.2	36.3	71
$Cd_{0.5}Zn_{0.5}S$ / MoS_2	-	300 W Xe lamp	96.0	-	63

2.4.1. Molybdenum carbides (MoC -Mo_2C)

Molybdenum carbides (MoC, Mo_2C) are a potential HER catalyst due to their d-band electronic structure, like platinum. However, their HER catalytic activities were not as well-performed as predicted compared to platinum. Elemental doping or material hybridization can increase their catalytic activity by modifying band topologies. A MoC-Mo_2C composite powder catalyst has shown increased electrocatalytic activity, but the fundamental process is uncertain. The catalyst also runs at a low current density for less than 30 hours at room temperature [73]. However, strong Mo-H bonds cause poor hydrogen desorption, resulting in a slow H_2 evolution rate. As a result, it is critical to study innovative ways for tuning the electron structure of Mo_2C to fast release hydrogen and increase hydrogen production rate [74].

In the literature, electrochemical experiments were often performed with MoC or Mo_2C. Wei et al. (2022) produced carbon-modified phase MoC-Mo_2C or MoC-Mo_2C@C, MMC nanosheets on a nanorod-sized $Cd_{0.5}Zn_{0.5}S$ catalyst. The inclusion of MMC considerably boosted the rate of hydrogen generation compared to the pure $Cd_{0.5}Zn_{0.5}S$ catalyst. While

the pure form generates 8.9 mmol g^{-1} h^{-1} of hydrogen, adding 1% by weight MMC increases the rate to 68.8 mmol g^{-1} h^{-1}. This work demonstrated that the MoC-Mo_2C structure may be employed for photocatalytic hydrogen generation. The quantum efficiency of 1-MMC/ZCS photocatalyst was tested using Na_2S/Na_2SO_3 as a hole sacrificial reagent and 420 nm monochromatic light, and it was 32.9% [75]. Construction of core-shell type nanostructures via linking the abundant hydrogen production catalyst Mo_2C to the excellent photo absorber CdS may be the ideal combination for photocatalytic hydrogen generation. Thus, for the first time, core-shell nanorods made of a CdS core and a Mo_2C-C shell were developed and produced by Yi et al. (2017). The generated CdS@Mo_2C-C nanorods had a higher hydrogen production rate of 17.24 mmol. g^{-1} h^{-1} than pure CdS. This could be attributed to the unique a one-dimensional nanostructure with extensive interaction among the core and shell materials, as well as an expanded visible light absorption range [76].

In this study, its activity in hydrogen production was examined by working with two different solvents (1,3-Diaminopropane (DAP) and Ethylenediamine (EDA)). Firstly, $Cd_XZn_{1-X}S$ was synthesized using DAP at different x ratios (0.7/0.3 and 0.3/0.7) and MoS_2 was added at different mass ratios (1% and 5%). The trials of the planned catalyst were designed with an experimental design, and the impact of three distinct parameters on the generation of hydrogen were investigated (catalyst amount (mg), x ratios and MoS_2%). The experimental design was made using MINITAB program and the experimental results were interpreted statistically. Another catalysts design was made using EDA. $Cd_{0.7}Zn_{0.3}S$ catalyst was synthesized at different EDA/water ratios and the catalyst was synthesized in nanorod structure. MoS_2 was added at different mass percentages (1%, 3%, 5%, 7%, 10%, and 15%) and its effect on activity was examined. In the last part of the study, MoC-Mo_2C was synthesized for the first time in the literature on the $Cd_{0.7}Zn_{0.3}S$/1% MoS_2/MoC-Mo_2C catalyst, which gave the best results, and its effect on hydrogen production was examined and interpreted by adding it in different ratios (0.5%, 1.0%, 1.5%, and 2.0%).

3. MATERIALS and METHODS

3.1. Preparation of Samples Using 1,3-Diaminopropane (DAP)

3.1.1. Materials

All the reagents were employed without additional purification. Chemicals utilized included cadmium nitrate ($Cd(NO_3)_2$•$4H_2O$, Merck), zinc acetate ($Zn(AC)_2$•$2H_2O$, Merck), thiourea (NH_2CSNH_2, Merck), sodium molybdate (Na_2MoO_4•$2H_2O$, Alfa Aesar), and 1,3-diaminopropane (1,3-DAP, TCI EUROPE NV). The materials used in Figure 3.1. are shown.

Figure 3.1 Chemicals used in the experiment.

3.1.2. Synthesis of $Cd_xZn_{1-x}S$ nanoparticles

$Cd_xZn_{1-x}S$ nanoparticles were created using a solvothermal technique [76]. $Cd(CH_3COO)_2 \cdot 2H_2O$ and $Zn(CH_3COO)_2 \cdot 2H_2O$ were dissolved (Cd/Zn = 7/3 and 3/7) in 1,3-DAP with vigorous magnetic stirring at room temperature. Then thiourea was added three times more than the total Cd and Zn mole number. After 60 minutes of stirring, the solution was transferred to a Teflon-coated stainless-steel autoclave to be kept at 180°C for 24 hours. After the autoclave was naturally cooled down, the precipitate was filtered, washed several times with water, and dried overnight at 65°C. In Figure 3.2., the synthesis procedure is visually given.

Figure 3.2 Images of (A) teflon-coated stainless-steel autoclave to be kept in the oven at 180°C for 24 hours, (B) solution obtained after autoclave, (C) filtration of the solution, (D) autoclave system used in the synthesis, and (E) obtained $Cd_xZn_{1-x}S$ catalyst.

3.1.3. Synthesis of $Cd_xZn_{1-x}S/MoS_2$

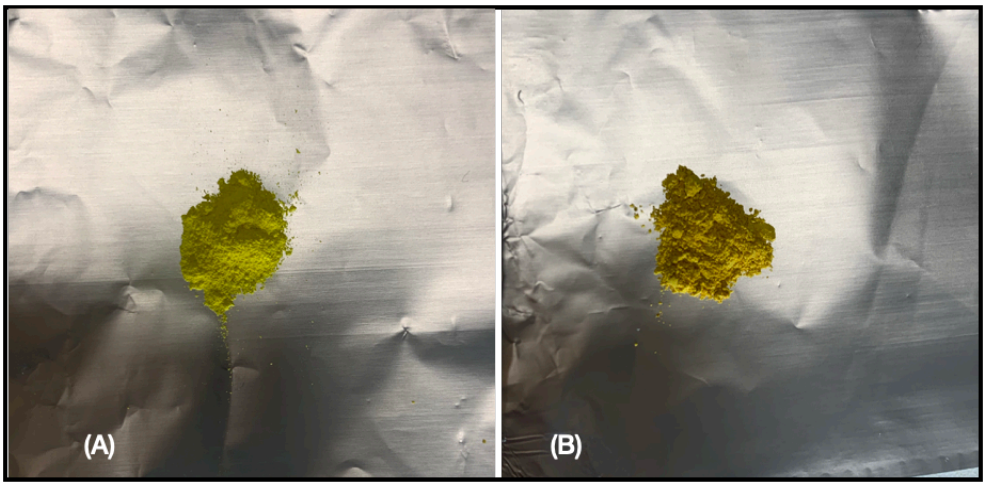

Figure 3.3 Images of (A) pure $Cd_{0.3}Zn_{0.7}S$ and (B) synthesized $Cd_{0.3}Zn_{0.7}S/5\%MoS_2$.

To create $Cd_xZn_{1-x}S$/1% MoS_2 and $Cd_xZn_{1-x}S$ /5% MoS_2 binary photocatalysts, $Cd_xZn_{1-x}S$ nanoparticles were suspended in water and $Na_2MoO_4 \cdot 2H_2O$ was added as a precursor. The MoS_2 concentration by weight was varied. Thiourea was used as a sulfurizing agent. After 60 minutes in an ultrasonic bath, the suspension was transferred to a Teflon-coated stainless-steel autoclave and stored at 180°C for 24 hours. After the autoclave had naturally cooled down, the precipitate was filtered, washed several times with water, and dried overnight at 65°C. The results are provided as the following compositions. $Cd_{0.7}Zn_{0.3}S$, $Cd_{0.3}Zn_{0.7}S$, $Cd_{0.7}Zn_{0.3}S/5\%MoS_2$, $Cd_{0.7}Zn_{0.3}S/1\%MoS_2$, $Cd_{0.3}Zn_{0.7}S/1\%MoS_2$, and $Cd_{0.3}Zn_{0.7}S/5\%MoS_2$. Figure 3.3A has pure $Cd_{0.3}Zn_{0.7}S$ and Figure 3.3B has images after the addition of MoS_2.

3.1.4. Electrochemical Measurement

For electrochemical measurements, it was mixed with DR Blade by mixing with enough sample ethylene glycol on the Ito glass. The conductivity was measured by voltmeter due to the lack of a conductor of the Ito glass, the conductivity was measured, and the conductive part was covered (Figure 3.4A-D). The first form of the coated samples is shown in Figure 3.4B. The samples were then dried at 50 °C in the magnetic active (Figure 3.4C). The visuals of all samples containing MoS_2 are shown in Figure 3.4D.

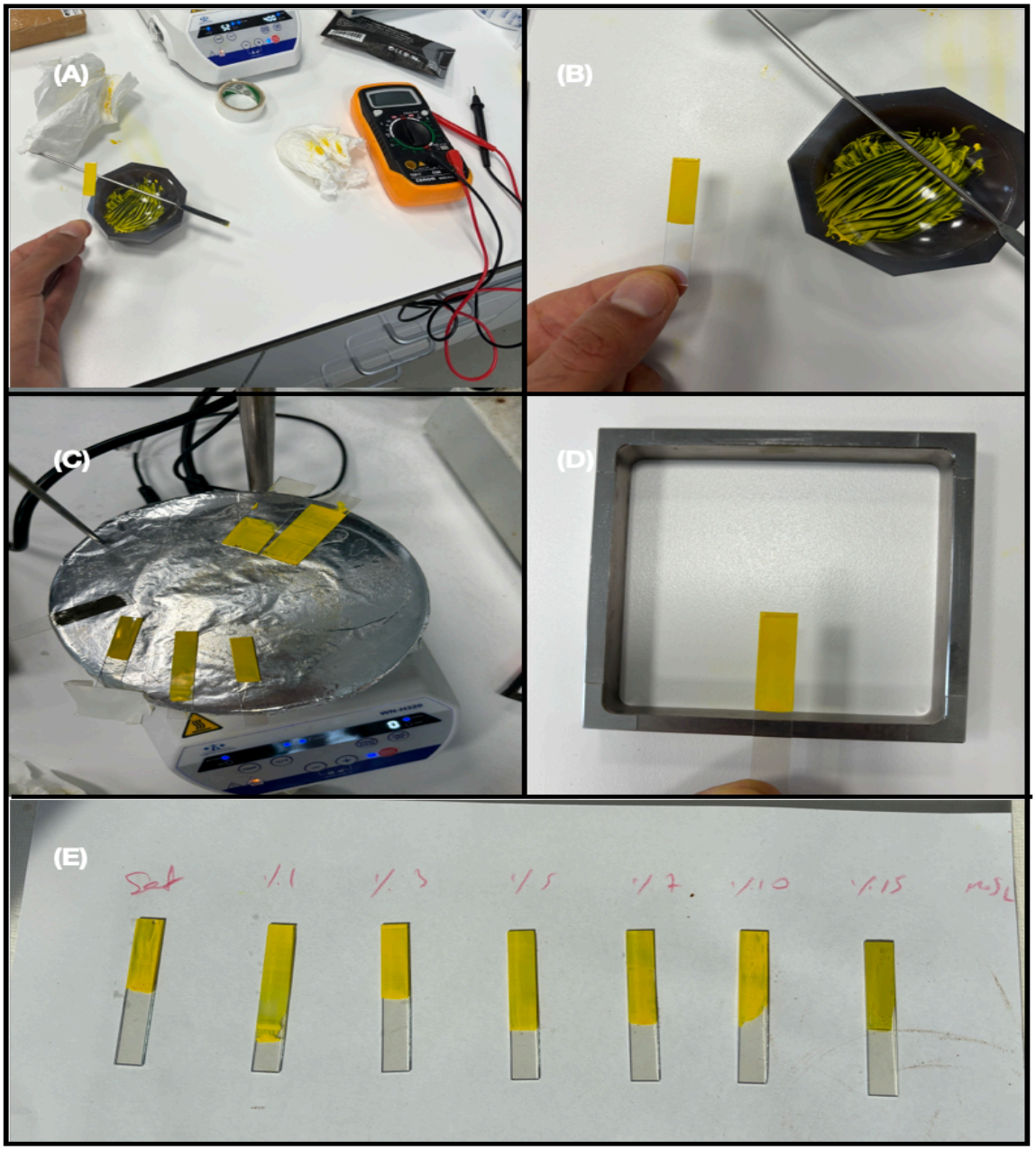

Figure 3.4 The studies of electrochemical applications.

3.2. Preparation of Samples Using Ethylenediamine (EDA)

3.2.1. Materials

All the reagents were employed without additional purification. Chemicals utilized included cadmium nitrate ($Cd(NO_3)_2$•$4H_2O$, Merck), zinc acetate ($Zn(AC)_2$•$2H_2O$, Merck), thiourea (NH_2CSNH_2, Merck), sodium molybdate (Na_2MoO_4•$2H_2O$, Merck), ethylenediamine (EDA, Sigma-Aldrich), and melamine ($C_3H_6N_6$, Merck).

3.2.2. Synthesis of $Cd_{0.7}Zn_{0.3}S$ with different ratios of EDA/water.

Nanorod $Cd_xZn_{1-x}S$ were created using a solvothermal technique with using ethylenediamine (EDA). $Cd(CH_3COO)_2 \cdot 2H_2O$ and $Zn(CH_3COO)_2 \cdot 2H_2O$ were dissolved (Cd/Zn = 7/3) in different EDA/water ratio with vigorous magnetic stirring at room temperature. Then thiourea was added three times more than the total Cd and Zn mole number. After 60 minutes of stirring, the solution was transferred to a Teflon-coated stainless-steel autoclave to be kept at 180°C for 24 hours. After the autoclave was naturally cooled down, the precipitate was filtered, washed several times with water, and dried overnight at 65°C. Figure 3.5. has a synthesis procedure scheme.

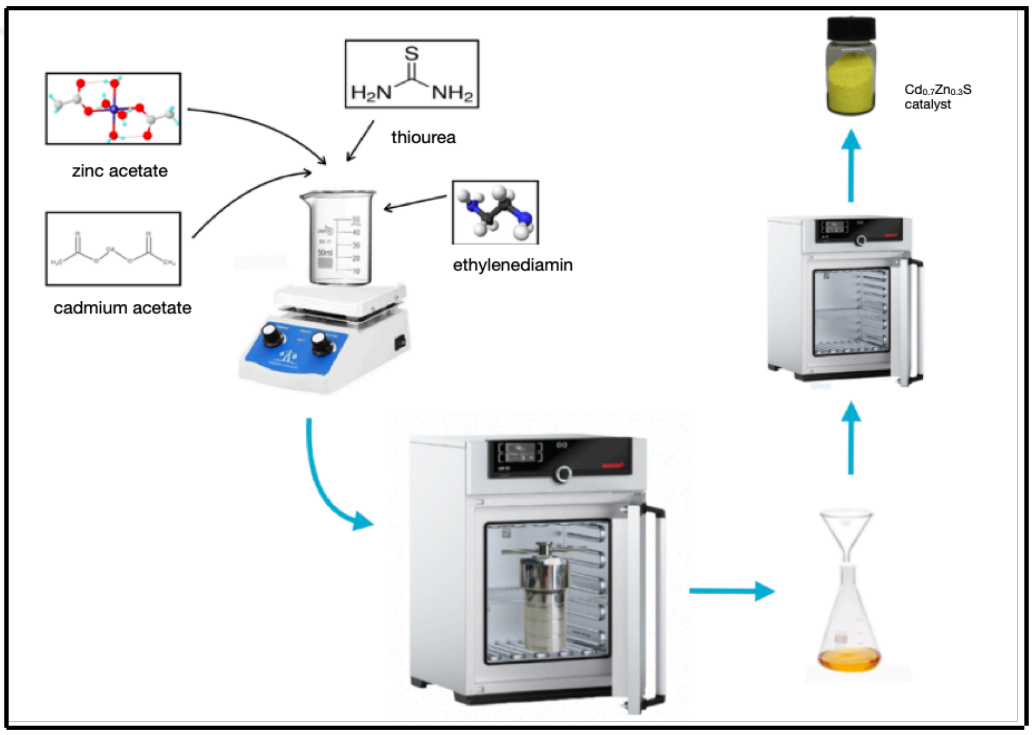

Figure 3.5 Schematic representation of the synthesis procedure of $Cd_{0.7}Zn_{0.3}S$ with different EDA/water ratios.

3.2.3. Synthesis of $Cd_{0.7}Zn_{0.3}S/MoS_2$

To create $Cd_{0.7}Zn_{0.3}S$/1% MoS_2, $Cd_{0.7}Zn_{0.3}S$/3% MoS_2, $Cd_{0.7}Zn_{0.3}S$/5% MoS_2, $Cd_{0.7}Zn_{0.3}S$/7% MoS_2, $Cd_{0.7}Zn_{0.3}S$/10% MoS_2, and $Cd_{0.7}Zn_{0.3}S$/15% MoS_2 binary photocatalysts, $Cd_{0.7}Zn_{0.3}S$ nanoparticles were suspended in water and $Na_2MoO_4 \cdot 2H_2O$ was added as a precursor. The MoS_2 concentration by weight was varied. Thiourea was used as a sulfurizing agent. After 60 minutes in an ultrasonic bath, the suspension was

transferred to a Teflon-coated stainless-steel autoclave and stored at 220°C for 24 hours. After the autoclave had naturally cooled down, the precipitate was filtered, washed several times with water, and dried overnight at 65°C. Figure 3.6. shows a schematic synthesis procedure to add MoS_2. In Figure 3.7., the visual appearance of catalysts is given.

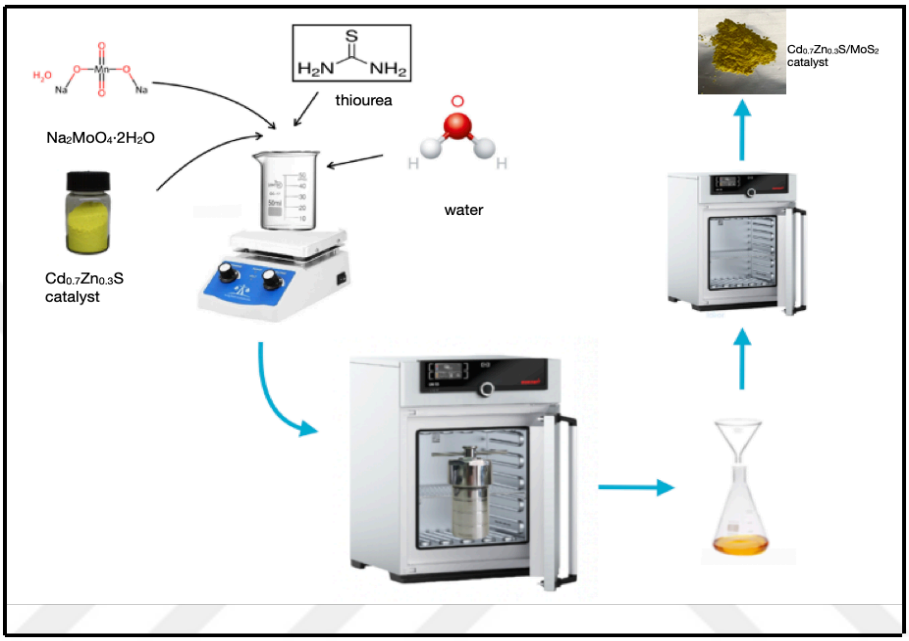

Figure 3.6 Schematic procedure of synthesis of MoS_2 on $Cd_{0.7}Zn_{0.3}S$ synthesized with hydrothermal method.

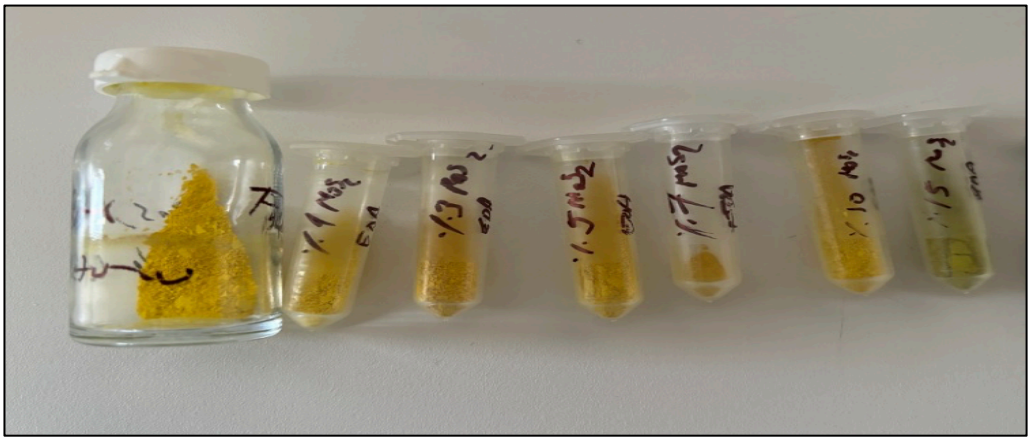

Figure 3.7 Images of $Cd_{0.7}Zn_{0.3}S/MoS_2$ catalysts synthesized with different MoS_2 ratios (MoS_2 ratio increases from left to right and MoS_2 synthesized alone is shown on the far left).

3.2.4. Synthesis of MoC-Mo_2C

MoC-Mo_2C nanoparticles were produced using a high-temperature calcination technique. To get a homogeneous solution, dissolve 1 g of sodium molybdate and 1.5 g of melamine in 80 mL of water and stir continuously in an 85 °C water bath. The solvent was evaporated until dry, and the resulting white powder was crushed and deposited in a quartz tube furnace. It was calcined at 800 °C for 2 hours under N_2 gas. The synthesized product was labeled as MoC-Mo_2C [75] (Figure 3.8.).

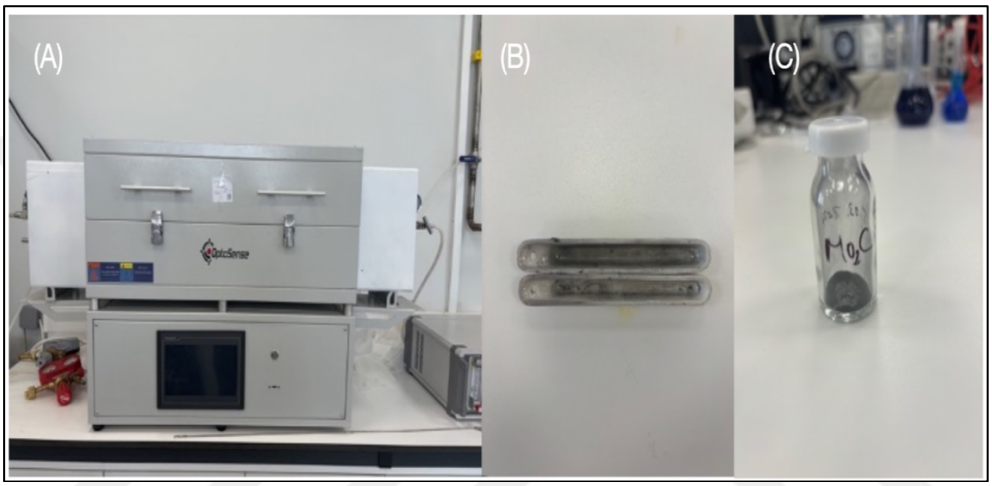

Figure 3.8 (A) Chemical vapor depositon (CVD), (B) tubes, and (C) the picture of MoC-Mo_2S.

3.2.5. Synthesis of $Cd_{0.7}Zn_{0.3}S$/1% MoS_2/MoC-Mo_2C

The synthesized MoC-Mo_2C was added to the $Cd_{0.7}Zn_{0.3}S$/1% MoS_2, the best catalyst in hydrogen production and electrochemical measurements. Figure 3.10 shows the synthesis procedure. MoC-Mo_2C has been added solidly on $Cd_{0.7}Zn_{0.3}S$/1% MoS_2 at different mass percentage rates (0.5 %, 1 %, 1.5 %, and 2 %) (Figure 3.9.). First of all, the required amount of $Cd_{0.7}Zn_{0.3}S$/1% MoS_2 and MoC-Mo_2C were weighed in the agat mortar and grinded for 1 hour. Necessary characterization and measurements were made after drying. The synthesized samples were called N-$Cd_{0.7}Zn_{0.3}S$/1% MoS_2/0.5% MoC-Mo_2C, N-$Cd_{0.7}Zn_{0.3}S$/1% MoS_2/1% MoC-Mo_2C, N-$Cd_{0.7}Zn_{0.3}S$/1% MoS_2/1.5% MoC-Mo_2C, and N-$Cd_{0.7}Zn_{0.3}S$/1% MoS_2/2% MoC-Mo_2C.

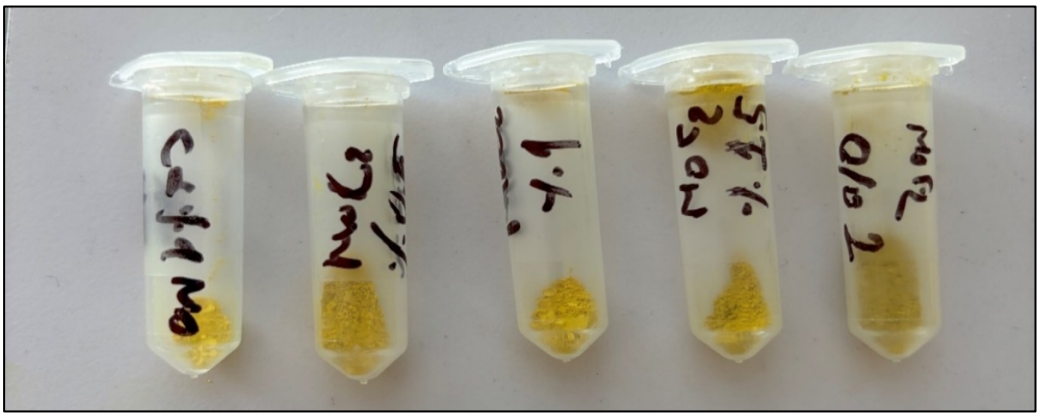

Figure 3.9 Images of catalysts after the addition of the synthesized MoC-Mo_2C.

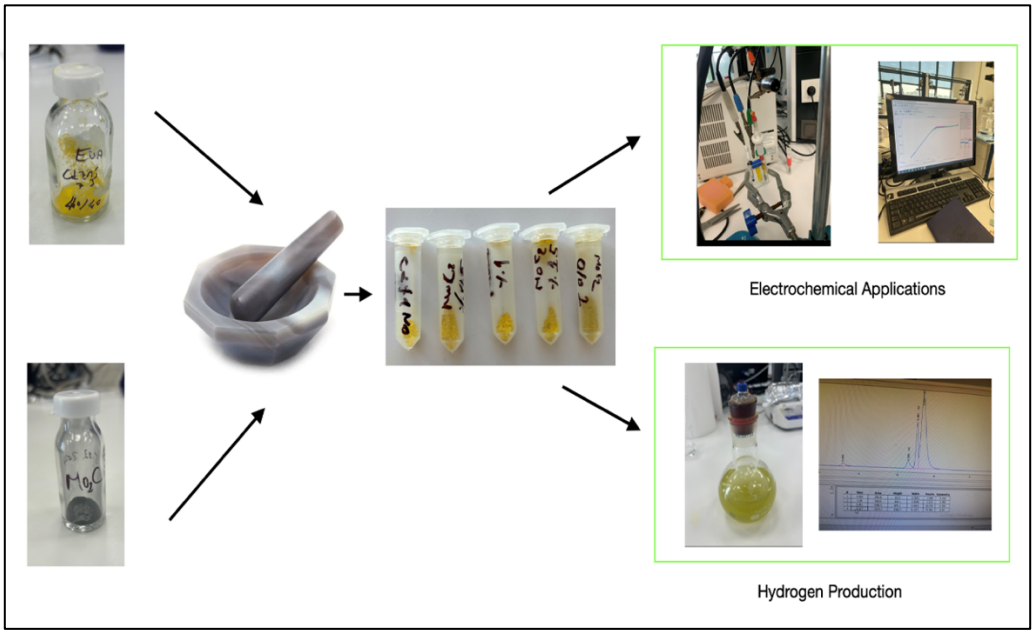

Figure 3.10 Synthesis procedure designed to add MoC-Mo_2C on $Cd_{0.7}Zn_{0.3}S$/1% MoS_2.

3.2.6. Photocatalytic Hydrogen Production

Photocatalytic hydrogen generation reactions were carried out in a 250 mL quartz reactor. In all studies, 150 ml of 0.25 M Na_2S-0.35 M Na_2SO_3 solution were utilized. The Philips 13095 halogen lamp was used to replicate sunlight, and the distance between the photocatalyst and the light source was adjusted to achieve a light intensity of 1000 W/m^2. The gas in the reactor was sampled using a gas syringe at regular intervals and examined using gas chromatography. Analysis was taken with a syringe for 5 hours and the hydrogen produced was calculated.

4. RESULTS AND DISCUSSION

4.1. Characterization Results of $Cd_xZn_{1-x}S/MoS_2$ Synthesized Using 1,3-Diaminopropane (DAP)

4.1.1. X-Ray Diffraction Analysis (XRD) Results of Samples with 1,3-Diaminopropane (DAP)

Figure 4.1. shows the XRD patterns of photocatalysts with varying Cd/Zn ratios and MoS_2 concentration. When $Cd_XZn_{1-X}S$ samples are studied, the diffraction patterns resemble hexagonal phase CdS (JCPDS card No. 41-1049) [78]. Peaks at 25.6, 27.09, 28.85, 37.72, 44.81, 48.88, and 53.11 correspond to the (100), (002), (101), (102), (110), (103), and (102) planes, respectively [26]. As the Cd/Zn ratio increased, the displacement of the peaks altered somewhat. The shift is small because the hexagonal phase of Cd is more stable than Zn.

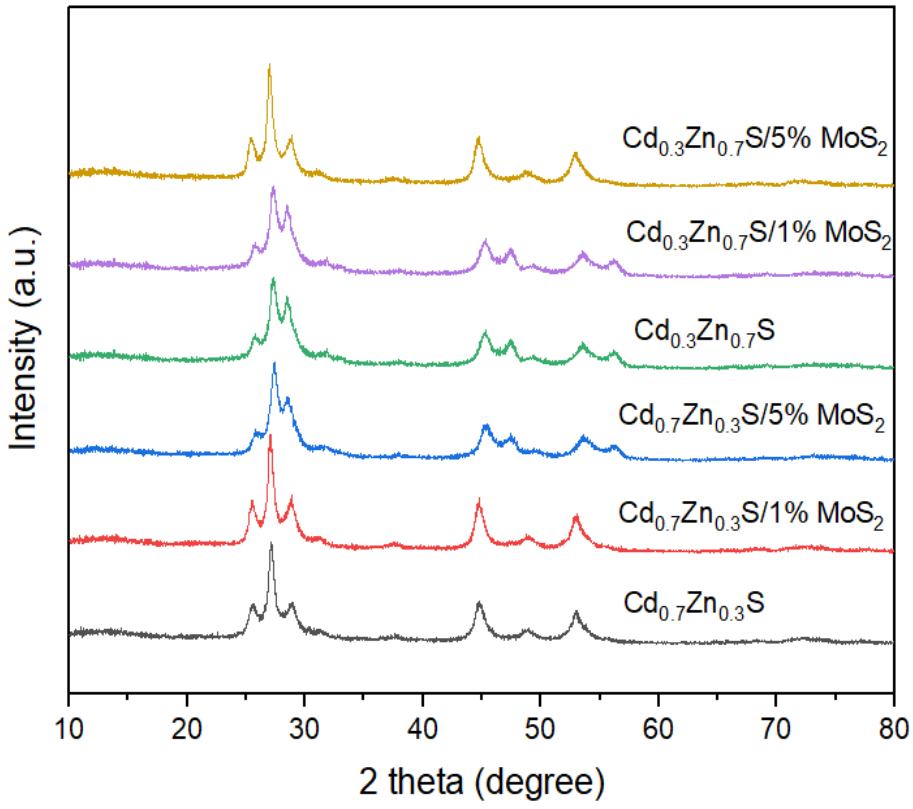

Figure 4.1 XRD patterns of $Cd_xZn_{1-x}S/MoS_2$ photocatalysts.

4.1.2. Transmission Electron Microscope (TEM) Images of Samples with 1,3-Diaminopropane (DAP)

TEM analysis was performed to evaluate the microstructure and morphology. Figures 4.2. and Figure 4.3. show the TEM images and elemental mapping of the $Cd_{0.7}Zn_{0.3}S$/1% MoS_2 photocatalyst, respectively. The photocatalyst exhibited an evenly dispersed nanocomposite form with a diameter of 15-35 nm and a length of 30-100 nm, resembling nanorods (Figure 4.2a-c). Figure 4.2d displays a HRTEM picture of the contact between $Cd_{0.7}Zn_{0.3}S$ and MoS_2. $Cd_{0.7}Zn_{0.3}S$ was detected in the (101) plane, which has a d-spacing of 0.33 nm [79], whereas MoS_2 had a d-spacing of 0.28 nm in the (002) plane [26]. The absence of noticeable peaks in the XRD examination of the $Cd_{0.7}Zn_{0.3}S$/1% MoS_2 and the absence of a defined lattice structure indicate that the MoS_2 structure is amorphous, which contributes to increased photocatalytic activity. Figure 4.3a shows a STEM image of a specific part of the $Cd_{0.7}Zn_{0.3}S$ /1%MoS_2. The photocatalyst sample's elemental mapping clearly identifies all elements, including Cd, Zn, S, and Mo, as shown in Figure 4.3b-f.

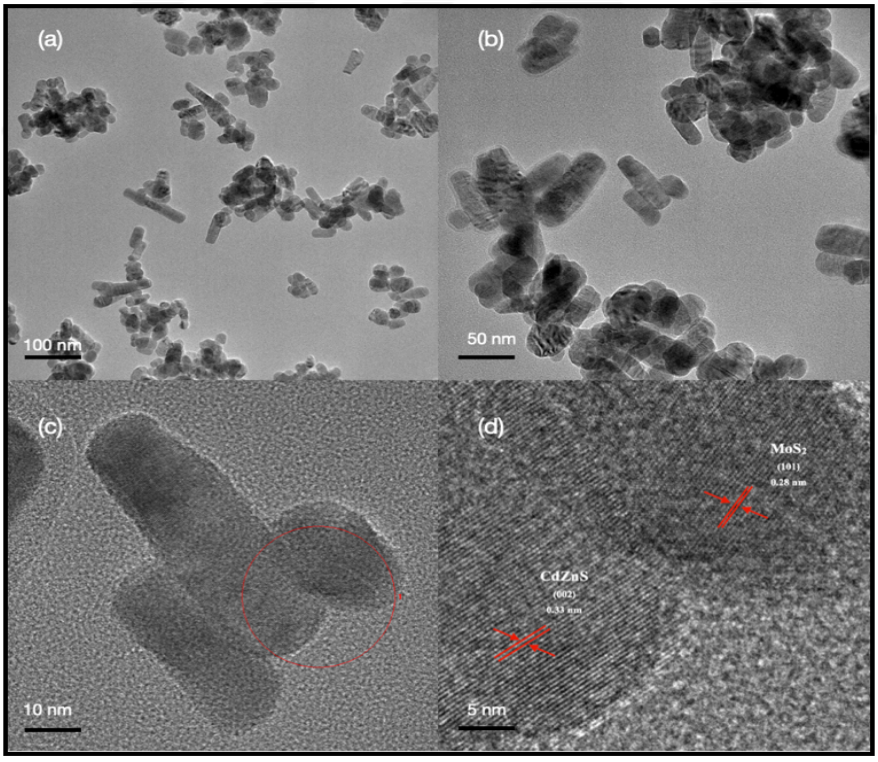

Figure 4.2 (a, b, c) TEM images of the $Cd_{0.7}Zn_{0.3}S$/1% MoS_2 nanocomposites; (d) HRTEM image of the interface between MoS_2 and $Cd_{0.7}Zn_{0.3}S$ in 5 nm.

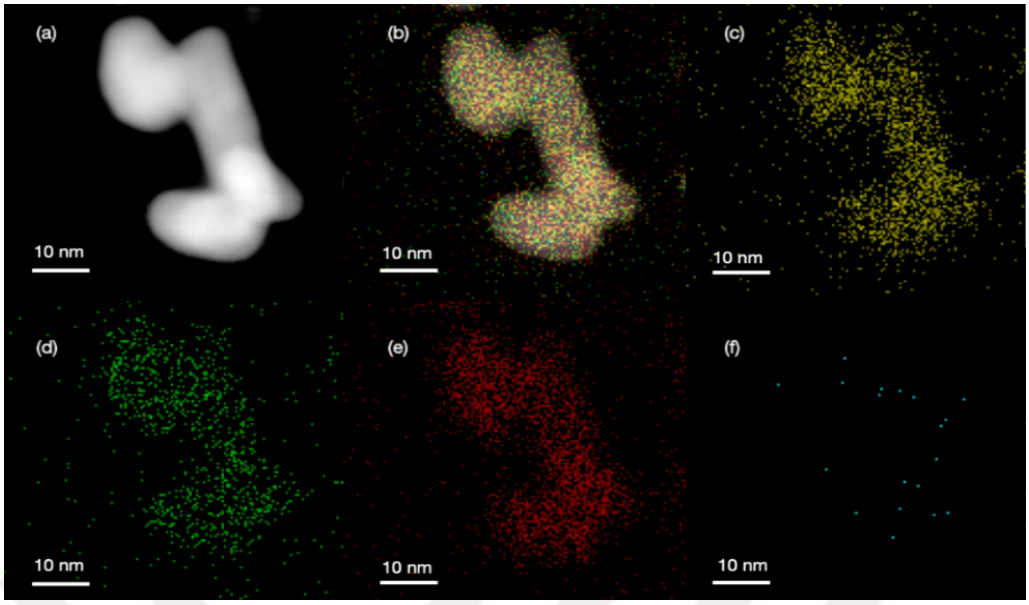

Figure 4.3 (a) STEM image of an interface; STEM image of the $Cd_{0.7}Zn_{0.3}S$/1% MoS_2 nanocomposites corresponding elemental distribution of (b) mix of elements, (c) Cd, (d) Zn, (e) S and (f) Mo.

4.1.3. Ultraviolet–Visible Diffuse Reflectance Spectroscopy (UV–Vis DRS) Results of Samples with 1,3-Diaminopropane (DAP)

Figure 4.4. shows the UV-vis absorption spectra of the photocatalysts, while table 4.1 presents the absorption wavelength edge and corresponding band gap values for each photocatalyst. Pure $Cd_{0.7}Zn_{0.3}S$ exhibited an absorption edge at approximately 528 nm, corresponding to a 2.34 eV band gap (Figure 4.4a); pure $Cd_{0.3}Zn_{0.7}S$ exhibited an absorption edge at approximately 522 nm, corresponding to a 2.37 eV band gap (Figure 4.4b). The band gap value rose due to the greater Zn ratio. Furthermore, adding MoS_2 progressively to both $Cd_{0.7}Zn_{0.3}S$ and $Cd_{0.3}Zn_{0.7}S$ resulted in a shift across the visible spectrum. The calculated direct band gaps are given in Table 4.1.

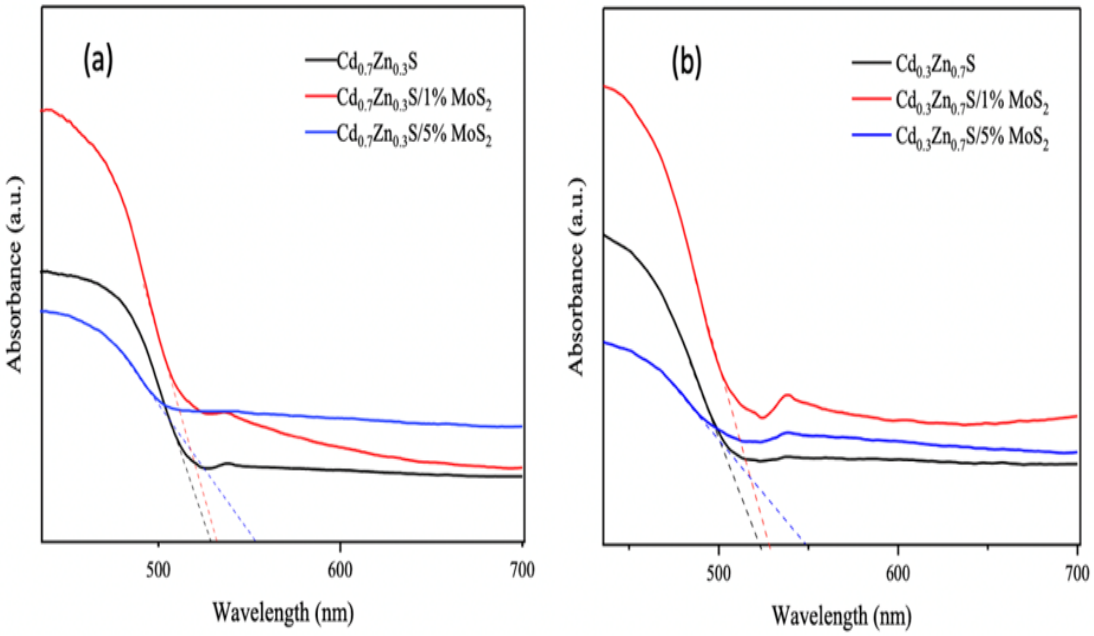

Figure 4.4 (a) UV-vis absorption spectra of $Cd_{0.7}Zn_{0.3}S$, $Cd_{0.7}Zn_{0.3}S$/1% MoS_2 and $Cd_{0.7}Zn_{0.3}S$/5% MoS_2 and (b) UV-vis absorption spectra of $Cd_{0.3}Zn_{0.7}S$, $Cd_{0.3}Zn_{0.7}S$/1% MoS_2 and $C_{0.3}Zn_{0.7}S$/5% MoS_2.

Table 4.1 UV-vis absorption wavelength edge and band gap values of photocatalysts.

Catalysts	Wavelength (nm)	Direct Band Gaps (eV)
$Cd_{0.3}Zn_{0.7}S$	522	2.37
$Cd_{0.3}Zn_{0.7}S$/1% MoS_2	527	2.35
$Cd_{0.3}Zn_{0.7}S$/5% MoS_2	549	2.26
$Cd_{0.7}Zn_{0.3}S$	528	2.34
$Cd_{0.7}Zn_{0.3}S$/1% MoS_2	533	2.32
$Cd_{0.7}Zn_{0.3}S$/5% MoS_2	555	2.23

4.2. Design of The Experiment and Interpretation of H_2 Production Results Using MINITAB

The effects of photocatalytic hydrogen production were examined using the Cd/Zn ratio (0.7/0.3 and 0.3/0.7), MoS_2 concentration (0, 1, and 5 w%), and photocatalyst loading (10, 25, and 50 mg). To investigate the impact of these parameters and their interactions, an experimental design was carried out using Minitab 19 statistical analysis software

[80][81]. Table 4.2. shows the 36 runs of the experiment and the findings required by this experimental design. The amount of hydrogen produced after 5 hours is given H_2 production rate (mmol g^{-1} h^{-1}).

Table 4.2 Experimental matrix of uncoded factors and responses.

No	Cd/Zn Ratio	MoS_2 %	Catalyst Amount (mg)	H_2 Production Rate (mmol g^{-1} h^{-1})
1	0.3/0.7	0	10	60
2	0.3/0.7	5	10	230
3	0.3/0.7	5	25	186
4	0.7/0.3	0	25	114
5	0.7/0.3	0	10	188
6	0.7/0.3	1	50	116
7	0.7/0.3	1	10	234
8	0.7/0.3	0	50	72,2
9	0.7/0.3	5	10	352
10	0.3/0.7	1	10	230
11	0.7/0.3	1	25	125
12	0.3/0.7	0	50	27
13	0.7/0.3	0	50	65
14	0.3/0.7	1	25	292
15	0.7/0.3	5	50	166
16	0.3/0.7	1	10	156
17	0.7/0.3	5	10	318
18	0.3/0.7	5	10	190
19	0.3/0.7	0	25	22
20	0.3/0.7	1	50	122
21	0.7/0.3	5	25	230
22	0.3/0.7	5	50	97
23	0.3/0.7	0	25	54
24	0.7/0.3	1	10	560

No	Cd/Zn Ratio	MoS_2 %	Catalyst Amount (mg)	H_2 Production Rate (mmol g^{-1} h^{-1})
25	0.3/0.7	0	10	77
26	0.7/0.3	0	10	177
27	0.7/0.3	1	50	43
28	0.3/0.7	5	25	168
29	0.7/0.3	0	25	140
30	0.3/0.7	1	50	45
31	0.7/0.3	5	50	155
32	0.7/0.3	5	25	151
33	0.3/0.7	5	50	122
34	0.3/0.7	0	50	19,9
35	0.3/0.7	1	25	142
36	0.7/0.3	1	25	97

The study's hydrogen production findings were expressed mathematically as Equation (4.1). The parameters affecting the design are specified in the formula as subscripts (Cd/Zn=0.7/0.3=2.33, Cd/Zn=0.3/0.7=0.42; 0, 1, and 5 are MoS_2 loading percentages; 10, 25, and 50 are the amount of catalyst used). Table 4.3. displays the linear, two-way interaction, and three-way interaction models used in the study's analysis of variance to determine the impacts of the three independent factors. P-values are used to investigate the influence of parameters on one another. Parameters with a P-value less than 0.05 have a significant influence on the study, whereas parameters with a higher P-value have a little impact [82]. The independent variables Cd/Zn ratio, catalyst amount (mg), and MoS_2 loading % had statistically significant ($P < 0.05$) influence on the dependent variable hydrogen generation. This research revealed the importance of linear and two-way interaction models. When two-way interactions are evaluated, it can be said that Cd/Zn and catalyst quantity are major independent factors influencing the analysis because of the high f value and low p value. When each parameter was studied independently, the linear results indicated that the catalyst loading quantity was the most critical parameter, however other parameters were essential in this study. The F value of the regression model created for the experimental design in ANOVA was found to be 4.36.

Responses (Hydrogen Production (mmol $g^{-1}h^{-1}$)) = 154.0 – 29.5*$Cd/Zn_{0.42}$ + 29.5*$Cd/Zn_{2.33}$ – 69.3*$MoS_{2\ 0}$ + 26.2*$MoS_{2\ 1}$ +43.1*$MoS_{2\ 5}$ + 77.0*Catalyst $Amount_{10}$ – 10.6* Catalyst $Amount_{25}$ -66.5* Catalyst $Amount_{50}$ (4.1)

Table 4.3 Analysis of variance.

Source	DF	Adj SS	Adj MS	F-Value	P-Value
Model	17	326674	19216	4.36	0.002
Linear	5	245123	49025	11.13	0.000
Cd/Zn	1	31388	31388	7.13	0.016
MoS_2	2	88176	44088	10.01	0.001
Catalyst Amount	2	125559	62780	14.25	0.000
2-Way Interactions	8	59604	7450	1.69	0.169
Cd/Zn*MoS_2	2	4029	2014	0.46	0.640
Cd/Zn*Catalyst Amount	2	36854	18427	4.18	0.032
MoS_2*Catalyst Amount	4	18721	4680	1.06	0.404
3-Way Interactions	4	21948	5487	1.25	0.327
Cd/Zn*MoS_2*Catalyst Amount	4	21948	5487	1.25	0.327
Error	18	79284	4405		
Total	35	405959			

Figure 4.5. shows the pareto chart of the hydrogen generation outcomes changing with independent parameters. After analyzing every parameter separately and through interaction in the Pareto chart, the critical t-value for the degree of freedom was determined to be 2.101 with a 95% confidence level and a 0.05 alpha value. When the parameters were examined, the amount of catalyst (mg) was found to be the most important parameter affecting it, and in decreasing order, MoS_2 loading percentage, Cd/Zn, catalyst amount (mg) with Cd/Zn etc. affects the parameters. The MoS_2 loading percentage can be useful for optimizing hydrogen generation because it significantly affects the results on itself. From the Pareto chart, the parameter that has the lowest

impact on the 2-way interaction's hydrogen production is the percentage of MoS_2 loading with Cd/Zn. Interaction graphs for the components involved in hydrogen generation are displayed in Figure 4.6. An important criterion is how the various components interact with one another to influence the optimization research on hydrogen generation. Interaction graphs can be used to examine each factor's impact. When the catalyst amount (mg) and MoS_2 loading percentage were compared, it was discovered that using catalysts of 25 and 50 mg improved the results of hydrogen production by increasing the MoS_2 loading percentage, while using catalysts of 10 mg significantly decreased the amount of hydrogen produced, from 1% to 5%. Moreover, increased hydrogen production was seen by increasing the Cd/Zn ratio and the MoS_2 loading percentage, regardless of the catalyst amount. The 10 mg sample showed a significant increase in hydrogen production when the Cd/Zn ratio was compared to the catalyst amount (mg), but not in the 25 or 50 mg tests. These data indicate that the $Cd_{0.7}Zn_{0.3}S$ catalyst will produce the greatest results in the 10 mg research; nevertheless, the interaction graph indicates that the catalyst performs better when the MoS_2 loading percentage increases to 1%.

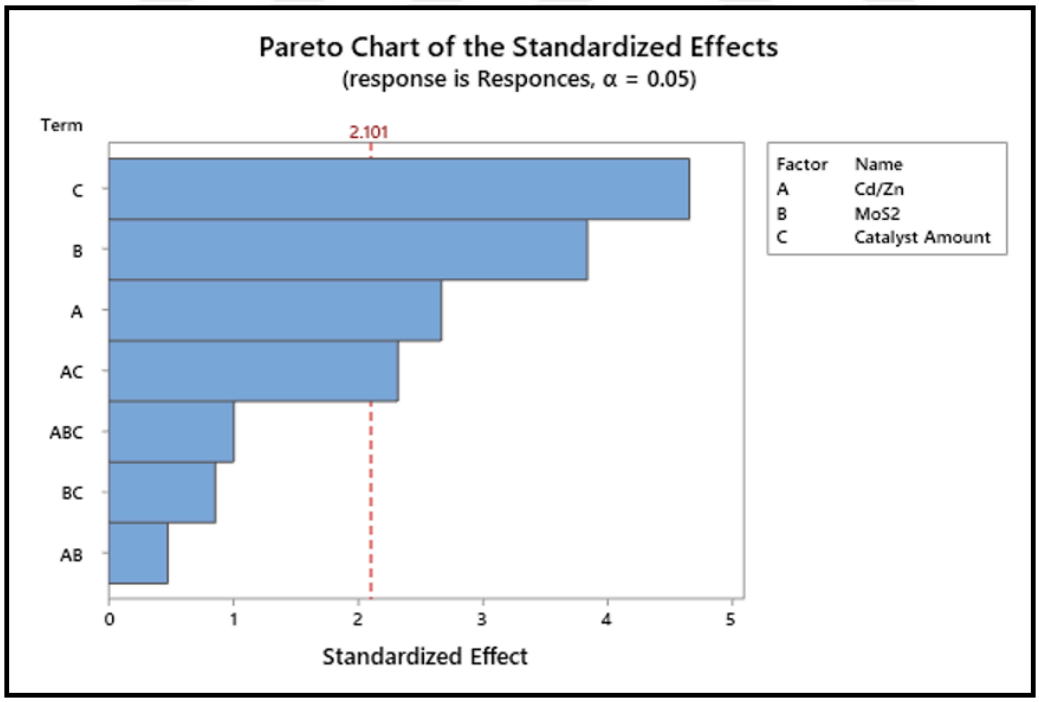

Figure 4.5 Pareto plot of independent variables affecting hydrogen production (mmol g^{-1} h^{-1})**.**

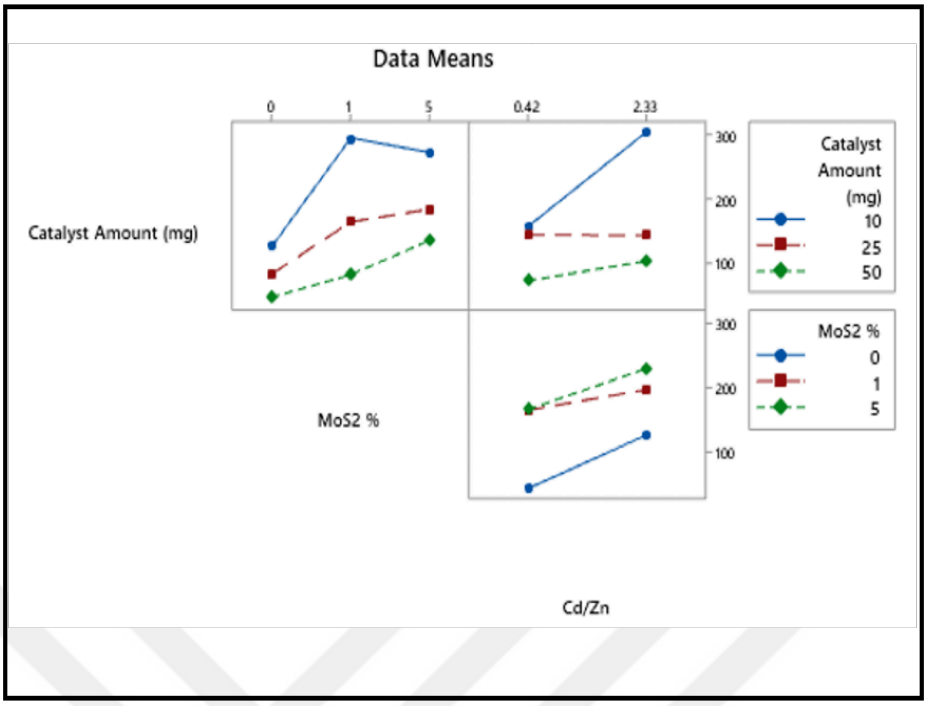

Figure 4.6 Interaction plots of the three independent parameters for hydrogen generation.

Figure 4.7. shows the graphs used to determine the factor with the least impact. The main effect graph makes it easy to see how each factor affects the other. The reference line is shown in the visuals as a gray dashed line. A significant decrease in the catalyst quantity (mg) curve occurs during component evaluation. Because of its substantial effect, more research on the amount of catalyst (mg) may be undertaken. Consequently, increasing the amount of catalyst (mg) reduces hydrogen generation. Higher Cd/Zn ratios led to increased production of hydrogen (mmol g^{-1} h^{-1}). Hydrogen production increased significantly from no MoS_2 to 1% MoS_2, but only modestly from 1% to 5% MoS_2, when the MoS_2 loading percentage was taken into consideration. Consequently, altering any parameter has a significant impact on the results. On the other hand, while increasing MoS_2 % and Cd/Zn increased hydrogen generation, increasing catalyst amount (mg) significantly decreased it. It is simpler to understand the consequences of each parameter with the help of this model graph.

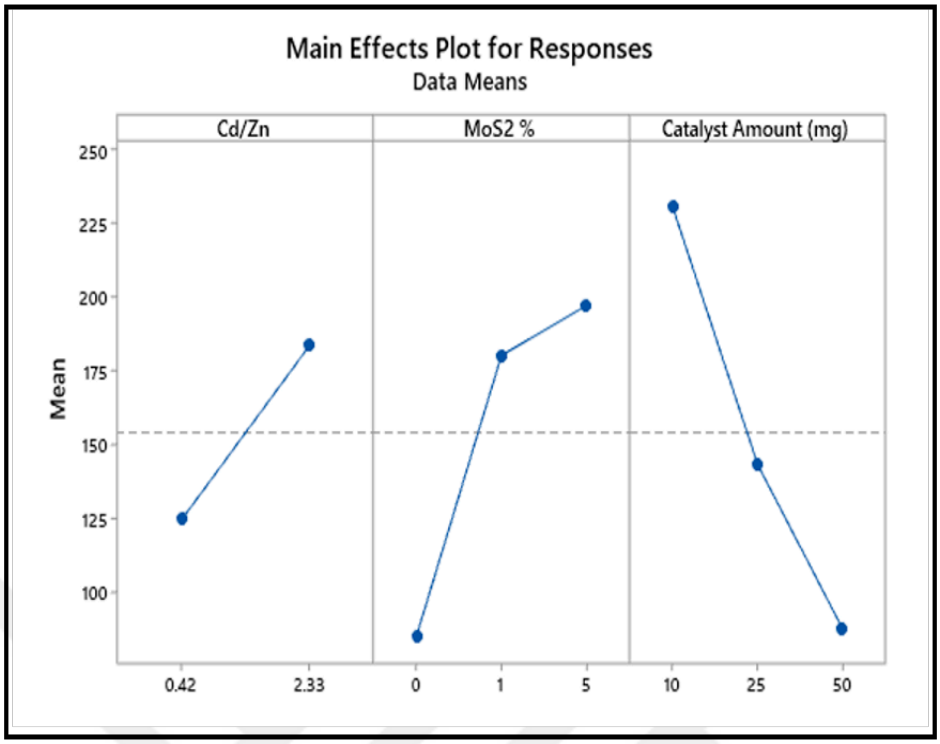

Figure 4.7 Main effect plots.

The contours show the impact of maintaining one component constant while changing the other two on hydrogen production responses (mmol g^{-1} h^{-1}). The green color contoured as the response color shows that the reaction rises from light to dark green. When the findings are studied independently of MoS_2%, it is projected that hydrogen production responses would rise when the catalyst amount (mg) is reduced, and the cadmium zinc ratio is raised (Figure 4.8a). When seen independently of the cadmium-zinc ratio, the color seems to darken, indicating better responsiveness as the amount of catalyst utilized decreases. With this reduction, the MoS_2 loading percentage offers better outcomes when used at typical levels of 1% to 5%. Figure 4.8b demonstrates that employing 3% MoS_2 loading in the research might yield better results. Unlike other graphs, this contour graph produced positive outcomes in selecting the most effective aspects for improving the work. The study examines hydrogen generation independent of the amount of catalyst. Figure 4.8c depicts the answers in mmol/h and increasing Cd/Zn and MoS_2% yields better results. However, larger MoS_2 loading percentages and Cd/Zn ratios cannot be entirely predicted. The contour plot results correspond with the interpretations found in other graphs (interaction and main effects plots). Furthermore, the capacity to forecast the progression of the study using these graphs sets it apart from other graphs.

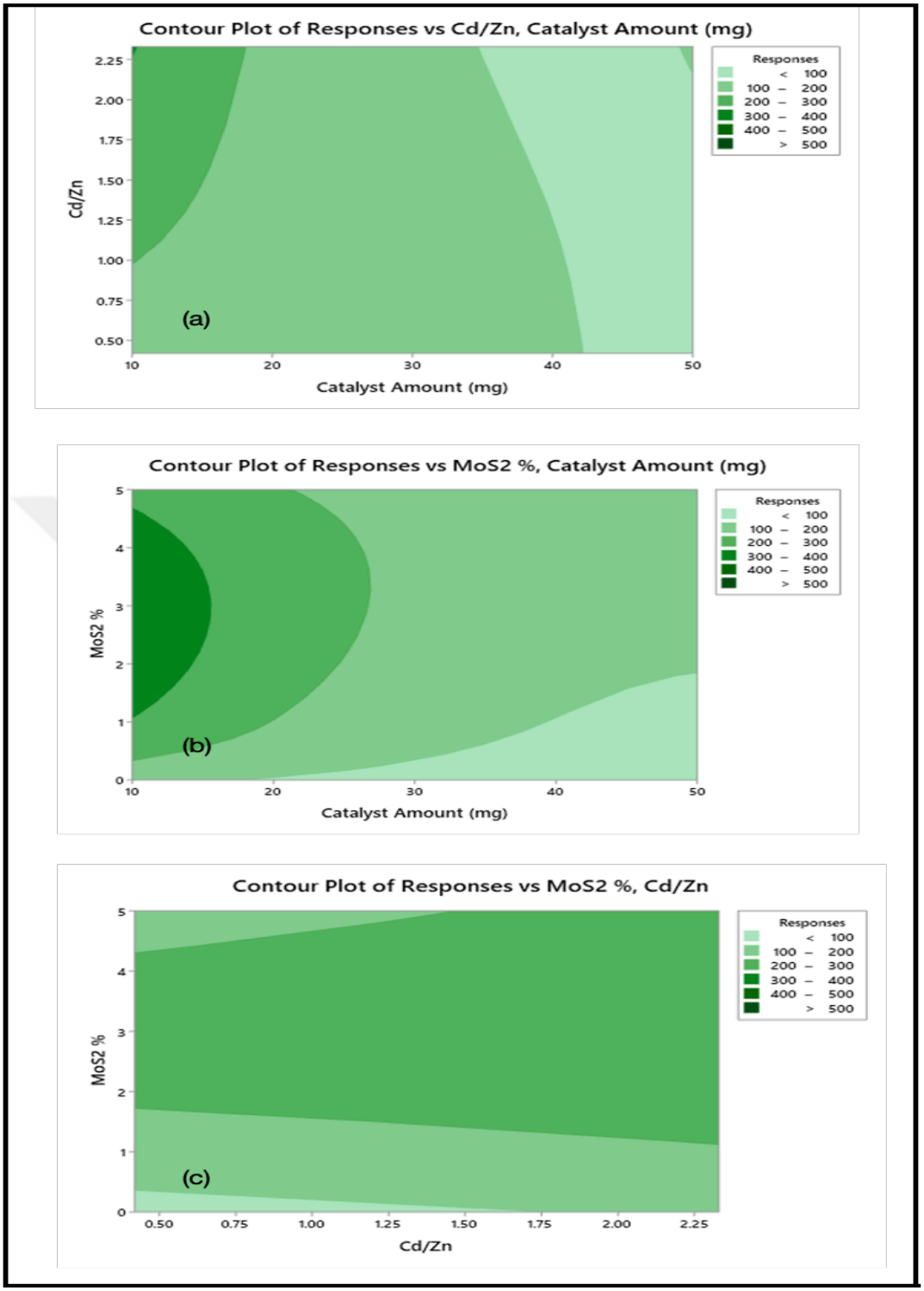

Figure 4.8 Contour graphs of the effect of (a) Cd/Zn and catalyst amount (mg), (b) MoS_2 % and catalyst amount (mg), (c) MoS_2 % and Cd/Zn on hydrogen production (mmol g^{-1} h^{-1}).

Surface curves showing the interaction of the change of independent parameters with the response in three dimensions, prepared by making use of the experimental design created using Full Factorial Design, are given in Figure 4.10. While drawing these curves, the effect of changing two parameters on the responses is examined while the other parameter is kept constant. Figure 4.10a illustrates the hydrogen production (mmol g^{-1} h^{-1}) versus the levels of catalyst amount (mg) and MoS_2 %. Like the two-dimensional contour graph, better responses were obtained at lower catalyst amounts and in the 1% to 5% MoS_2 loading range. In Figure 4.10b, the effect of catalyst amount (mg) and Cd/Zn on the answers is examined in 3D. However, no effective results were observed from the 3D graph as compared to the 2D graph (Figure 4.8a). It can be said that the answers are slightly better at low catalyst amounts and high Cd/Zn. It can be said that a good analysis can be made when these two graphs are examined together. When Figure 4.10c was examined, similar results were seen with the 2D graph (Figure 4.8c). It is seen that the effect of adding MoS_2 % at low Cd/Zn levels is low. Increasing both factors have a positive effect on the responses. The normal probability plot of the responses is given in Figure 4.9. The normal probability plot is a graphical tool for observing the normal distribution of data. The p-value and associated AD statistic for the accuracy of the distribution are also provided in the graph.

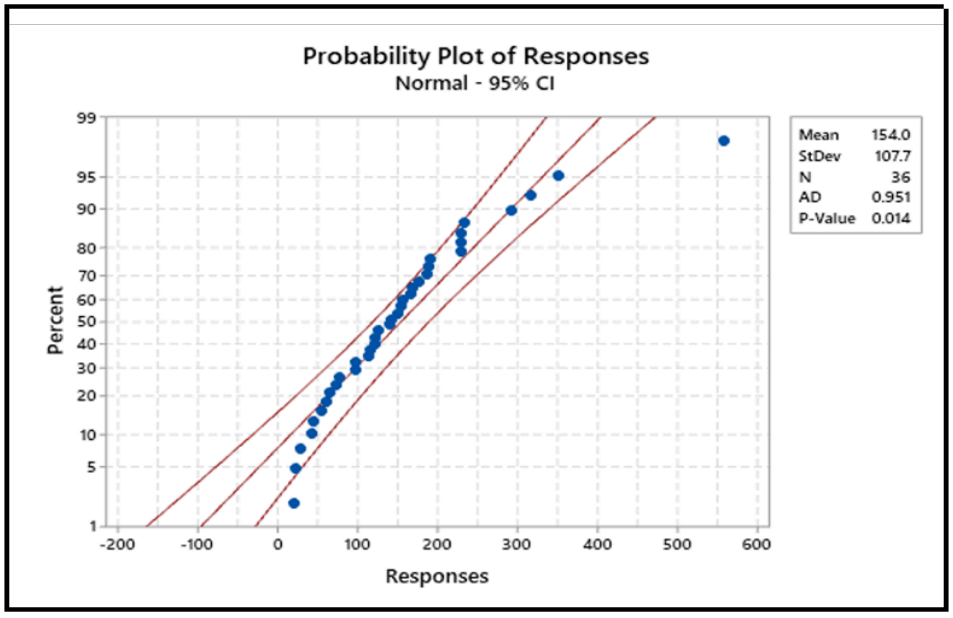

Figure 4.9 Normal probability plot.

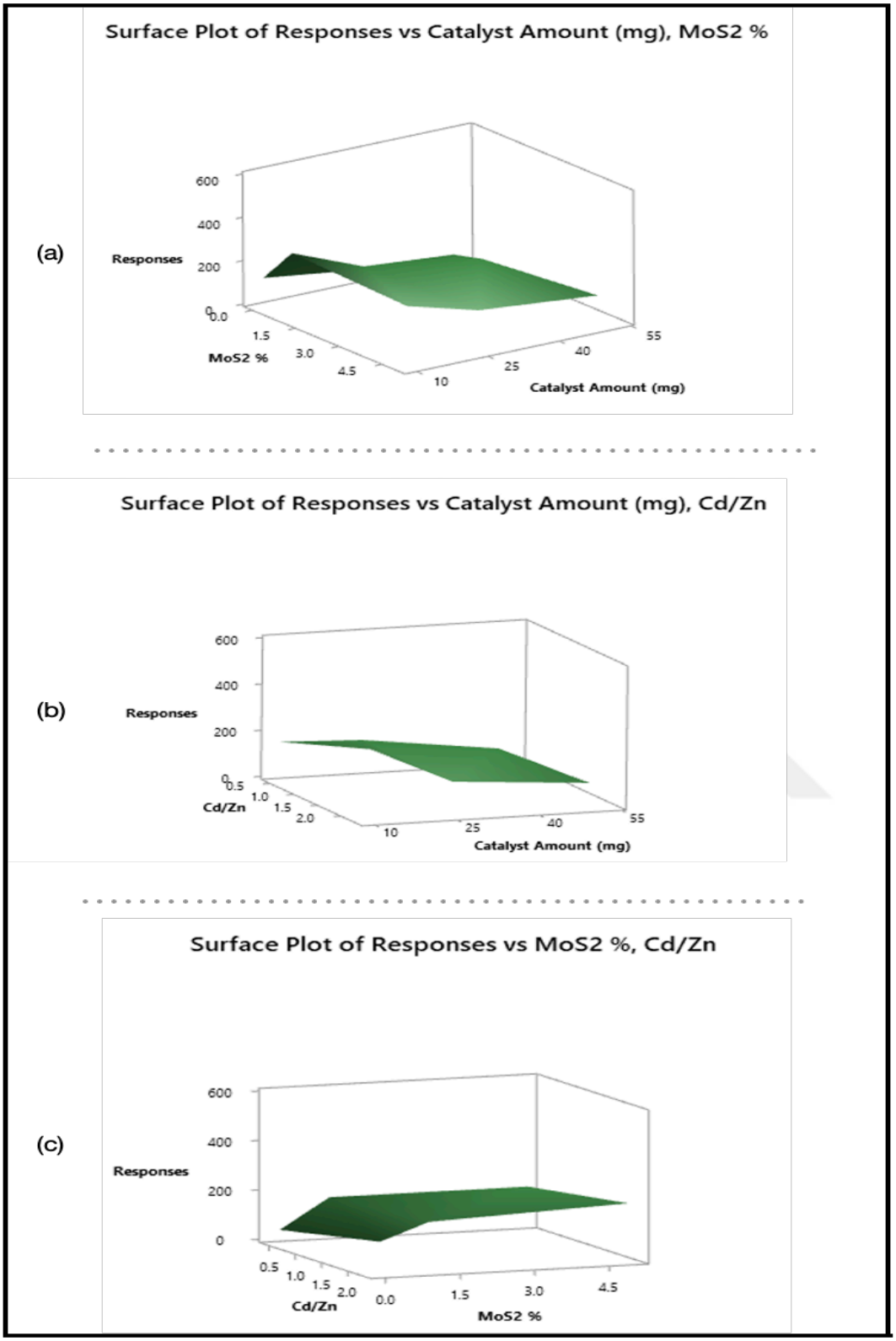

Figure 4.10 3D interaction effect plot of the effect of independent factors (a) catalyst amount and MoS_2 %, (b) catalyst amount and Cd/Zn, (c) MoS_2 % and Cd/Zn on hydrogen production (mmol g^{-1} h^{-1}).

4.3. Characterization Results of Nanorod $Cd_{0.7}Zn_{0.3}S/MoS_2$ Catalyst Synthesized Using Ethylenediamine (EDA)

4.3.1. SEM Images of Nanorod $Cd_{0.7}Zn_{0.3}S$ Catalyst with EDA

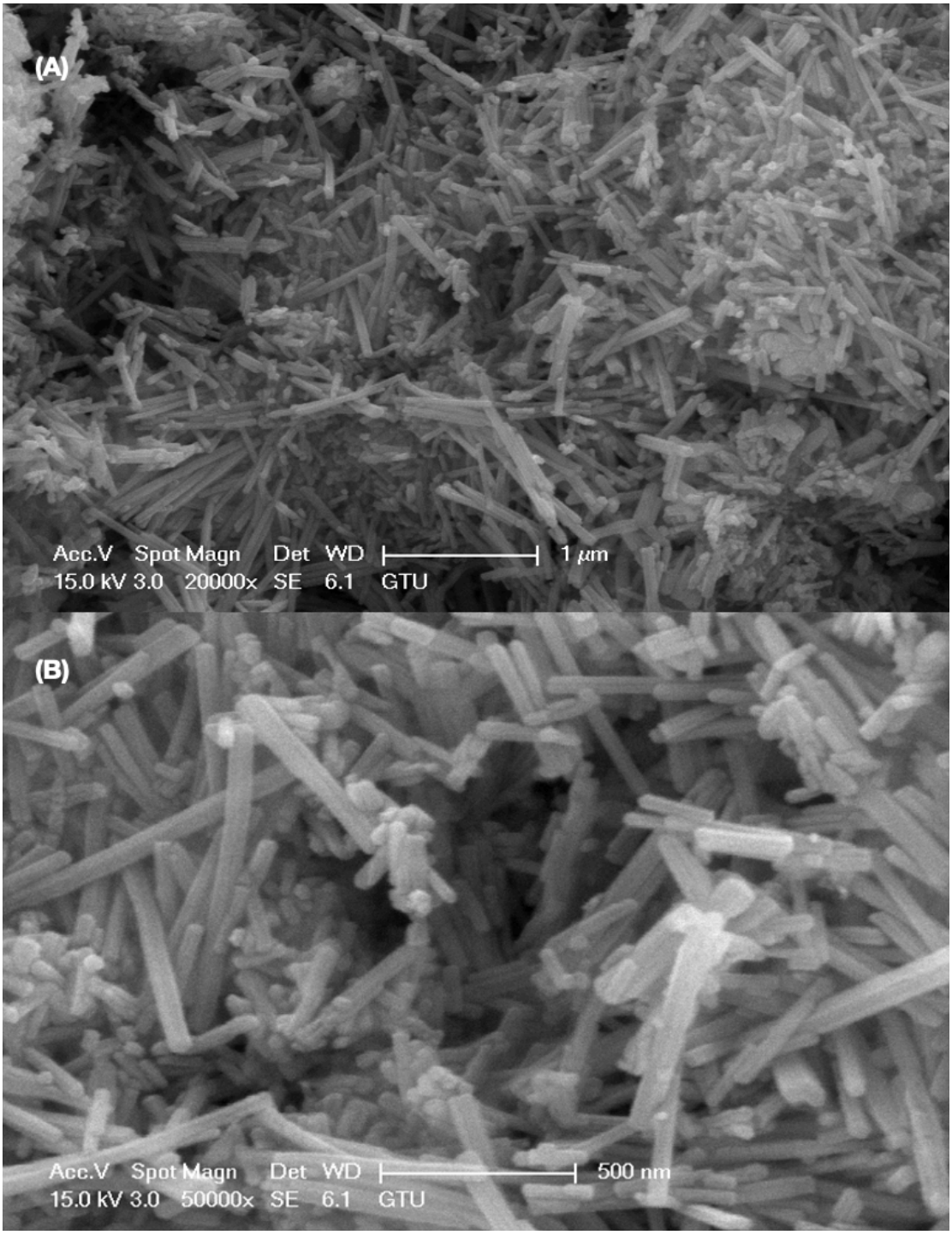

Figure 4.11 SEM images of the $Cd_{0.7}Zn_{0.3}S$/1% MoS_2 nanocomposites with using 40 ml EDA- 40 ml water.

In the synthesis procedure, synthesis was performed with a total of 80 ml of solvent. Experiments were carried out by changing the solution ratio used (EDA/water). In the example shown in Figure 4.11., 40 ml EDA and 40 ml water were used. In Figure 4.11a, SEM analysis was carried out with 1 micrometer and 20000 times magnification. It can be seen that the catalyst is in nanorod form, distributed homogeneously and without agglomeration. In Figure 4.11b, SEM analysis was carried out at 500 nanometers and 50000 times magnification. It has been clearly shown that the catalyst is in the form of nanorods. In the example shown in Figure 4.12., 60 ml EDA and 20 ml water were used. In Figure 4.12a, SEM analysis was carried out with 1 micrometer and 20000 times magnification. It has been shown that the catalyst approaches the rod form but is not fully synthesized as nanorods. The catalyst is in lump form. In Figure 4.12b, SEM analysis was carried out at 500 nanometers and 50000 times magnification. In the example shown in Figure 4.13., 80 ml EDA was used. In Figure 4.13a, SEM analysis was carried out with 1 micrometer and 20000 times magnification. The catalyst is clustered and does not have a specific shape. In Figure 4.13b, SEM analysis was carried out at 500 nanometers and 50000 times magnification [23][47][51].

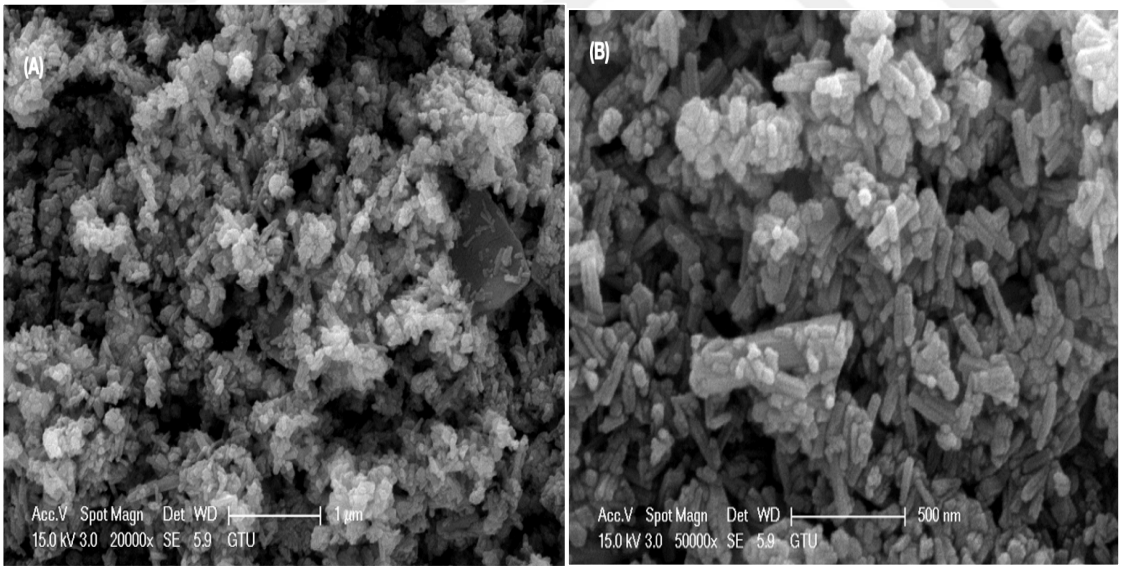

Figure 4.12 SEM images of the $Cd_{0.7}Zn_{0.3}S$/1% MoS_2 nanocomposites with using 60 ml EDA- 20 ml water.

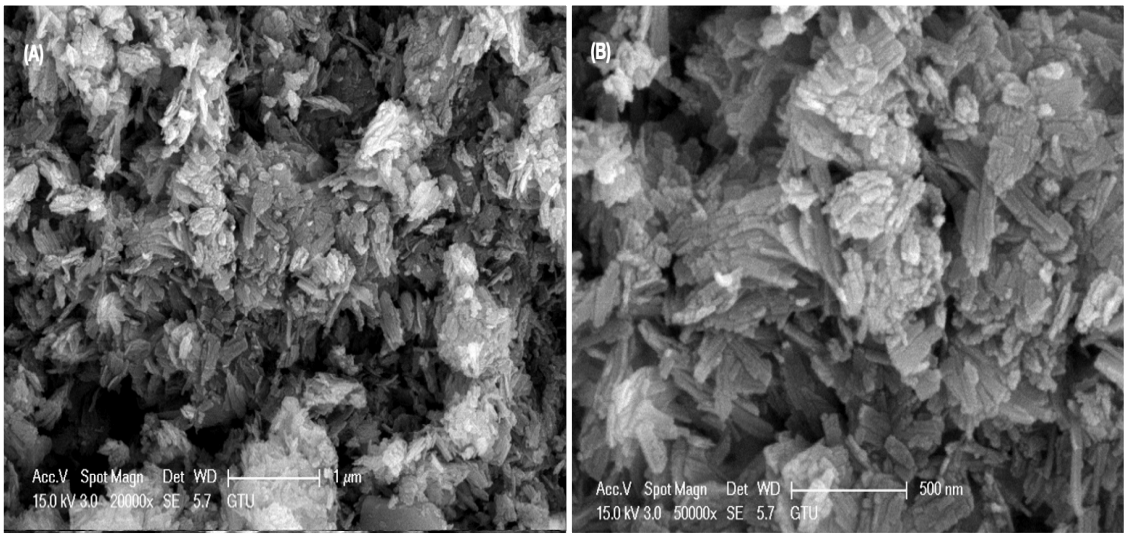

Figure 4.13 SEM images of the $Cd_{0.7}Zn_{0.3}S$/1% MoS_2 nanocomposites with using 80 ml EDA.

4.3.2. UV–Vis DRS Results of Nanorod $Cd_{0.7}Zn_{0.3}S$/ MoS_2 Catalyst

The optical characteristics and band gap of the materials were investigated using UV-Vis diffuse reflectance spectroscopy (UV-Vis DRS). In diffuse reflectance spectroscopy, the device analyzes diffusely reflected light. The system under investigation consists of a substrate coated with a substance of interest that is irradiated with diffuse monochromatic radiation. The Tauc-plots (plot of hv f(R) vs. photon energy (hv)) used for calculating the direct band gap values were obtained from reflectance measurements by converting the Kubelka-Munk function (Equation 4.2). K and S represent the K-M absorption and scattering coefficients, respectively [82] [83].

$$f(R) = \frac{\mathrm{K}}{\mathrm{S}} = \frac{(1-\mathrm{R})^2}{2\mathrm{R}} \qquad (4.2)$$

In Figure 4.15., UV-vis absorption spectra of N-$Cd_{0.7}Zn_{0.3}S$, N-$Cd_{0.7}Zn_{0.3}S$/1% MoS_2, N-$Cd_{0.7}Zn_{0.3}S$/3% MoS_2, N-$Cd_{0.7}Zn_{0.3}S$/5% MoS_2, N-$Cd_{0.7}Zn_{0.3}S$/7% MoS_2, N-$Cd_{0.7}Zn_{0.3}S$/10% MoS_2, N-$Cd_{0.7}Zn_{0.3}S$/15% MoS_2 and MoS_2 are also shown. In Figure 4.14., the $Cd_{0.7}Zn_{0.3}S$ synthesized as nanorods and the $Cd_{0.7}Zn_{0.3}S$/1% MoS_2 catalyst with the highest hydrogen production rate (mmol g^{-1} $h^{-}1$) are drawn. It was observed that with the addition of MoS_2, the wavelength (nm) increased, and the direct band gap (eV) decreased.

Estimated direct band gap energies (Eg) as a function of photon energy $[\alpha hv]^2$ based on the Kubelka-Munk function were calculated [85]. Additionally, in Table 4.4., the wavelengths (nm) and calculated direct band gaps (eV) of all catalysts synthesized by adding MoS_2 are given. The direct band gaps were 2.37 eV, 2.36 eV, 2.35 eV, 2.36 eV, 2.35, 2.34, and 2.33 eV, corresponding to N-$Cd_{0.7}Zn_{0.3}S$, N-$Cd_{0.7}Zn_{0.3}S$/1% MoS_2, N-$Cd_{0.7}Zn_{0.3}S$/3% MoS_2, N-$Cd_{0.7}Zn_{0.3}S$/5% MoS_2, N-$Cd_{0.7}Zn_{0.3}S$/7% MoS_2, N-$Cd_{0.7}Zn_{0.3}S$/10% MoS_2, N-$Cd_{0.7}Zn_{0.3}S$/15% MoS_2, respectively. The band gap decreased in samples with MoS_2 added; this can be explained by the fact that the charge transfer between pure N-$Cd_{0.7}Zn_{0.3}S$ and added MoS_2 results in a lower energy transition.

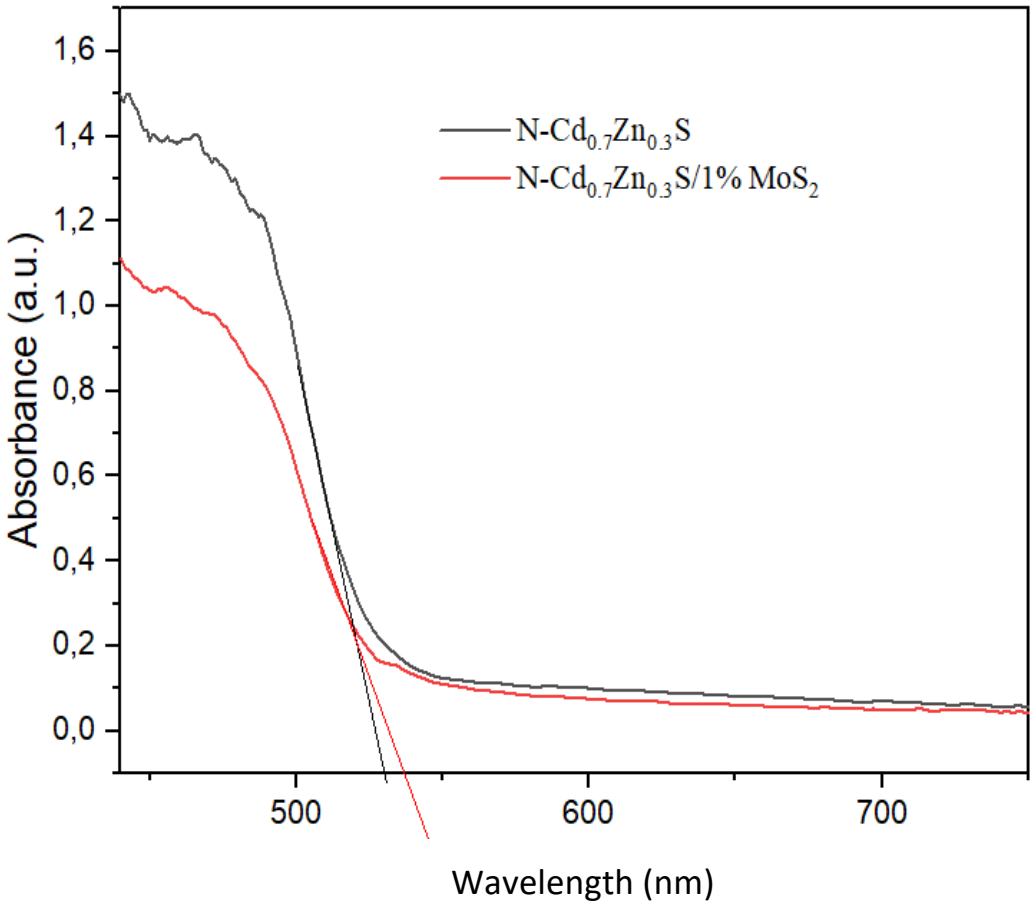

Figure 4.14 UV-DRS absorption spectra of nanorod $Cd_{0.7}Zn_{0.3}S$ -nanorod $Cd_{0.7}Zn_{0.3}S$/1% MoS_2.

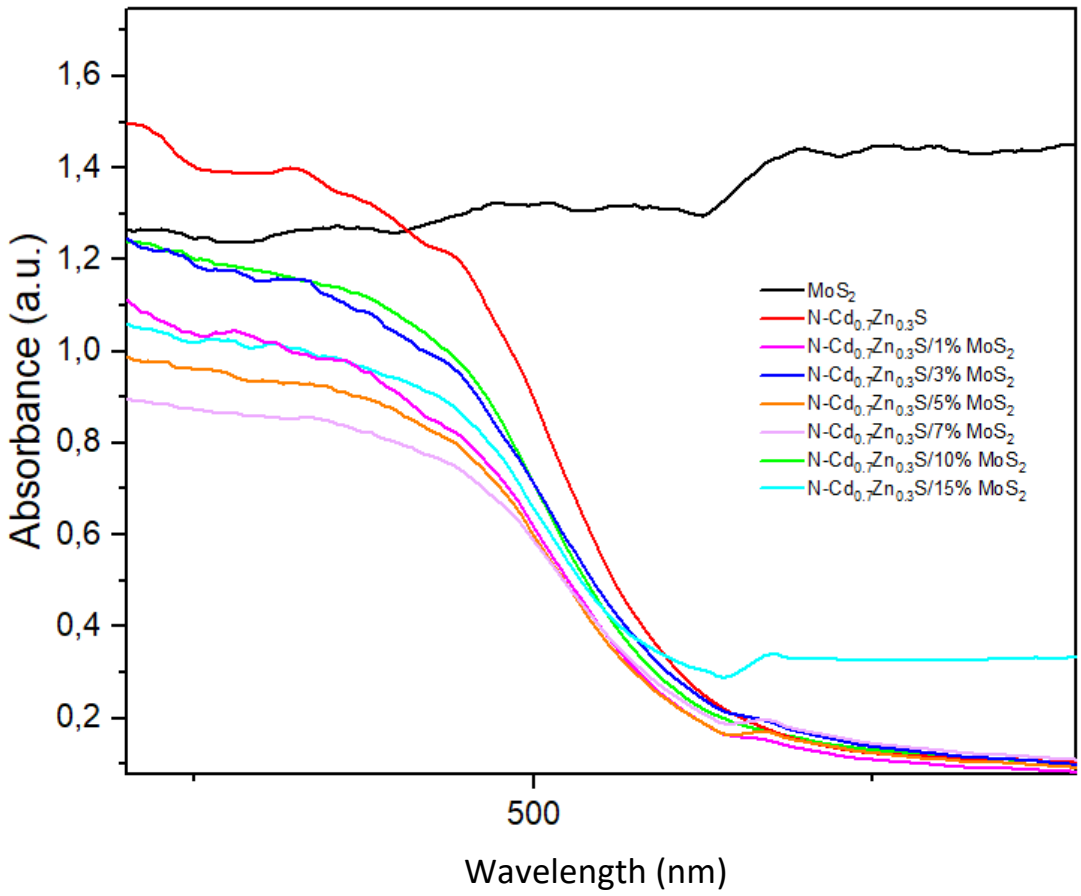

Figure 4.15 UV-DRS absorption spectra of N-$Cd_{0.7}Zn_{0.3}S$, N-$Cd_{0.7}Zn_{0.3}S$/1% MoS_2, N-$Cd_{0.7}Zn_{0.3}S$/3% MoS_2, N-$Cd_{0.7}Zn_{0.3}S$/5% MoS_2, N-$Cd_{0.7}Zn_{0.3}S$/7% MoS_2, N-$Cd_{0.7}Zn_{0.3}S$/10% MoS_2, N-$Cd_{0.7}Zn_{0.3}S$/15% MoS_2 and MoS_2.

Table 4.4 UV-vis absorption wavelength edge and band gap values of nanorod photocatalysts.

Catalysts	Wavelength (nm)	Direct Band Gaps (eV)
N-$Cd_{0.7}Zn_{0.3}S$	522	2.37
N-$Cd_{0.7}Zn_{0.3}S$/1% MoS_2	524	2.36
N-$Cd_{0.7}Zn_{0.3}S$/3% MoS_2	526	2.35
N-$Cd_{0.7}Zn_{0.3}S$/5% MoS_2	525	2.36
N-$Cd_{0.7}Zn_{0.3}S$/7% MoS_2	526	2.35
N-$Cd_{0.7}Zn_{0.3}S$/10% MoS_2	530	2.34
N-$Cd_{0.7}Zn_{0.3}S$/15% MoS_2	531	2.33

4.4. Photocatalytic Hydrogen Evolution of Nanorod $Cd_{0.7}Zn_{0.3}S/MoS_2$ Catalyst

Photocatalysts produced in the form of nanorods were tested for photocatalytic activity under visible light using Na_2S/Na_2SO3 (0.35 M/0.25 M) as a sacrificial agent. Figure 4.16. depicts the H_2 generation rates, whereas Figure 4.17. depicts the time dependent H_2 evolution of N-$Cd_{0.7}Zn_{0.3}S$ following addition of different MoS_2 concentrations. The photocatalytic performance was compared by adding MoS_2. N-$Cd_{0.7}Zn_{0.3}S$/1% MoS_2 produced H_2 at a rate of 131.8 mmol g^{-1} h^{-1}, 3.5 times more than N-$Cd_{0.7}Zn_{0.3}S$. Increasing the quantity of MoS_2 resulted in a reduction in H_2 production rates because MoS_2 inhibited light absorption. N-$Cd_{0.7}Zn_{0.3}S$/1% MoS_2 was chosen as the greatest hydrogen-yielding catalyst for use in the MoC-Mo_2C addition tests. As shown in Figure 4.17., the experiment continued 5 hours, with analysis performed every hour. The experimental results reveal that hydrogen generation rises hourly. Furthermore, the addition of MoS_2 caused an increase in the rate of hydrogen generation in all samples.

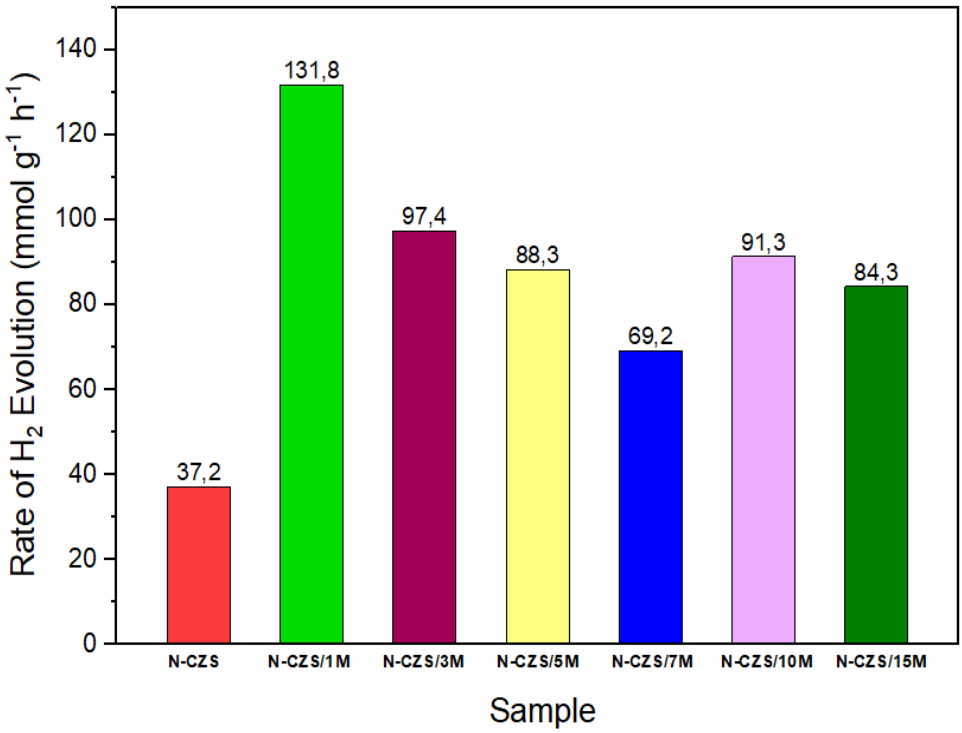

Figure 4.16 Photocatalytic H_2 production rates of N-$Cd_{0.7}Zn_{0.3}S$, N-$Cd_{0.7}Zn_{0.3}S$/1% MoS_2, N-$Cd_{0.7}Zn_{0.3}S$/3% MoS_2, N-$Cd_{0.7}Zn_{0.3}S$/5% MoS_2, N-$Cd_{0.7}Zn_{0.3}S$/7% MoS_2, N-$Cd_{0.7}Zn_{0.3}S$/10% MoS_2, and N-$Cd_{0.7}Zn_{0.3}S$/15% MoS_2 samples.

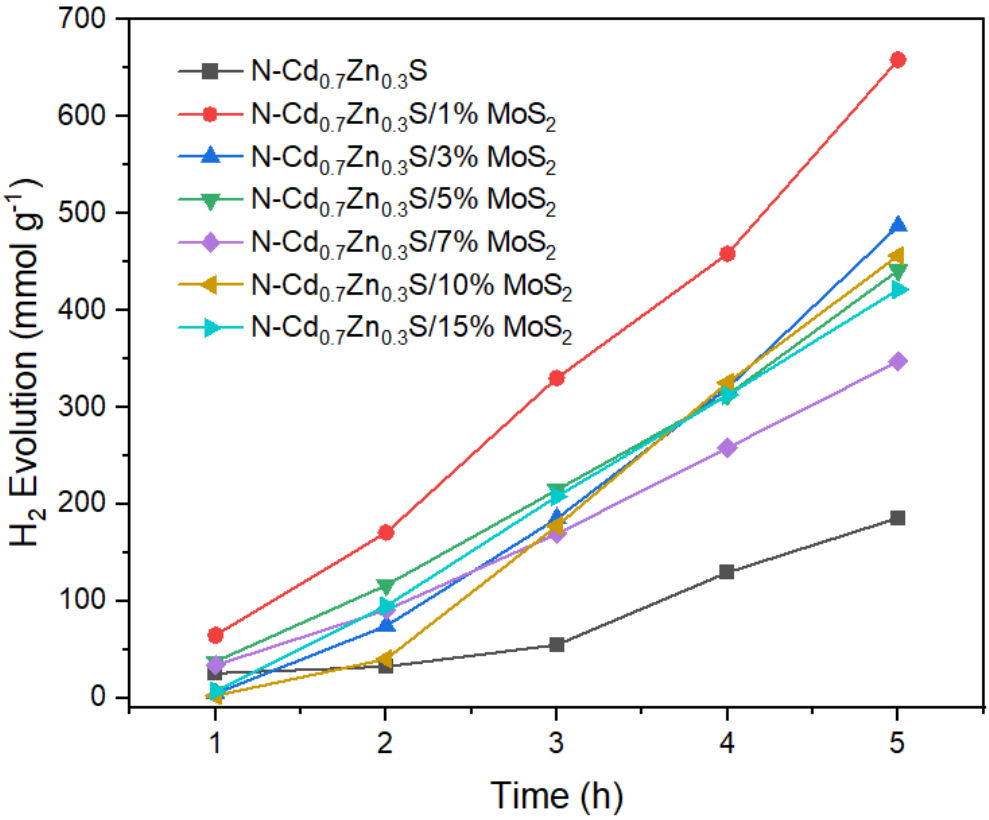

Figure 4.17 Time-dependent H_2 production activities of N-$Cd_{0.7}Zn_{0.3}S$, N-$Cd_{0.7}Zn_{0.3}S$/1% MoS_2, N-$Cd_{0.7}Zn_{0.3}S$/3% MoS_2, N-$Cd_{0.7}Zn_{0.3}S$/5% MoS_2, N-$Cd_{0.7}Zn_{0.3}S$/7% MoS_2, N-$Cd_{0.7}Zn_{0.3}S$/10% MoS_2, and N-$Cd_{0.7}Zn_{0.3}S$/15% MoS_2 samples.

4.5. Electrochemical Applications of Nanorod $Cd_{0.7}Zn_{0.3}S/MoS_2$ Catalyst

Chronoamperometry was used to assess the catalyst's stability throughout time that it was being investigated electrochemically (Figure 4.18.). The relationship between time and current produced by photogenerated electrons was examined. Chronoamperometry study was done on all photocatalysts at a potential of 0 V. Table 4.5. shows the photocurrent responses derived from the synthesized photocatalysts. According to these results, the N-$Cd_{0.7}Zn_{0.3}S$/1% MoS_2 photocatalyst produced the best photocurrent result. Compared to pure N-$Cd_{0.7}Zn_{0.3}S$, the photocurrent increased by adding of 1% MoS_2. This demonstrates that heterojunctions considerably enhance the transmission of photogenerated charges [86]. This finding is supported by hydrogen production rate results. The inclusion of 10% and 15% MoS_2 results in lower photocurrent values compared to pure N-$Cd_{0.7}Zn_{0.3}S$. The

findings obtained were shown to be higher than the study conducted with the same type of catalyst [87].

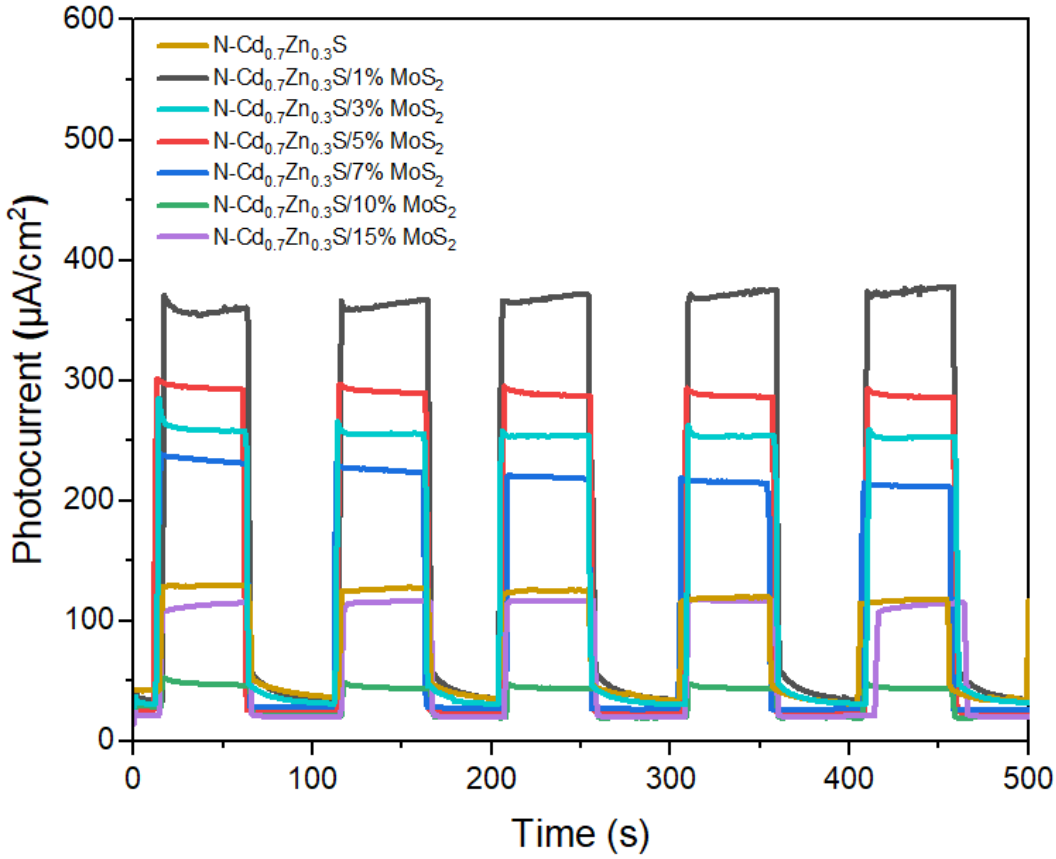

Figure 4.18 Transient photo current curves of N-$Cd_{0.7}Zn_{0.3}S$, N-$Cd_{0.7}Zn_{0.3}S$/1% MoS_2, N-$Cd_{0.7}Zn_{0.3}S$/3% MoS_2, N-$Cd_{0.7}Zn_{0.3}S$/5% MoS_2, N-$Cd_{0.7}Zn_{0.3}S$/7% MoS_2, N-$Cd_{0.7}Zn_{0.3}S$/10% MoS_2, N-$Cd_{0.7}Zn_{0.3}S$/15% MoS_2 samples.

Table 4.5 Photo-current response of the synthesized catalysts.

Catalysts	Photocurrent Response (μA/cm²)
N-$Cd_{0.7}Zn_{0.3}S$	82
N-$Cd_{0.7}Zn_{0.3}S$/1% MoS_2	318
N-$Cd_{0.7}Zn_{0.3}S$/3% MoS_2	225
N-$Cd_{0.7}Zn_{0.3}S$/5% MoS_2	278
N-$Cd_{0.7}Zn_{0.3}S$/7% MoS_2	212
N-$Cd_{0.7}Zn_{0.3}S$/10% MoS_2	35
N-$Cd_{0.7}Zn_{0.3}S$/15% MoS_2	120

Linear Sweep Voltammetry (LSV) was used on all catalysts coated with ITO. LSV analysis was carried out in visible light. Figure 4.19. shows the resultant photocurrent response. The figure displays three distinct sample findings; pure N-$Cd_{0.7}Zn_{0.3}S$, N-$Cd_{0.7}Zn_{0.3}S$/1% MoS_2 loaded catalyst gave the best hydrogen results and N-$Cd_{0.7}Zn_{0.3}S$/15% MoS_2 maximum MoS_2 loaded catalyst. The results show that photocatalysts' visible light spectrum are active. It has been demonstrated that photocurrent rises depending on whether the light is turned off or on. Studies have also shown that the addition of MoS_2 suppresses electron-hole recombination while increasing photocatalytic activity in the visible band. The findings are congruent with the chronoamperometry results.

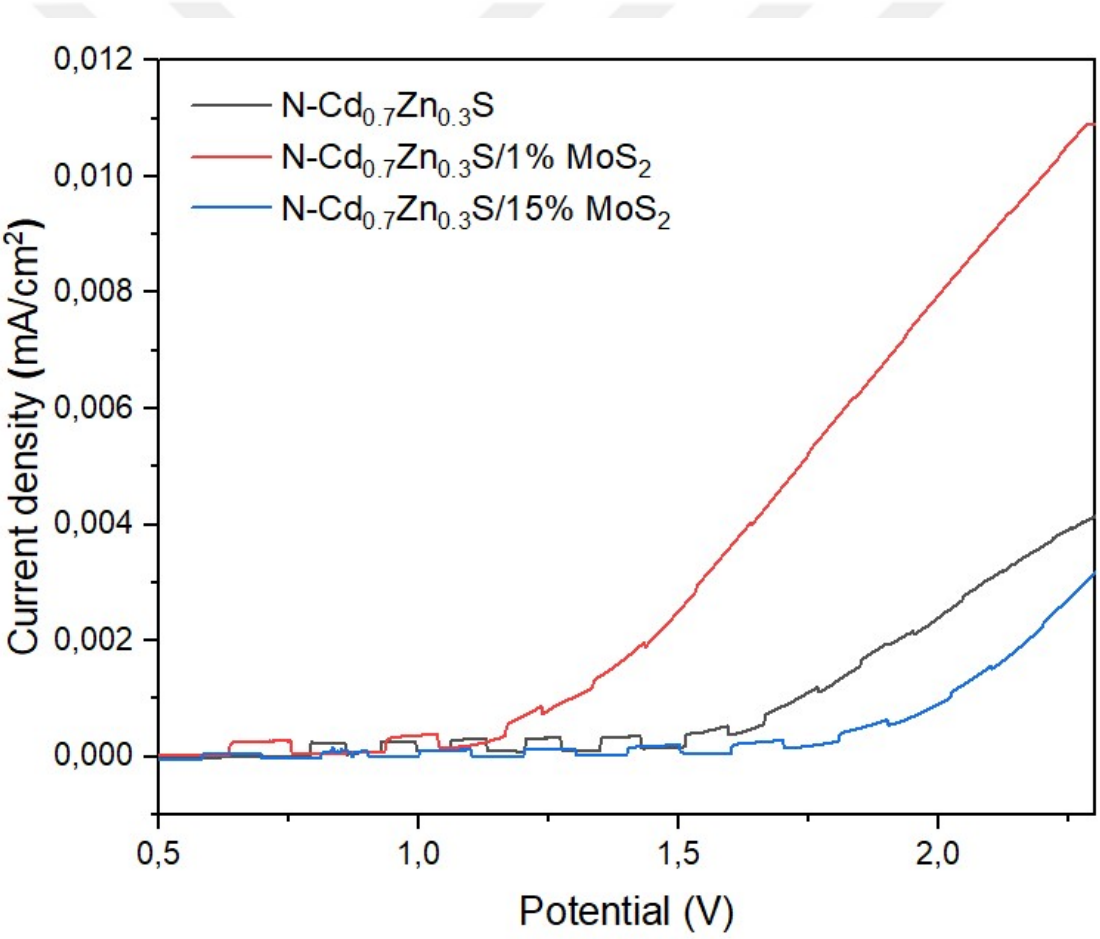

Figure 4.19 LSV of N-$Cd_{0.7}Zn_{0.3}S$, N-$Cd_{0.7}Zn_{0.3}S$/1% MoS_2, N-$Cd_{0.7}Zn_{0.3}S$/3% MoS_2, N-$Cd_{0.7}Zn_{0.3}S$/5% MoS_2, N-$Cd_{0.7}Zn_{0.3}S$/7% MoS_2, N-$Cd_{0.7}Zn_{0.3}S$/10% MoS_2, N-$Cd_{0.7}Zn_{0.3}S$/15% MoS_2 samples.

4.6. Characterization Results of Nanorod $Cd_{0.7}Zn_{0.3}S$/1% MoS_2/ MoC-Mo_2C Catalyst

4.6.1. X-Ray Diffraction Analysis (XRD) Results of MoC-Mo_2C

Figure 4.20. shows the XRD patterns of the synthesized MoC-Mo_2C. XRD analysis was used to study the synthesized sample's structure and phase advancement. As shown in Figure 4.20., the sample's XRD pattern indicates the development of MoC (ICDD card no. 03-065-6664) and Mo_2C (ICDD card no. 00-035-0787) phases in the manufactured powder sample [88]. As demonstrated in the experiments, XRD examination revealed no unsynthesized C or Mo peaks. This suggests that the intended MoC-Mo_2S structure was synthesized pure [89]. In this study using CVD, MoC-Mo_2S was synthesized and then its effect on hydrogen production was studied by adding it in different mass percentages to the N-$Cd_{0.7}Zn_{0.3}S$/1% MoS_2 catalyst, which gives the best hydrogen production rate (mmol g^{-1} h^{-1}) and shows good results in electrochemical applications.

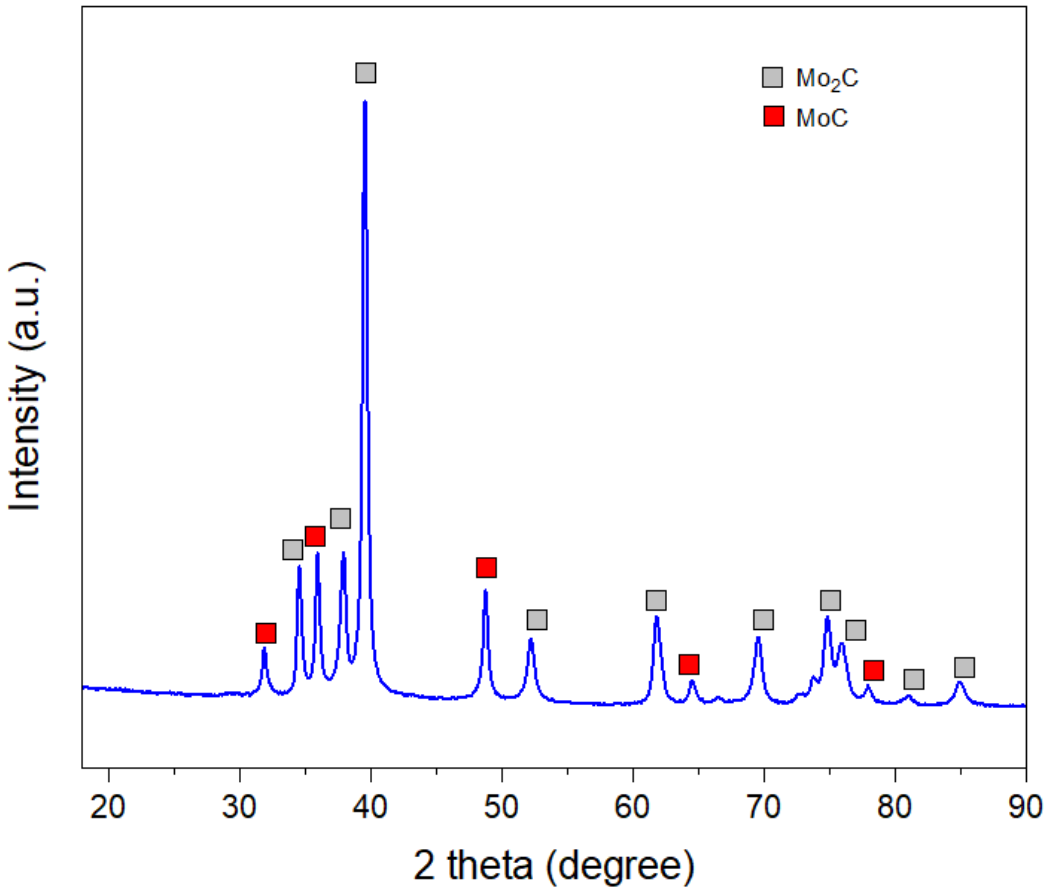

Figure 4.20 XRD patterns of MoC-Mo_2C.

4.6.2. UV–Vis DRS Results of N-$Cd_{0.7}Zn_{0.3}S$/1% MoS_2/MoC-Mo_2C

UV-Vis DRS measurements were made for MoC-Mo_2C and 4 samples to which MoC-Mo_2C was added (Figure 4.21.). In Figure 4.22., the N-$Cd_{0.7}Zn_{0.3}S$/1% MoS_2 catalyst with the highest hydrogen production rate (mmol g^{-1} h^{-1}) and the N-$Cd_{0.7}Zn_{0.3}S$/1% MoS_2/1.0% MoC-Mo_2C catalyst with the most efficient hydrogen production by adding MoC-Mo_2C are drawn. It has been shown that the band gaps decrease with the addition of MoC-Mo_2C. This type of characterization also confirms the synthesis of the catalyst. Calculated band gaps in Table 4.6. are shown below. The direct band gaps were 2.36 eV, 2.36 eV, 2.33 eV, 2.32, and 2.31 eV, corresponding to N-$Cd_{0.7}Zn_{0.3}S$/1% MoS_2, N-$Cd_{0.7}Zn_{0.3}S$/1% MoS_2/0.5% MoC-Mo_2C, N-$Cd_{0.7}Zn_{0.3}S$/1% MoS_2/1.0% MoC-Mo_2C, N-$Cd_{0.7}Zn_{0.3}S$/1% MoS_2/1.5% MoC-Mo_2C, N-$Cd_{0.7}Zn_{0.3}S$/1% MoS_2/2.0% MoC-Mo_2, respectively.

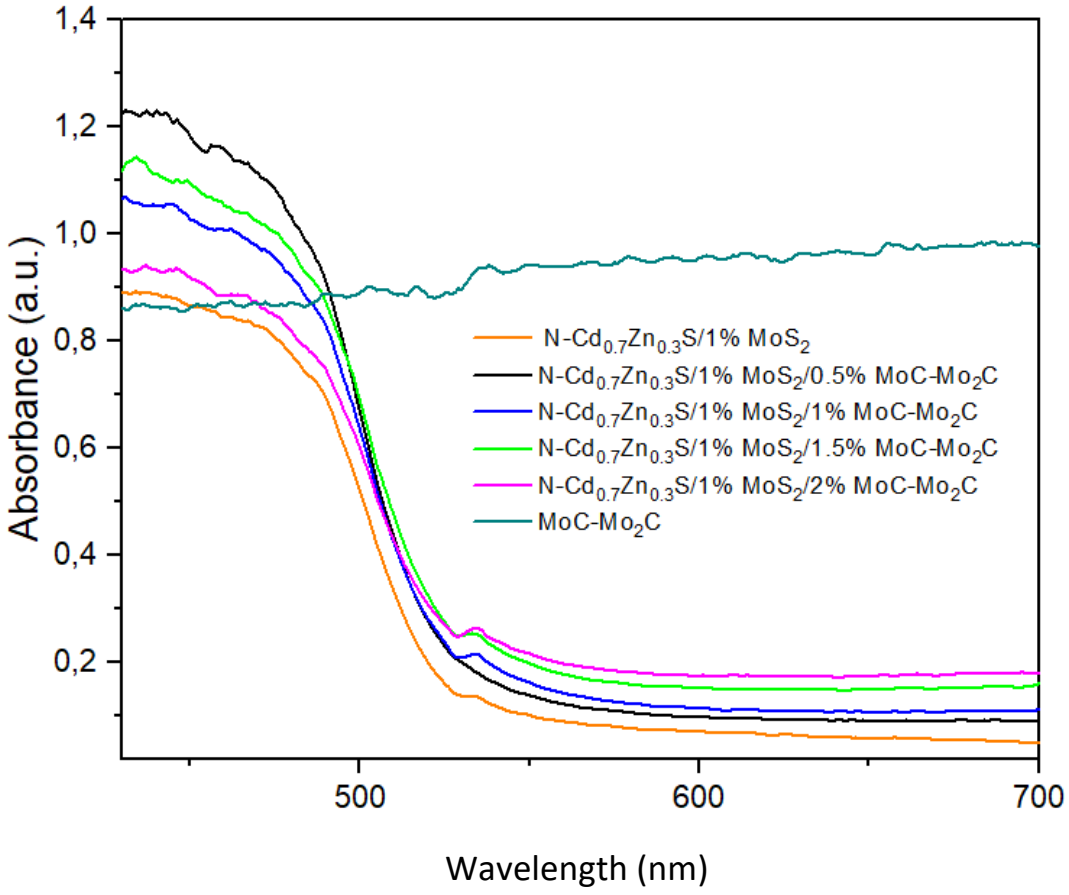

Figure 4.21 UV-DRS absorption spectra of N-$Cd_{0.7}Zn_{0.3}S$/1% MoS_2, N-$Cd_{0.7}Zn_{0.3}S$/1% MoS_2/0.5% MoC-Mo_2C, N-$Cd_{0.7}Zn_{0.3}S$/1% MoS_2/1.0% MoC-Mo_2C, N-$Cd_{0.7}Zn_{0.3}S$/1% MoS_2/1.5% MoC-Mo_2C, N-$Cd_{0.7}Zn_{0.3}S$/1% MoS_2/2.0% MoC-Mo_2C and MoC-Mo_2C.

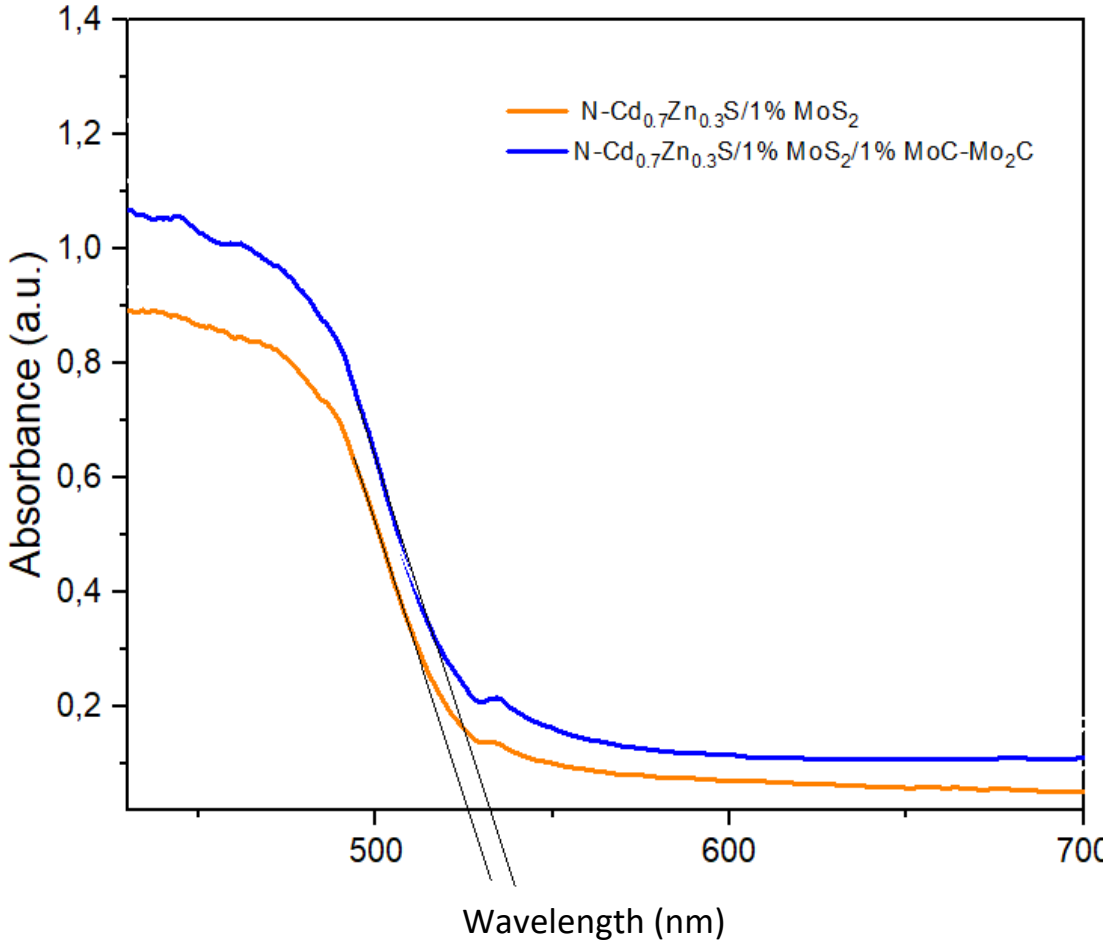

Figure 4.22 UV-DRS absorption spectra of N-$Cd_{0.7}Zn_{0.3}S$/1% MoS_2 and N-$Cd_{0.7}Zn_{0.3}S$/1% MoS_2/1.0% MoC-Mo_2C.

Table 4.6 UV-vis absorption wavelength edge and band gap values.

Catalysts	Wavelength (nm)	Direct Band Gaps (eV)
N-$Cd_{0.7}Zn_{0.3}S$/1% MoS_2	524	2.36
N-$Cd_{0.7}Zn_{0.3}S$/1% MoS_2/0.5% MoC-Mo_2C	525	2.36
N-$Cd_{0.7}Zn_{0.3}S$/1% MoS_2/1.0% MoC-Mo_2C	532	2.33
N-$Cd_{0.7}Zn_{0.3}S$/1% MoS_2/1.5% MoC-Mo_2C	534	2.32
N-$Cd_{0.7}Zn_{0.3}S$/1% MoS_2/2.0% MoC-Mo_2C	536	2.31

4.7. Photocatalytic Hydrogen Evolution of N-$Cd_{0.7}Zn_{0.3}S$/1% MoS_2/MoC-Mo_2C

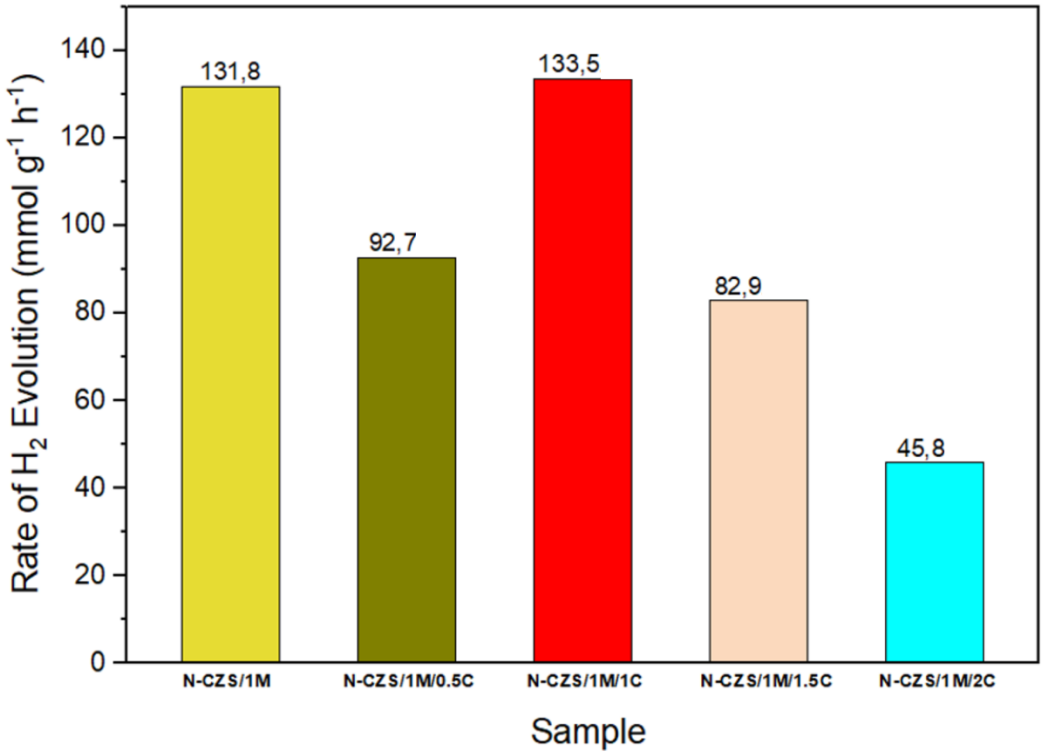

Figure 4.23 Photocatalytic H_2 production rates of N-$Cd_{0.7}Zn_{0.3}S$/1% MoS_2, N-$Cd_{0.7}Zn_{0.3}S$/1% MoS_2/0.5% MoC-Mo_2C, N-$Cd_{0.7}Zn_{0.3}S$/1% MoS_2/1.0% MoC-Mo_2C, N-$Cd_{0.7}Zn_{0.3}S$/1% MoS_2/1.5% MoC-Mo_2C, N-$Cd_{0.7}Zn_{0.3}S$/1% MoS_2/2.0% MoC-Mo_2C samples.

The catalysts, whose activity was examined by adding MoC-Mo_2C, were tested for photocatalytic activity under visible light, using Na_2S/Na_2SO3 (0.35 M/0.25 M) as a sacrificial agent, at a constant weight of 10 mg and a light intensity of 1000 W/m^2. Figure 4.23. shows the H_2 production rates, and Figure 4.24. shows the time-dependent H_2 evolution of N-$Cd_{0.7}Zn_{0.3}S$/1% MoS_2 after adding different MoC-Mo_2C mass percentage. The photocatalytic performance was compared by adding MoC-Mo_2C. N-$Cd_{0.7}Zn_{0.3}S$/1% MoS_2 produced hydrogen at a rate of 131.8 mmol g^{-1} h^{-1}, while N-$Cd_{0.7}Zn_{0.3}S$/1% MoS_2/1.0% MoC-Mo_2C produced 133.5 mmol g^{-1} h^{-1}. It has been shown that hydrogen production decreases with the addition of 0.5%, 1.5% and 2.0% MoC-Mo_2C. These results are supported by electrochemical measurements and UV-DRS results. In studies conducted with MoC-Mo_2C, low amounts were added by mass because it prevents light absorption [75][76]. It can be said that this is because the excessive amount of MoC-

Mo_2C co-catalyst on the N-$Cd_{0.7}Zn_{0.3}S$/1% MoS_2 surface and the strong light absorption capacity of black MoC-Mo_2C inhibits the light absorption of N-$Cd_{0.7}Zn_{0.3}S$/1% MoS_2 catalyst, and as a result, the hydrogen evolution rate for 1.5% and 2% MoC-Mo_2C decreases. In this study, the optimum MoC-Mo_2C percentage was found to be 1.0%. As shown in Figure 4.24., the experiment continued for 5 hours, with analysis taken every hour. Experimental results revealed that hydrogen production increased hourly. In addition, the addition of MoC-Mo_2C caused an hourly increase in all samples, but the sample that gave higher hydrogen production than its best and purest form was N-$Cd_{0.7}Zn_{0.3}S$/1% MoS_2/1.0% MoC-Mo_2C.

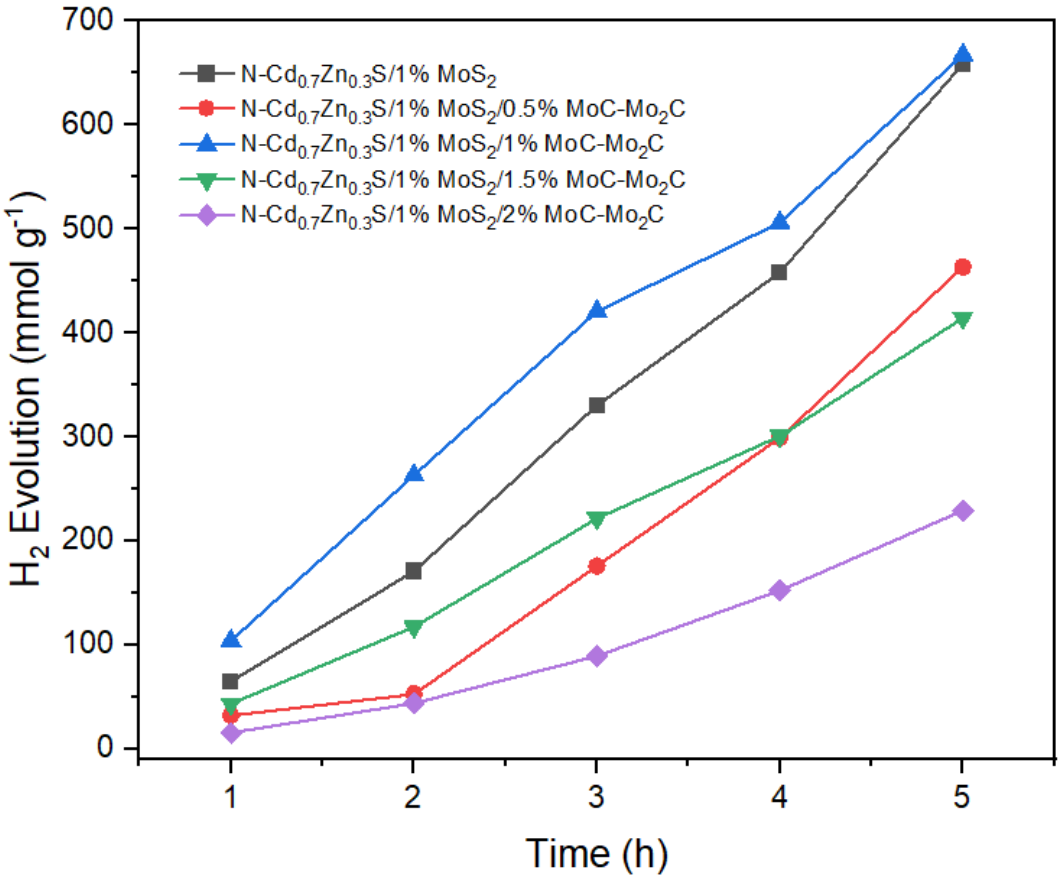

Figure 4.24 Time-dependent H_2 production activities of N-$Cd_{0.7}Zn_{0.3}S$/1% MoS_2, N-$Cd_{0.7}Zn_{0.3}S$/1% MoS_2/0.5% MoC-Mo_2C, N-$Cd_{0.7}Zn_{0.3}S$/1% MoS_2/1.0% MoC-Mo_2C, N-$Cd_{0.7}Zn_{0.3}S$/1% MoS_2/1.5% MoC-Mo_2C, N-$Cd_{0.7}Zn_{0.3}S$/1% MoS_2/2.0% MoC-Mo_2C samples.

4.8. Electrochemical Applications of N-$Cd_{0.7}Zn_{0.3}S$/1% MoS_2/MoC-Mo_2C

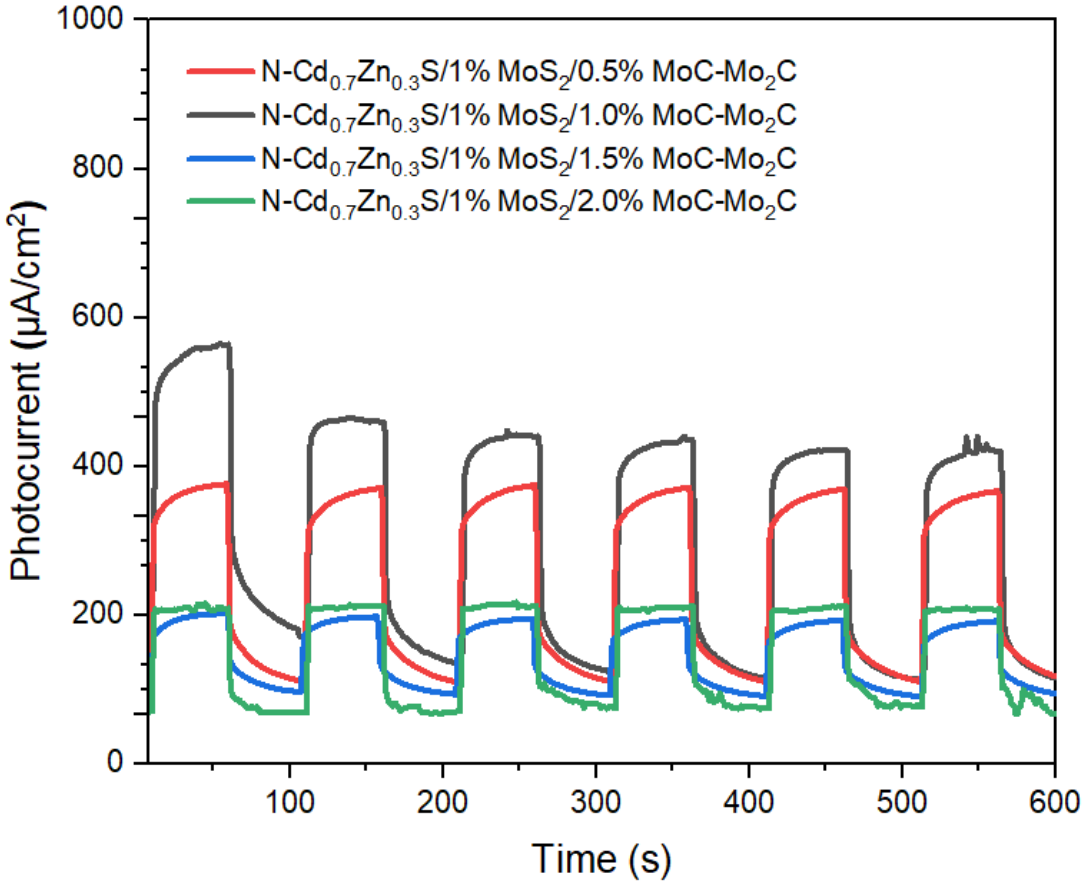

Figure 4.25 Transient photo current curves of N-$Cd_{0.7}Zn_{0.3}S$/1% MoS_2/0.5% MoC-Mo_2C, N-$Cd_{0.7}Zn_{0.3}S$/1% MoS_2/1.0% MoC-Mo_2C, N-$Cd_{0.7}Zn_{0.3}S$/1% MoS_2/1.5% MoC-Mo_2C, N-$Cd_{0.7}Zn_{0.3}S$/1% MoS_2/2.0% MoC-Mo_2C samples.

Chronoamperometry was performed to evaluate the catalyst's stability during electrochemical testing (Figure 4.25.). The connection between time and current created by photogenerated electrons was investigated. All photocatalysts were subjected to a chronoamperometry examination at a potential of 0 V. According to these conclusions, the N-$Cd_{0.7}Zn_{0.3}S$/1% MoS_2/1.0% MoC-Mo_2C photocatalyst provided the highest photocurrent value. The photocurrent generation of the N-$Cd_{0.7}Zn_{0.3}S$/1% MoS_2/0.5% MoC-Mo_2C catalyst was lower than that of the N-$Cd_{0.7}Zn_{0.3}S$/1% MoS_2/1.0% MoC-Mo_2C catalyst, as well as 1.5% and 2.0% MoC-Mo_2C. The graph shows that photocurrent drops with the addition of MoC-Mo_2C. This observation is corroborated by the hydrogen generation rate.

MoC-Mo_2C added samples were coated on ITO, and LSV was utilized in visible light. Photocurrent responses were measured in four samples: N-$Cd_{0.7}Zn_{0.3}S$/1% MoS_2/0.5% MoC-Mo_2C, N-$Cd_{0.7}Zn_{0.3}S$/1% MoS_2/1.0% MoC-Mo_2C, N-$Cd_{0.7}Zn_{0.3}S$/1% MoS_2/1.5% MoC-Mo_2C, N-$Cd_{0.7}Zn_{0.3}S$/1% MoS_2/2.0% MoC-Mo_2C (Figure 4.26.). The results reveal that the photocatalysts created by adding MoC-Mo_2C are active in the visible light spectrum. It has been demonstrated that the photocurrent varies depending on whether the light is turned off or on. Studies have also demonstrated that the addition of MoC-Mo_2C increases photocatalytic activity in the visible range while suppressing electron-hole recombination. The results were found to be similar with the chronoamperometry findings.

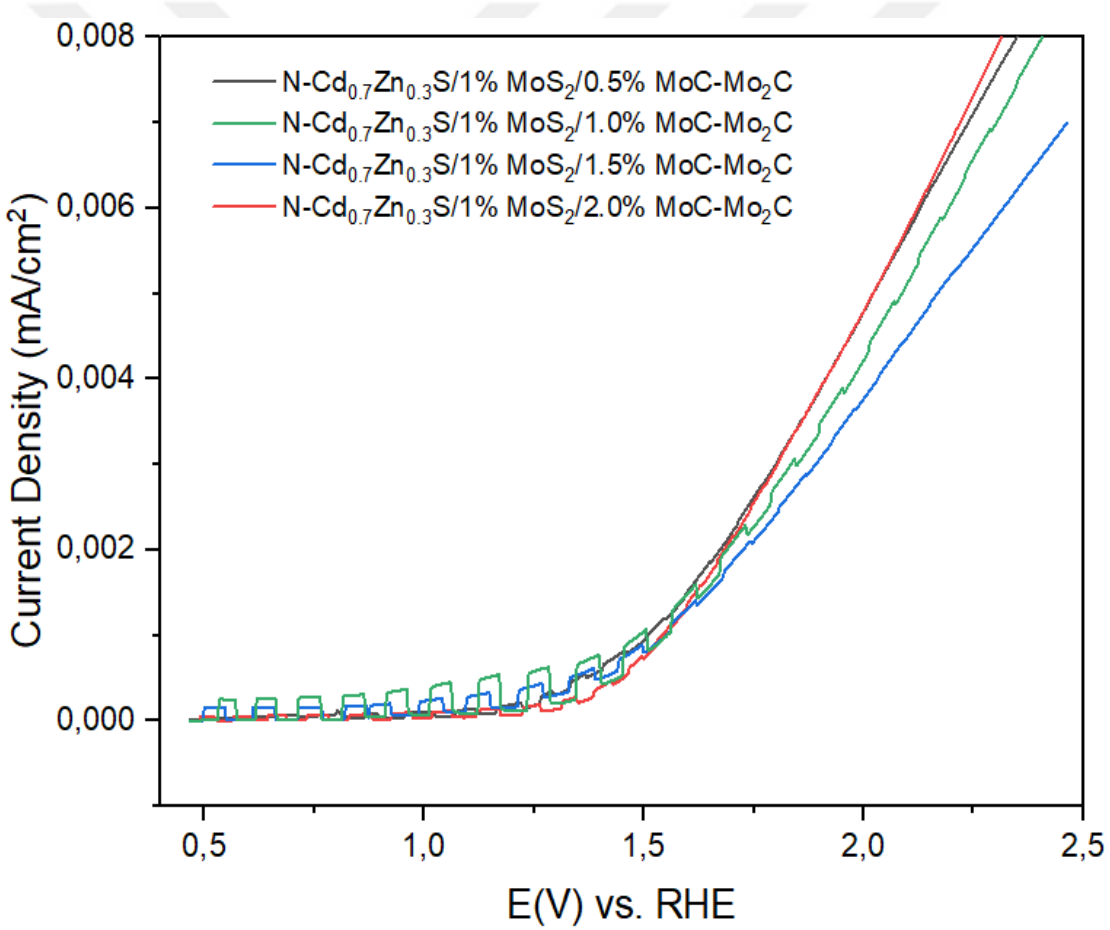

Figure 4.26 LSV of N-$Cd_{0.7}Zn_{0.3}S$/1% MoS_2/0.5% MoC-Mo_2C, N-$Cd_{0.7}Zn_{0.3}S$/1% MoS_2/1.0% MoC-Mo_2C, N-$Cd_{0.7}Zn_{0.3}S$/1% MoS_2/1.5% MoC-Mo_2C, N-$Cd_{0.7}Zn_{0.3}S$/1% MoS_2/2.0% MoC-Mo_2C samples.

5. CONCLUSION

In this study, photocatalyst synthesis and optimization were studied to increase the activity in photocatalytic H_2 production. First, photocatalyst synthesis conditions were optimized in terms of H_2 amount produced using Full Factorial Design by Minitab 19. Cadmium zinc sulfide ($Cd_xZn_{1-x}S$) photocatalyst was studied because CdS has fast electron-hole recombination, so the $Cd_xZn_{1-x}S$ structure was used to increase the activity. As the first synthesis method, DAP, which is not used in the literature before, was preferred and $Cd_xZn_{1-x}S$ photocatalysts were synthesized by solvothermal method in DAP. The important parameters for the amount of produced H_2 are the change in x value or namely Cd/Zn ratio, the amount of catalyst used in the photocatalytic H_2 production reaction (mg) and the MoS_2% aimed to be added to the $Cd_xZn_{1-x}S$ catalyst. $Cd_{0.7}Zn_{0.3}S$ and $Cd_{0.3}Zn_{0.7}S$ were studied for x value; 10, 25, and 50 mg were selected as amounts of catalyst used in the photocatalytic H_2 production; and 1% and 5% were selected for MoS_2 addition. In the statistical interpretations of ANOVA, the Catalyst Amount was found to be significant for the single factor effect, and the Cd/Zn*Catalyst Amount was found to be significant for double interactions because the p value was below 0.05. As a result, these parameters were determined as the main factors affecting H_2 production. Graphically, the effects of pareto charts, interaction plots, main effect plots, contour graphs and 3D interaction effect plots are discussed and interpreted. For the highest hydrogen producing catalyst, a production rate of 560 mmol g^{-1} h^{-1} H_2 was found by using 10 mg of $Cd_{0.7}Zn_{0.3}S$ sample and adding 1% MoS_2. XRD, TEM, HRTEM, STEM, and UV–Vis DRS were used for the characterization of the photocatalysts. It was observed that the peaks in XRD did not change with the change in MoS_2%. When examined morphologically, it is seen that it is nanosized and synthesized approximately in the form of nanorods. It has been proven by STEM elemental mapping, $Cd_{0.7}Zn_{0.3}S/1\%MoS_2$ contains Cd, Zn, S, and Mo. With DRS analysis, it is seen that the band gap decreases as MoS_2 is added. The direct band value for the highest hydrogen producing catalyst was calculated to be approximately 2.32 eV.

For the second part of the study, the aim was to synthesize a photocatalyst in nanorod form and utilizing the results obtained from optimization in the first part. The $Cd_{0.7}Zn_{0.3}S$ catalyst was selected for synthesis in nanorod form. At this stage, one of the factors influencing the synthesis parameters, namely the solvent type, was altered, and EDA was

chosen. It was synthesized using 3 different EDA/water ratios. in Figure 4.11. as shown, the photocatalyst synthesized using 40 mL EDA and 40 mL water is in nanorod form. N-$Cd_{0.7}Zn_{0.3}S$ photocatalyst showed 37.2 mmol g^{-1} h^{-1} hydrogen production. After, different percentages (1, 3, 5, 7, 10, and 15 %) of MoS_2 were added to increase the activity. N-$Cd_{0.7}Zn_{0.3}S$/1% MoS_2 photocatalyst, which had the highest hydrogen production, showed 131.8 mmol g^{-1} h^{-1} hydrogen production. This value increased by 3.5 times compared to its bare value. The same catalyst also gave the highest photocurrent difference in electrochemical measurements.

Then, MoC-Mo_2C was synthesized by using CVD and added to $Cd_{0.7}Zn_{0.3}S$/1% MoS_2 photocatalyst in various percentages. N-$Cd_{0.7}Zn_{0.3}S$/1%MoS_2/1.0%MoC-Mo_2C photocatalyst showed the best results with 133.5 mmol H_2 g^{-1} h^{-1}. It has been found that hydrogen production is increased by adding the MoS_2/MoC-Mo_2C structure. In DRS analysis, the band gap of the N-$Cd_{0.7}Zn_{0.3}S$/1% MoS_2 photocatalyst was calculated to be approximately 2.36 eV, while the N-$Cd_{0.7}Zn_{0.3}S$/1% MoS_2/1.0% MoC-Mo_2C was calculated to be approximately 2.32 eV. Hydrogen production results and electrochemical measurements support each other. In this study, N-$Cd_{0.7}Zn_{0.3}S$/1% MoS_2/1.0% MoC-Mo_2C structure, which was proposed for the first time in the literature, was developed as a efficient and stable photocatalyst for H_2 production. It is aimed that the study will provide impact for the literature and hydrogen production applications.

REFERENCES LIST

1. Wei, L., Chen, Y., Lin, Y., Wu, H., Yuan, R., & Li, Z. 2014. "MoS_2 as non-noble-metal co-catalyst for photocatalytic hydrogen evolution over hexagonal ZnIn2S4 under visible light irradiations", Applied Catalysis B: Environmental, 144, 521-527.

2. Chang, K., Li, M., Wang, T., Ouyang, S., Li, P., Liu, L., & Ye, J. 2015. "Drastic layer-number-dependent activity enhancement in photocatalytic H2 evolution over nMoS_2/CdS (n≥ 1) under visible light", Advanced Energy Materials, 5(10), 1402279.

3. Lv, B., Feng, X., Xi, X., Feng, X., Yuan, Z., Yang, Y., & Zhang, F. (2021). Noble-metal-free Cd0. 3Zn0. 7S-Ni (OH) 2 for high efficiency visible light photocatalytic hydrogen production. Journal of Colloid and Interface Science, 601, 177-185.

4. Acar, C., Dincer, I., & Naterer, G. F. (2016). Review of photocatalytic water-splitting methods for sustainable hydrogen production. International Journal of Energy Research, 40(11), 1449-1473.

5. Oliveira, L. G., Machado, B., de Souza, L. P., Corrêa, G. C. G., Polinarski, M. A., Trevisan, S. V. C., ... ve Alves, H. J. 2022. "Dry reforming of biogas in a pilot unit: Scale-up of catalyst synthesis and green hydrogen production", International Journal of Hydrogen Energy, 47(84), 35608-35625.

6. Joshi, A. S., Dincer, I., & Reddy, B. V. (2010). Exergetic assessment of solar hydrogen production methods. *International Journal of Hydrogen Energy*, *35*(10), 4901-4908.

7. Huang, H. B., Fang, Z. B., Yu, K., Lü, J., & Cao, R. (2020). Visible-light-driven photocatalytic H 2 evolution over CdZnS nanocrystal solid solutions: interplay of twin structures, sulfur vacancies and sacrificial agents. Journal of materials chemistry A, 8(7), 3882-3891.

8. Huang, H. B., Fang, Z. B., Yu, K., Lü, J., & Cao, R. (2020). Visible-light-driven photocatalytic H 2 evolution over CdZnS nanocrystal solid solutions: interplay of twin structures, sulfur vacancies and sacrificial agents. Journal of materials chemistry A, 8(7), 3882-3891.

9. Jiang, D., Sun, Z., Jia, H., Lu, D., & Du, P. (2016). "A cocatalyst-free CdS nanorod/ZnS nanoparticle composite for high-performance visible-light-driven hydrogen production from water", Journal of Materials Chemistry A, 4(2), 675-683.

10. Cheng, L., Xiang, Q., Liao, Y., & Zhang, H. (2018). "CdS-based photocatalysts", Energy & Environmental Science, 11(6), 1362-1391.

11. Yuan, J., Wen, J., Zhong, Y., Li, X., Fang, Y., Zhang, S., & Liu, W. (2015). Enhanced photocatalytic H 2 evolution over noble-metal-free NiS cocatalyst modified CdS nanorods/gC 3 N 4 heterojunctions. Journal of Materials Chemistry A, 3(35), 18244-18255.

12. Yang, Y., Zhou, C., Wang, W., Xiong, W., Zeng, G., Huang, D., ... & Ouyang, Z. (2021). Recent advances in application of transition metal phosphides for photocatalytic hydrogen production. Chemical Engineering Journal, 405, 126547.

13. Wang, Z., Li, C., & Domen, K. (2019). "Recent developments in heterogeneous photocatalysts for solar-driven overall water splitting", Chemical Society Reviews, 48(7), 2109-2125.

14. Li, T., Tsubaki, N., & Jin, Z. (2024). S-scheme heterojunction in photocatalytic hydrogen production. Journal of Materials Science & Technology, 169, 82-104.

15. Tahir, M., Tasleem, S., & Tahir, B. (2020). Recent development in band engineering of binary semiconductor materials for solar driven photocatalytic hydrogen production. International Journal of Hydrogen Energy, 45(32), 15985-16038.

16. Debnath, B., Dhingra, S., & Nagaraja, C. M. (2021). "Recent Developments in the Design of $Cd_xZn_{1-x}S$-Based Photocatalysts for Sustainable Production of Hydrogen", Solar RRL, 5(7), 2100226.

17. Kumaravel, V., Imam, M., Badreldin, A., Chava, R., Do, J., Kang, M., & Abdel-Wahab, A. (2019). Photocatalytic hydrogen production: role of sacrificial reagents on the activity of oxide, carbon, and sulfide catalysts. Catalysts 9: 276.

18. Huang, S., Lin, Y., Yang, J. H., & Yu, Y. (2013). CdS-based semiconductor photocatalysts for hydrogen production from water splitting under solar light. In Nanotechnology for Sustainable Energy (pp. 219-241). American Chemical Society.

19. Jiang, D., Sun, Z., Jia, H., Lu, D., & Du, P. (2016). "A cocatalyst-free CdS nanorod/ZnS nanoparticle composite for high-performance visible-light-driven hydrogen production from water", Journal of Materials Chemistry A, 4(2), 675-683.

20. Cheng, L., Xiang, Q., Liao, Y., & Zhang, H. (2018). CdS-based photocatalysts. Energy & Environmental Science, 11(6), 1362-1391.

21. Wu, A., Tian, C., Jiao, Y., Yan, Q., Yang, G., & Fu, H. (2017). "Sequential two-step hydrothermal growth of MoS_2/CdS core-shell heterojunctions for efficient visible light-driven photocatalytic H_2 evolution", Applied Catalysis B: Environmental, 203, 955-963.

22. Liu, S., Ma, Y., Chi, D., Sun, Y., Chen, Q., Zhang, J., ... & Liu, B. (2022). Hollow heterostructure CoS/CdS photocatalysts with enhanced charge transfer for photocatalytic hydrogen production from seawater. International Journal of Hydrogen Energy, 47(15), 9220-9229.

23. Ran, J., Yu, J., & Jaroniec, M. (2011). Ni (OH) 2 modified CdS nanorods for highly efficient visible-light-driven photocatalytic H 2 generation. Green Chemistry, 13(10), 2708-2713.

24. Li, F., Yang, J., Gao, J., Liu, Y., & Gong, Y. (2020). Enhanced photocatalytic hydrogen production of CdS embedded in cationic hydrogel. International Journal of Hydrogen Energy, 45(3), 1969-1980.

25. Liu, H., Chen, J., Guo, W., Xu, Q., & Min, Y. (2022). A high efficiency water hydrogen production method based on CdS/WN composite photocatalytic. Journal of Colloid and Interface Science, 613, 652-660.

26. Zhao, H., Fu, H., Yang, X., Xiong, S., Han, D., & An, X. (2022). MoS2/CdS rod-like nanocomposites as high-performance visible light photocatalyst for water splitting photocatalytic hydrogen production. International Journal of Hydrogen Energy, 47(13), 8247-8260.

27. Sun, D., Shi, J. W., Ma, D., Zou, Y., Sun, G., Mao, S., ... & Cheng, Y. (2020). CdS/ZnS/ZnO ternary heterostructure nanofibers fabricated by electrospinning for excellent photocatalytic hydrogen evolution without co-catalyst. Chinese Journal of Catalysis, 41(9), 1421-1429.

28. Ma, D., Shi, J. W., Zou, Y., Fan, Z., Ji, X., Niu, C., & Wang, L. (2017). Rational design of CdS@ ZnO core-shell structure via atomic layer deposition for drastically enhanced photocatalytic H2 evolution with excellent photostability. Nano Energy, 39, 183-191.

29. Wang, X., Liu, M., Chen, Q., Zhang, K., Chen, J., Wang, M., ... & Guo, L. (2013). Synthesis of CdS/CNTs photocatalysts and study of hydrogen production by photocatalytic water splitting. International journal of hydrogen energy, 38(29), 13091-13096.

30. Jia, Y., Wang, Z., Qiao, X. Q., Huang, L., Gan, S., Hou, D., ... & Li, D. S. (2021). A synergistic effect between S-scheme heterojunction and Noble-metal free cocatalyst to promote the hydrogen evolution of ZnO/CdS/MoS2 photocatalyst. Chemical Engineering Journal, 424, 130368.

31. Ma, D., Shi, J. W., Sun, L., Sun, Y., Mao, S., Pu, Z., ... & Cheng, Y. (2022). Knack behind the high performance CdS/ZnS-NiS nanocomposites: Optimizing synergistic effect between cocatalyst and heterostructure for boosting hydrogen evolution. Chemical Engineering Journal, 431, 133446.

32. Zhou, Q., Li, L., Xin, Z., Yu, Y., Wang, L., & Zhang, W. (2020). Visible light response and heterostructure of composite CdS@ ZnS–ZnO to enhance its photocatalytic activity. Journal of Alloys and Compounds, 813, 152190.

33. Reddy, C. V., Shim, J., & Cho, M. (2017). Synthesis, structural, optical, and photocatalytic properties of CdS/ZnS core/shell nanoparticles. Journal of Physics and Chemistry of Solids, 103, 209-217.

34. Sharma, K., Raizada, P., Hasija, V., Singh, P., Bajpai, A., Nguyen, V. H., ... & Van Le, Q. (2021). ZnS-based quantum dots as photocatalysts for water purification. Journal of Water Process Engineering, 43, 102217.

35. Kanakaraju, D., & Chandrasekaran, A. (2023). Recent advances in TiO2/ZnS-based binary and ternary photocatalysts for the degradation of organic pollutants. Science of The Total Environment, 868, 161525.

36. Lin, Y., Zhang, Q., Li, Y., Liu, Y., Xu, K., Huang, J., ... & Peng, F. (2020). The evolution from a typical type-I CdS/ZnS to type-II and Z-scheme hybrid structure for efficient and stable hydrogen production under visible light. ACS sustainable chemistry & engineering, 8(11), 4537-4546.

37. Zhang, D., Teng, J., Yang, H., Fang, Z., Song, K., Wang, L., ... & Yang, W. (2023). Air-condition process for scalable fabrication of CdS/ZnS 1D/2D heterojunctions toward efficient and stable photocatalytic hydrogen production. Carbon Energy, 5(7), e277.

38. Lee, G. C., Lyu, L. M., Hsiao, K. Y., Huang, Y. S., Perng, T. P., Lu, M. Y., & Chen, L. J. (2022). Induction of a piezo-potential improves photocatalytic hydrogen production over ZnO/ZnS/MoS2 Heterostructures. Nano Energy, 93, 106867.

39. Jin, Z., Liu, Y., & Hao, X. (2020). Self-assembly of zinc cadmium sulfide nanorods into nanoflowers with enhanced photocatalytic hydrogen production activity. Journal of colloid and interface science, 567, 357-368.

40. Ran, J., Yu, J., & Jaroniec, M. (2011). Ni (OH) 2 modified CdS nanorods for highly efficient visible-light-driven photocatalytic H 2 generation. Green Chemistry, 13(10), 2708-2713.

41. Su, D. W., Ran, J., Zhuang, Z. W., Chen, C., Qiao, S. Z., Li, Y. D., & Wang, G. X. (2020). Atomically dispersed Ni in cadmium-zinc sulfide quantum dots for high-performance visible-light photocatalytic hydrogen production. Science advances, 6(33), eaaz8447.

42. Zu, S., Wang, Z., Liu, B., Fan, X., & Qian, G. (2009). Synthesis of nano-CdxZn1− xS by precipitate-hydrothermal method and its photocatalytic activities. Journal of Alloys and Compounds, 476(1-2), 689-692.

43. Medina-Ramírez, I., Hernández-Ramírez, A., & Maya-Trevino, M. L. (2015). Synthesis methods for photocatalytic materials. Photocatalytic Semiconductors: Synthesis, Characterization, and Environmental Applications, 69-102.

44. Debnath, B., Dhingra, S., & Nagaraja, C. M. (2021). Recent Developments in the Design of CdxZn1− xS-Based Photocatalysts for Sustainable Production of Hydrogen. Solar RRL, 5(7), 2100226.

45. Zhao, S., Huang, J., Huo, Q., Zhou, X., & Tu, W. (2016). “A non-noble metal MoS_2–$Cd_{0.5}Zn_{0.5}S$ photocatalyst with efficient activity for high H 2 evolution under visible light irradiation”, Journal of Materials Chemistry A, 4(1), 193-199.

46. Wang, Y., Yang, C., Guo, L., Yang, Z., Jin, B., Du, R., ... & Wang, D. (2023). "Plate-on-plate structured $MoS_2/Cd_{0.6}Zn_{0.4}S$ Z-scheme heterostructure with enhanced photocatalytic hydrogen production activity via hole sacrificial agent synchronously strengthen half-reactions", Journal of Colloid and Interface Science, 630, 341-351.

47. Li, Y., Wan, S., Lin, C., Gao, Y., Lu, Y., Wang, L., & Zhang, K. (2021). "Engineering of 2D/2D $MoS_2/Cd_xZn_{1-x}S$ photocatalyst for solar H_2 evolution coupled with degradation of plastic in alkaline solution", Solar RRL, 5(6), 2000427.

48. Wang, Y., Wu, J., Zheng, J., & Xu, R. (2011). "Highly active $Zn_xCd_{1-x}S$ photocatalysts containing earth abundant elements only for H2 production from water under visible light", Catalysis Science & Technology, 1(6), 940-947.

49. Li, Q., Meng, H., Zhou, P., Zheng, Y., Wang, J., Yu, J., & Gong, J. (2013). "$Zn_{1-x}Cd_xS$ solid solutions with controlled bandgap and enhanced visible-light photocatalytic H2-production activity", Acs Catalysis, 3(5), 882-889.

50. Wang, J., Li, B., Chen, J., Li, L., Zhao, J., & Zhu, Z. (2013). Hierarchical assemblies of CdxZn1− xS complex architectures and their enhanced visible-light photocatalytic activities for H2-production. Journal of alloys and compounds, 578, 571-576.

51. Yu, K., Huang, H. B., Zeng, X. Y., Xu, J. Y., Yu, X. T., Liu, H. X., ... & Cao, R. (2020). "CdZnS nanorods with rich sulphur vacancies for highly efficient photocatalytic hydrogen production", Chemical Communications, 56(56), 7765-7768.

52. Shi, J., Liang, Z., Lu, X., Tong, Y., Su, C., & Liu, H. (2011). "The roles of defect states in photoelectric and photocatalytic processes for Zn x Cd 1− x S", Energy & Environmental Science, 4(2), 466-470.

53. Pei, L., Liu, J., Xu, Y., Han, Y., Wu, J., Wang, Z., & Zhang, X. (2019). “Hierarchical Zn1 xCdxS microclusters with superior visible-light-driven photocatalytic hydrogen generation performance”, Journal of Alloys and Compounds, 809, 151869.

54. Li, Q., Meng, H., Zhou, P., Zheng, Y., Wang, J., Yu, J., & Gong, J. (201)3. “$Zn_{1-x}Cd_xS$ solid solutions with controlled bandgap and enhanced visible-light photocatalytic H2-production activity”, Acs Catalysis, 3(5), 882-889.

55. Zhang, K., Jing, D., Xing, C., & Guo, L. (2007). “Significantly improved photocatalytic hydrogen production activity over Cd1-xZnxS photocatalysts prepared by a novel thermal sulfuration method”, International Journal of Hydrogen Energy, 32(18), 4685-4691.

56. Nazir, M. A., Najam, T., Altaf, M., Ahmad, K., Hossain, I., Assiri, M. A., ... & Shah, S. S. A. (2024). Tuning the photocatalytic hydrogen production via co-catalyst engineering. Journal of Alloys and Compounds, 174378.

57. Liu, M., Xia, P., Zhang, L., Cheng, B., & Yu, J. (2018). Enhanced photocatalytic H2-production activity of g-C3N4 nanosheets via optimal photodeposition of Pt as cocatalyst. ACS Sustainable Chemistry & Engineering, 6(8), 10472-10480.

58. Han, B., & Hu, Y. H. (2016). MoS2 as a co-catalyst for photocatalytic hydrogen production from water. Energy Science & Engineering, 4(5), 285-304.

59. Wu, A., Tian, C., Jiao, Y., Yan, Q., Yang, G., & Fu, H. (2017). “Sequential two-step hydrothermal growth of MoS_2/CdS core-shell heterojunctions for efficient visible light-driven photocatalytic H_2 evolution”, Applied Catalysis B: Environmental, 203, 955-963.

60. Jayachitra, S., Mahendiran, D., Ravi, P., Murugan, P., & Sathish, M. (2022). Highly conductive NiSe2 nanoparticle as a co-catalyst over TiO2 for enhanced photocatalytic hydrogen production. Applied Catalysis B: Environmental, 307, 121159.

61. Li, Y., Sun, B., Lin, H., Ruan, Q., Geng, Y., Liu, J., ... & Tam, K. C. (2020). Efficient visible-light induced H2 evolution from T-CdxZn1-xS/defective MoS2 nano-hybrid with both bulk twinning homojunctions and interfacial heterostructures. Applied Catalysis B: Environmental, 267, 118702.

62. Su, T., Xiao, L., Gao, Y., Liu, T., Peng, X., Yuan, H., ... & Wang, X. (2019). Multifunctional MoS2 ultrathin nanoflakes loaded by Cd0. 5Zn0. 5S QDs for enhanced photocatalytic H2 production. International Journal of Energy Research, 43(11), 5678-5686.

63. Chen, Y. C., Huang, Y. S., Huang, H., Su, P. J., Perng, T. P., & Chen, L. J. (2020). "Photocatalytic enhancement of hydrogen production in water splitting under simulated solar light by band gap engineering and localized surface plasmon resonance of ZnxCd1-xS nanowires decorated by Au nanoparticles", Nano Energy, 67, 104225.

64. Hinnemann, B., Moses, P. G., Bonde, J., Jørgensen, K. P., Nielsen, J. H., Horch, S., ... & Nørskov, J. K. (2005). "Biomimetic hydrogen evolution: MoS2 nanoparticles as catalyst for hydrogen evolution", Journal of the American Chemical Society, 127(15), 5308-5309.

65. Zhu, B., Lin, B., Zhou, Y., Sun, P., Yao, Q., Chen, Y., & Gao, B. (2014). "Enhanced photocatalytic H_2 evolution on ZnS loaded with graphene and MoS 2 nanosheets as cocatalysts", Journal of Materials Chemistry A, 2(11), 3819-3827.

66. He, G., Zhang, Y., & He, Q. (2019). "MoS_2/CdS heterostructure for enhanced photoelectrochemical performance under visible light", Catalysts, 9(4), 379.

67. Ertis, I. F., & Boz, I. (2017). "Synthesis and characterisation of MoS_2–CdS catalyst for photocatalytic degradation of methylene blue from aqueous solution", Journal of Chemical Research, 41(9), 529-533.

68. Wu, A., Tian, C., Jiao, Y., Yan, Q., Yang, G., & Fu, H. (2017). “Sequential two-step hydrothermal growth of MoS_2/CdS core-shell heterojunctions for efficient visible light-driven photocatalytic H_2 evolution”, Applied Catalysis B: Environmental, 203, 955-963.

69. Saadati, M., Akhavan, O., & Fazli, H. (2021). Single-layer MoS2-MoO3-x heterojunction nanosheets with simultaneous photoluminescence and co-photocatalytic features. Catalysts, 11(12), 1445.

70. Du, R., Zhang, Y., Li, B., Yu, X., Liu, H., An, X., & Qu, J. (2016). Biomolecule-assisted synthesis of defect-mediated Cd 1− x Zn x S/MoS 2/graphene hollow spheres for highly efficient hydrogen evolution. Physical Chemistry Chemical Physics, 18(24), 16208-16215.

71. Li, Y., Wan, S., Lin, C., Gao, Y., Lu, Y., Wang, L., & Zhang, K. (2021). “Engineering of 2D/2D $MoS_2/Cd_xZn_{1-x}S$ photocatalyst for solar H_2 evolution coupled with degradation of plastic in alkaline solution”, Solar RRL, 5(6), 2000427.

72. Yin, X. L., Li, L. L., Jiang, W. J., Zhang, Y., Zhang, X., Wan, L. J., & Hu, J. S. (2016). MoS2/CdS nanosheets-on-nanorod heterostructure for highly efficient photocatalytic H2 generation under visible light irradiation. ACS applied materials & interfaces, 8(24), 15258-15266.

73. Liu, W., Wang, X., Wang, F., Du, K., Zhang, Z., Guo, Y., ... & Wang, D. (2021). A durable and pH-universal self-standing MoC–Mo2C heterojunction electrode for efficient hydrogen evolution reaction. Nature Communications, 12(1), 6776.

74. Liu, J., Wang, P., Fan, J., Yu, H., & Yu, J. (2021). Hetero-phase MoC-Mo 2 C nanoparticles for enhanced photocatalytic H 2-production activity of TiO 2. Nano Research, 14, 1095-1102.

75. Wei, T., Zhang, T., Jin, Z., Li, F., & Xu, L. (2022). Fabrication of nanocomposite MoC–Mo 2 C@ C/Cd 0.5 Zn 0.5 S: promoted electron migration and improved photocatalytic hydrogen evolution. Dalton Transactions, 51(30), 11397-11403.

76. Yi, S. S., Yan, J. M., Wulan, B. R., & Jiang, Q. (2017). Efficient visible-light-driven hydrogen generation from water splitting catalyzed by highly stable CdS@ Mo 2 C–C core–shell nanorods. Journal of materials chemistry A, 5(30), 15862-15868.

77. Yu, K., Huang, H. B., Zeng, X. Y., Xu, J. Y., Yu, X. T., Liu, H. X., ... & Cao, R. (2020). CdZnS nanorods with rich sulphur vacancies for highly efficient photocatalytic hydrogen production. Chemical communications, 56(56), 7765-7768.

78. Rao, B. S., Kumar, B. R., Reddy, V. R., Rao, T. S., & Chalapathi, G. J. C. L. (2011). Preparation and characterization of CdS nanoparticles by chemical co-precipitation technique. Chalcogenide Lett, 8(3), 177-185.

79. Hamid, M. A. S., Zengin, Y., & Boz, I. (2024). Synergistic effects of sulphur vacancies and MoS2 on the photocatalytic activity of CdxZn1-xS for H2 evolution. International Journal of Hydrogen Energy, 52, 1229-1238.

80. Achutha Kini, U., Shettar, M., Sharma, S., Hiremath, P., Gowrishankar, M. C., Hegde, A., & Siddhartha, D. (2019). Effect of hygrothermal aging on the mechanical properties of nanoclay-glass fiber-epoxy composite and optimization using full factorial design. Materials Research Express, 6(6).

81. Krishnan, T., & Purushothaman, R. (2017, July). Optimization and influence of parameter affecting the compressive strength of geopolymer concrete containing recycled concrete aggregate: using full factorial design approach. In IOP Conference Series: Earth and Environmental Science (Vol. 80, No. 1, p. 012013). IOP Publishing.

82. Di Leo, G., & Sardanelli, F. (2020). Statistical significance: p value, 0.05 threshold, and applications to radiomics—reasons for a conservative approach. European radiology experimental, 4, 1-8.

83. Chen, H. W., Ku, Y., & Kuo, Y. L. (2007). Effect of Pt/TiO2 characteristics on temporal behavior of o-cresol decomposition by visible light-induced photocatalysis. Water research, 41(10), 2069-2078.

84. Landi Jr, S., Segundo, I. R., Freitas, E., Vasilevskiy, M., Carneiro, J., & Tavares, C. J. (2022). Use and misuse of the Kubelka-Munk function to obtain the band gap energy from diffuse reflectance measurements. Solid state communications, 341, 114573.

85. Zheng, A. L. T., Sabidi, S., Ohno, T., Maeda, T., & Andou, Y. (2022). Cu2O/TiO2 decorated on cellulose nanofiber/reduced graphene hydrogel for enhanced photocatalytic activity and its antibacterial applications. Chemosphere, 286, 131731.

86. Sun, B., Liang, Z., Qian, Y., Xu, X., Han, Y., & Tian, J. (2020). Sulfur vacancy-rich O-doped 1T-MoS2 nanosheets for exceptional photocatalytic nitrogen fixation over CdS. ACS applied materials & interfaces, 12(6), 7257-7269.

87. Fu, H., Zhao, H., Li, X., Chen, F., Yang, X., Xiong, S., ... & An, X. (2023). High-performance visible-light-driven MoS2/CdZnS nanorods for photocatalytic hydrogen production by water splitting. Powder Technology, 429, 118889.

88. Upadhyay, S., & Pandey, O. P. (2022). Synthesis of Mo 2 C/MoC/C nanocomposite for hydrogen evolution reaction. Journal of Solid State Electrochemistry, 1-6.

89. Mir, R. A., Sharma, P., & Pandey, O. P. (2017). Thermal and structural studies of carbon coated Mo2C synthesized via in-situ single step reduction-carburization. Scientific Reports, 7(1), 3518.

CURRICULUM VITAE

Name: İbrahim

Surname: KABA

EDUCATION STATUS

B.Sc. License: 2022, Marmara University, Chemical Engineering

PUBLICATIONS

Articles

ÖZKUL, S. L. Ç., KABA, İ., ÖZDEMİR OLGUN, F. A. (2024). Unravelling the potential of magnetic nanoparticles: a comprehensive review of design and applications in analytical chemistry. Analytical Methods. (SCI-E, Q2, Review Article)

Conferences

KABA, İ., and KERKEZ KUYUMCU, Ö., (2024). Synthesis of $Cd_{0.7}Zn_{0.3}S/MoS_2$ Catalysts and Investigation of Their Activities in Photocatalytic H_2 Production. IHTEC 2024: The 8th International Hydrogen Technologies Congress, Diyarbakir, Turkey. (Oral Presentation)

YILMAZ, E. T., KABA, İ., KERKEZ KUYUMCU, Ö., (2024). Synthesis of $CuS/CuInS_2/TiO_2$ Catalysts and Investigation of Their Activities in Photocatalytic H_2 Production. IHTEC 2024: The 8th International Hydrogen Technologies Congress, Diyarbakir, Turkey. (Oral Presentation)

KABA, İ., & BOZKURT, R. N., (2024). Kavun Meyvesi (Cucumis Melo L.) Atıklarından Çinko Oksit Nanopartiküllerin Yeşil Sentezi, Karakterizasyonu Ve Yanıt Yüzey Metodolojisiyle Optimizasyonu. 17. Ulusal Spektroskopi Kongresi, Zonguldak, Turkey. (Poster Presentation)